Phylogeographic patterning of three co-distributed forest-dwelling reptile species along the east coast of South Africa

By

Theo Busschau

Thesis presented in partial fulfilment of the requirements for the degree Master of Science in Zoology at Stellenbosch University
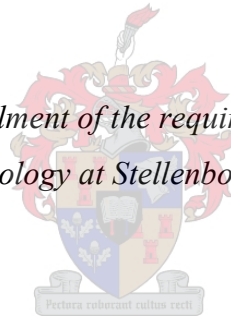
Supervisor: Prof. Savel R. Daniels

Co-supervisor: Mr. Werner Conradie

Faculty of Science

Department of Botany and Zoology

December 2019

Declaration

By submitting this thesis electronically, I declare that the entirety of the work contained therein is my own, original work, that I am the authorship owner thereof (unless to the extent explicitly otherwise stated) and that I have not previously in its entirety or in part submitted it for obtaining any qualification.

December 2019

Abstract

This study investigates the phylogeographic structure of three co-distributed forest-living reptile species, the Pondo flat gecko (*Afroedura pondolia*), the forest thread snake (*Leptotyphlops sylvicolus*) and the Natal black snake (*Macrelaps microlepidotus*), by sampling specimens from the Eastern Cape and KwaZulu-Natal provinces of South Africa. Phylogenetic results, using Bayesian inferences and maximum likelihood, from the combined mitochondrial sequence data (*ND4* and *cyt b*), along with population genetic analyses suggest the presence of broadly congruent biogeographic breaks among the study taxa. Sequence divergence values suggest that *A. pondolia* and *L. sylvicolus* represent species complexes comprising several cryptic species while *M. microlepidotus* exhibits population level differentiation. Divergence-time estimates indicate that cladogenesis within the study taxa occurred during the late Miocene to the Plio/Pleistocene climatic shifts, suggesting that cladogenesis was driven by climatic oscillations and suitable habitat fragmentation. We further investigate the species level divergence within *A. pondolia* and *L. sylvicolus* by including two partial nuclear loci (*PRLR* and *RAG1*) and employing several species delimitation methods (ABGD, bGMYC, PTP and STACEY). The species delimitation results were generally incongruent, estimating between two and 14 species nested within *A. pondolia* and between ten and 12 species nested within *L. sylvicolus*. In both taxa, the species hypotheses retrieved by STACEY based on the total-evidence data were preferred and used to define groups in the morphological analyses. In *A. pondolia* the multivariate morphological analyses indicate statistically significant differences among the four putative species, corroborating the presence of four species. In *L. sylvicolus* the morphological analyses exhibit large overlap among the ten putative species but indicate differences between grassland and forest species. The narrow distributions of the putative species identified in the present study have further implications for the conservation status of *A. pondolia* and *L. sylvicolus* and suggest that the fragmented forest habitat along the east coast of South Africa may harbor significantly higher levels of diversity than currently recognized.

III

Acknowledgements

Table of contents

List of tables

List of figures

List of appendices

Chapter 1
General introduction

Oscillations in global climatic conditions together with geomorphological changes have played a major role in the habitat shifts of terrestrial taxa through repeated habitat contraction and expansion cycling, promoting both cladogenesis and extinction events (Hewitt, 2000, 2003, 2004). Southern Africa experienced several dramatic climatic ameliorations as a consequence of global climatic shifts (Deacon, 1983; Tyson, 1986). These climatic changes significantly impacted biome structure and composition, resulting in numerous contractions, extinction and expansion episodes for organisms, creating a complex mosaic of interconnectivity and isolation among populations and facilitating diversification.

One of the South African biomes most affected by climatic shifts is the forest biome. The forest biome is the smallest biome in South Africa and occupies an estimated 7177km^2 or < 0.56% of the total land area (Rutherford and Westfall, 1994; Low and Rebelo, 1996; Mucina and Rutherford, 2006). After an initial period of uplift and formation of the great escarpment following the breakup of Gondwanaland, South Africa's geology remained stable between 130 and 30 million years ago (Mya) (Clark et al., 2011; Neumann and Bamford, 2015). During the Paleocene and Eocene (65-38 Mya) South Africa was warmer with higher levels of precipitation, resulting in expansion of the Afrotemperate forest biome (Feakins and Demenocal, 2010; Deacon, 1983). The eastern continental margin of southern Africa was inundated by marine transgressions followed by regression during the Oligocene (34–23 Mya) (Perissinotto et al., 2013). Climatic ameliorations at the onset of the Oligocene resulted in a cooler xeric climatic shift due to the development of the first permanent Antarctic ice sheet and the formation of the proto Benguela current along the west coast of southern Africa (Feakins and Demenocal, 2010; Siesser, 1980). This initiated the contraction of Afrotemperate forest habitat to areas with high precipitation along mountain ranges in the adjacent interior and initiated the fragmentation of the forest biome in South Africa.

During the early Miocene (23 Mya) mesic conditions were once again established due to warmer temperatures, resulting in increased precipitation and the expansion of the Afrotemperate forest biome (Deacon, 1983). From the middle Miocene a steeper climatic gradient from the equator to the poles is thought to have led to the global establishment of grasslands and savannas as well as the formation of fire prone ecosystems, further isolating forest fragments (Linder, 2003; Mucina and Rutherford, 2006). From the late Miocene marked expansion of the Antarctic ice sheets caused the climate in South Africa to become arid, again leading to a shift in the distribution of forest habitats to areas of suitable climatic conditions, generally higher elevations or sheltered valleys (Mucina and Rutherford, 2006; Lawes, 1990).

The cooling Benguela current led to the establishment of seasonal rainfall patterns in South Africa, with the Western Cape experiencing winter rainfall and more arid conditions (Deacon et al., 1992; Scott et al., 1997; Roberts et al., 2013). In contrast, along the east coast the warm Agulhas current, together with the Great Escarpment created a rain shadow effect that maintained a subtropical climatic regime along the Great Escarpment's eastern slopes as well as monsoonal summer rainfall (Neumann and Bamford, 2015). As a result, isolated forest patches persisted along the east coast since the Miocene while in the remainder of southern Africa forest patches became established at higher altitude areas (Sepulchre et al., 2006). The continued xeric climatic shifts intensified during the Plio/Pleistocene further accelerating the fragmentation of the forest biome.

During the last 2 million years there were repeated glacial-interglacial cycles with periodicity of about 100 000 years (Deacon, 1983; Tyson, 1986). Interglacial periods were characterized by a warmer and wetter climate and the expansion of more mesic habitats like forests in South Africa while glacial periods were characterized as being cooler and more arid and resulted in the contraction of forest habitats (Deacon, 1983). The last interglacial period was between 130 000-40 000 BP after which temperatures decreased and conditions became much drier towards the last glacial maximum (LGM) about 18000 BP (Deacon, 1983; Tyson, 1986). During the LGM winter conditions in the eastern parts of South Africa, where current forest habitat occur, were cold and dry with strong wind and cold air draining from the Drakensberg mountains leading to increased aridification, especially so in the south where higher mountains are closer to the coast (Eeley et al., 1999). Sea surface temperatures were also cooler during the LGM, along with the cooler and weaker Agulhas current, contributing to the decrease in temperature and aridification in the eastern parts of South Africa (Van Zinderen Bakker, 1982; Prell et al., 1980). With the climatic history of South Africa, the majority of forest types have been fragmented throughout most of their evolutionary history by severe climate changes in the quaternary (Eeley et al., 1999). Wetter conditions were re-established by 15000 – 17000 BP and temperatures were warmer by 8000 BP during the Holocene altithermal, allowing once again for the expansion of forest habitat (Tyson, 1986).

Contemporary indigenous forests in South Africa are highly fragmented, occurring in patches along the eastern and southern margins of the country with most patches being less than 100ha and imbedded within larger biomes such as fynbos, grassland, Albany thicket and savannah (Low and Rebelo, 1996; Midgley et al., 1997). Forests typically occur in areas characterized by high precipitation but specialized forest types can be found along drainage lines or in deep river valleys in more arid regions (Mucina and Rutherford, 2006). There are a large diversity of forest types in South Africa due to spatial variation in climate, altitude, latitude, and topography across the region, but they are generally divided into two major types, inland Afrotemperate forests and Indian Ocean Coastal Belt forest (IOCB) types (Midgley et

al, 1997; Von Maltitz et al., 2003; Mucina and Rutherford, 2006). Afrotemperate forest form part of the larger biome that extends into the Zimbabwean highlands, Malawi, the East Africa mountain arch and Ethiopia (Mucina and Rutherford, 2006). The coastal forests of South Africa form part of the Tongaland-Pondoland Regional Mosaic sharing some elements with adjacent forests from the Zanzibar-Inhambane Regional Mosaic (White, 1983). The Tongaland-Pondoland Regional Mosaic stretches from southern Mozambique to the shores of Algoa Bay in the Eastern Cape. The latter region is considered a biodiversity hotspot (Van Wyk and Smith, 2001).

Afrotemperate forests are ancient and have persisted in South Africa since the Miocene while the Indian Ocean Coastal Belt (IOCB) forests expanded along the Mozambique coast recently following the last glacial maximum, after 8000 BP (Lawes, 1990; Eeley et al., 1999). Afrotemperate forests are generally small, discontinuous and isolated to higher elevations or sheltered valleys where they are separated by dry low land barriers and fire regimes in the surrounding habitat (Mucina and Rutherford, 2006). The much younger coastal forests occur along the coastal margins of the Eastern Cape and KwaZulu-Natal provinces of South Africa in areas that were historically submerged during marine transgressions (Mucina and Geldenhuys, 2006). Between these two forest types is a narrow band of scarp forests. Due to expansion of forests during the Holocene, there was potential for a mixing of Afrotemperate and Indian Ocean coastal belt forests along the scarp forest belt (Eeley et al., 1999). Thus, scarp forests comprise a mixture of pallaeoendemic species, coastal communities and species assemblages with strong Afrotemperate affinities (Lawes, 1990; MacDevette et al., 1989; Van Wyk, 1990).

Because scarp forests are relatively large and located on coastal escarpments close to the sea they are thought to have acted as relatively unaffected refugia for Afrotemperate fauna during quaternary climate change (Lawes, 1990; Lawes et al., 2007). These refugia were small and isolated patches of favorable conditions where forests survived as important remnants (Eeley et al., 1999). Much of the Afrotemperate forest faunal recolonization after the LGM came from these scarp forest refugia (Lawes, 1990; Eeley et al, 1999; Lawes et al. 2007). As a result Afrotemperate forests show lower species richness and fewer forest specialists compared to coastal or scarp forests (Lawes et al., 2007). Geldenhuys (1992) suggested that the present composition of both Afrotemperate and coastal types indicates that the similarity between different forests may have been established before the late-Miocene when the forest biome experienced major fragmentation due to increased aridity.

The contraction of forest habitat during cooler drier periods is thought to be the main driver of cladogenesis in forest-living species (White, 1978; Lawes, 1990). However, cladogenesis in the forest-living fauna of South Africa appears to be largely understudied. Research on forest-

dwelling taxa such as mammals, velvet worms and chameleons (Lawes, 1990; Lawes et al., 2000a,b; Lawes et al., 2007; Tolley et al., 2008; Daniels et al., 2016) suggest that paleoclimatic changes and subsequent isolation through habitat fragmentation drove allopatric speciation among forest-living taxa. Not much attention has been given to other forest-living reptiles in South Africa, especially not so at the population genetic level. For some South African reptiles it has been suggested that Miocene and Pleistocene climatic oscillations have shaped current distributions (e.g. Kulenkampff et al., 2019; Barlow et al., 2013; Engelbrecht et al., 2013; Tolley et al., 2008). The majority of these examples suggest that cladogenic activity within taxa were driven by vicariance events such as isolation through habitat fragmentation in response to climatic changes, topographic uplift or increases in CO_2 levels.

Forests in South Africa are generally characterized by rich local and regional faunal assemblages (Geldenhuys and MacDevette, 1989) and the country exhibits high levels of reptile diversity with more than 422 described taxa (Bates et al., 2014), however, there appears to be a proportionately low number of forest-living reptiles in South Africa (Branch, 1998; Bates et al,. 2014). This may be because of the relatively recent establishment of the coastal forests while the older Afrotemperate forests contain lower reptile diversity because these forests generally only contain species that are either highly vagile, enabling them to disperse among geographically isolated forest patches, generalist species from the surrounding habitat that occupy vacant niches, or resilient taxa that survived extinction filtering events during glacial maxima (Lawes, 2007). Ecologically sensitive taxa are removed during extinction filtering processes and the resultant communities are generally species-poor but ecologically robust and persistent (Balmford, 1996). Reptiles are less likely to disperse over large distances and because of their ectothermic life styles appear to be particularly sensitive to climatic oscillations, rendering them ideal organisms with which to test the impact of climatic events as cladogenic drivers. During the present study we will focus on three co-distributed forest-dwelling reptile species, the Natal black snake (*Macrelaps microlepidotus*), the forest thread snake (*Leptotyphlops sylvicolus*) and the Pondo flat gecko (*Afroedura pondolia*). These taxa are distributed along the east coast and the adjacent interior of the Eastern Cape and KwaZulu-Natal provinces of South Africa.

Afroedura pondolia occurs from the eastern parts of the Eastern Cape into central KwaZulu-Natal where it favors wooded habitat and is found on trees and rocky outcrops and frequents human dwellings (Bates et al., 2014, Branch, 1998). Recent molecular studies on *Afroedura* highlight the high genetic diversity and morphological similarities within this genus (Jacobsen et al., 2014; Makhubo et al., 2015). Makhubo et al. (2015) observed that the molecular phylogeny of *Afroedura* species is congruent with geography, with sister species being geographically close to one another. With *Afroedura* being substrate specialists for rupicolous habitats or trees and have low vagility, grasslands between rocky outcrops or potentially forest

patches are thought to impede gene flow (Makhubo et al., 2015). These results are reflected in other South African lizard species showing high substrate specificity and low vagility (e.g. Mouton and Van Wyk, 1994; Tolley et al., 2008). Furthermore, the long branch lengths within *A. pondolia* in the phylogeny by Makhubo et al*.* (2015) suggest the presence of genetically distinct lineages.

The monotypic *Macrelaps microlepidotus* is a medium sized fossorial snake with a maximum snout to vent length (SVL) of 938 mm (Branch, 1998). The species has a strong affinity to forest habitats where it burrows in loamy soils and is generally active on the surface on warm humid evenings (Branch, 1998; Bates et al., 2014). It occurs along the Eastern Cape Province coastal belt and adjacent interior from East London to northern KwaZulu-Natal province (Bates et al., 2014) and is co-distributed with *Leptotyphlops sylvicolus*, a small (SVL) 105 mm fossorial snake species (Broadley and Wallach, 1997) initially reported from three isolated forest habitats along the east coast by Broadley and Broadley (1999). Species boundaries in well adapted fossorial reptiles have largely been obscured by the conservation of morphological characters where molecular data has frequently been used to delineate species boundaries (e.g. Daniels et al., 2002, 2005, 2006, 2009; Adalsteinsson et al., 2009; Parham and Papenfuss, 2009; Heideman et al., 2011; Siler et al., 2011; Valente et al., 2014). Marked genetic differentiation and taxonomic diversity has been observed among other fossorial reptiles in South Africa, particularly within the well-studied fossorial skinks (Daniels et al. 2009, Lamb et al. 2010; Engelbrecht et al. 2013; Busschau et al. 2017). This is especially so where populations are disjunct, suggesting that fossorial forest-living snakes should exhibit high levels of cryptic differentiation among assumed conspecific populations. Adalsteinsson *et al.* (2009) demonstrated the presence of deeply structured *Leptotyphlops* species, suggesting the possible presence of yet undescribed lineages.

By obtaining molecular data it will be possible to examine the evolutionary history of forest-dwelling reptiles in South Africa. Congruent patterns among such co-distributed taxa would suggest that they share a common history in response to paleoclimatic oscillations and geological changes. To understand the biogeographic history of these taxa we have to compare the relative timing of cladogenic events to the timing of major environmental changes that could have led to habitat fragmentation and isolation within taxa. The aim is to document the phylogeographic diversity in the three co-distributed forest dwelling reptile species and examine the species boundaries in *L. sylvicolus* and *A. pondolia*. Since the three taxa are forest-living and largely co-distributed along the east coast of South Africa it is expected that they would show congruent phylogeographic patterns and have responded similarly to historic biogeographic breaks. Smaller animals and substrate specialists such as *L. sylvicolus* and *A. pondolia*, are expected to be less likely to disperse across large geographic distances characterized by unsuitable habitat. Therefore, these species are likely to demonstrate a

higher degree of genetic structure compared to the larger *M. microlepidotus.* However, all taxa are likely to reflect the impact of forest habitat fragmentation due to past climatic ameliorations. The results of this study may have further implications on the conservation status of these taxa, particularly so if there are isolated cryptic lineages.

Research questions:

I.   Are there cryptic lineages among the study taxa?

II.   What is the degree of phylogeographic congruence among the taxa under study?

III.   Is cladogenesis in the three study taxa related to climatic ameliorations that impacted the forest biome along the east coast of South Africa?

Hypotheses:

I.   All three species will exhibit marked genetic differentiation at the population genetic level, but *A. pondolia* and *L. sylvicolus* will exhibit deeper species level divergence among populations.

II.   Divergence time analyses are likely to reveal different evolutionary histories of the three taxa in their respective forest habitat, while some levels of cladogenesis are likely to coincide with habitat fragmentation due to paleoclimatic events.

Chapter 2

Evidence for cryptic diversification in a rupicolous forest-dwelling gecko (Gekkonidae: *Afroedura pondolia*) from a biodiversity hotspot

*This work formed the bases of a peer reviewed publication:

2.1 Introduction

Among the South African reptiles, lizard fauna exhibit the highest levels of diversity and endemism with an estimated 266 described lizard species of which geckos comprise an estimated 33.1% (Branch, 1998; Bates et al., 2014; Tolley et al., 2019). Branch et al. (2006) estimated that rupicolous gecko species in the genera *Afroedura*, *Lygodactylus* and *Pachydactylus* included the largest number of undiscovered cryptic lineages in southern Africa. Recent taxonomic revisions of the three aforementioned genera revealed a plethora of novel species (Heinicke et al., 2011, 2017a; Jacobsen et al., 2014; Makhubo et al., 2015; Röll et al., 2010; Travers et al., 2014). In the two rock-dwelling gecko genera *Afroedura* and *Lygodactylus*, molecular systematic research has revealed the presence of several point endemic species that were frequently isolated to single massifs or mountain tops in the northern Drakensberg Mountain region (Jacobsen et al., 2014; Travers et al., 2014). Similarly, in the highly diverse *Pachydactylus,* allopatric speciation of small rock-dwelling species account for most of the diversity in the group because of their smaller range sizes and higher rates of diversification (Heinicke et al., 2017a).

In southern Africa, *Afroedura* historically contained 15 species and three subspecies (Branch, 1998); however, recent molecular studies suggest high levels of cryptic diversity obscured by morphologically conserved characters (Jacobsen et al., 2014; Makhubo et al., 2015; Branch et al., 2017). The molecular phylogeny by Jacobsen et al. (2014) is only partially congruent with the morphological groups assigned by Onderstall (1984) and Jacobsen (1992). The focal species of the present study, *Afroedura pondolia,* was found to be distantly related to the remainder of Jacobsen's (1992) *A. pondolia* complex from the northern Drakensberg in the Limpopo, Mpumalanga and northern KwaZulu-Natal provinces, which was subsequently renamed the *"marleyi"* group (Jacobsen et al., 2014). Molecular research by both Jacobsen et al. (2014) and Makhubo et al. (2015) retrieved strong support for *Afroedura pondolia* as part of the "*nivaria"* group (an extensive clade of species from the Eastern Cape, Free State and

KwaZulu-Natal provinces) and as the sister species to *A. nivaria*. Furthermore, Jacobsen et al. (2014) described nine new species from the northern Drakensberg region while Makhubo et al. (2015) revealed several potential cryptic species within the "*nivaria*" group among specimens formerly identified as *A. amatolica*, *A. halli* and *A. nivaria*.

The Pondo flat gecko, *Afroedura pondolia*, occurs along the coast and interior of the eastern portions of the Eastern Cape Province into the central portions of the KwaZulu-Natal Province of South Africa, and has a large distribution in comparison to its congeners (Bates et al., 2014; Branch, 1998; Tolley et al. 2019). The latter region forms part of the greater Maputaland-Pondoland-Albany (MPA) biodiversity hotspot along the east coast of southern Africa, below the Great Escarpment, where the herpetofauna exhibits the highest vertebrate endemism (Perera et al., 2011). *Afroedura pondolia* favors forested habitat where it typically occurs on trees and rocky outcrops and also frequents human dwellings (Bates et al., 2014; Branch, 1998).

Along South Africa's east coast there are two main forest types, the fragmented ancient Afrotemperate forests in the interior and the more continuous younger Indian Ocean Coastal Belt (IOCB) forests along the coast (Mucina et al., 2006; Mucina and Geldenhuys, 2006). Paleoclimatic and geomorphological changes have caused numerous contractions and expansions of forest habitat in this region (Eeley et al., 1999; Mucina et al., 2006; Mucina and Geldenhuys, 2006; Neumann and Bamford, 2015). Past expansion and contraction of these forests and the formation of dispersal barriers, caused by landscape and climatic change, may have affected gene flow and facilitated diversification of forest-associated species along the east coast of South Africa. Several recent surveys of the fauna of these forests have revealed novel species in a diversity of faunal groups (Barnes and Daniels, 2019; Daniels, 2017; Daniels et al., 2017; Tolley et al., 2018).

The late Miocene to early Pliocene was a period characterized by marked changes in geological (Thomas and Shaw, 1993; Partridge and Maud, 2000) and climatic conditions (Van Zinderen Bakker and Mercer, 1986; Coetzee 1993; Tyson and Partridge, 2000) that would have led to habitat fragmentation, isolation and subsequent cladogenesis in habitat specialists like *A. pondolia*. Uplift throughout the late Tertiary contributed to the formation of South Africa's great escarpment (Clark et al., 2011). Coupled with continuous erosion, uplift may have provided possible vicariance opportunities for taxa associated with the escarpment and adjacent regions (Clark et al., 2011; Thomas and Shaw, 1993; Partridge and Maud, 2000).

Warmer and moister conditions prior to the late Miocene maintained widespread forests in southern Africa (Coetzee, 1986; Scott et al., 1997). However, the onset of the late Miocene global cooling resulted in widespread aridification and the contraction of mesic habitats such as forests (Sepulchre et al., 2006). The warm Aghulhas current along the east coast of South

Africa in conjunction with the Great Escarpment created a rain shadow effect, which maintained a subtropical climate along the eastern slopes of the escarpment, while isolating the interior plateau and contributing to its aridification (Neumann and Bamford, 2015; Sepulchre et al., 2006). Higher precipitation and the high elevation of the Eastern Escarpment produced many deep valleys that would have allowed forest patches to persist during glacial periods throughout the Plio/Pleistocene. Reduced atmospheric CO_2 caused the spread of savanna and grasslands and a shift from C3- to more C4-dominant vegetation (Bredenkamp et al., 2002; Lee-Thorp et al., 2007), contributing to the contraction and fragmentation of forested habitats and the subsequent isolation of forest-dwelling taxa.

The most northern forests in the MPA biodiversity hotspot likely acted as refugia (Eeley et al., 1999; Mazus, 2000; Lawes et al., 2007), while the contraction of forests in the Pleistocene caused localized extinctions or contraction of forest-dwelling taxa to refugial areas (Eeley et al., 1999; Lawes et al., 2007; Tolley et al., 2018). Throughout its distribution *A. pondolia* is recorded from coastal and scarp forests along the Indian Ocean Coastal belt (IOCB). Most of the northern IOCB (Maputaland) was, however, inundated until about 10 million years ago, and coastal forests expanded down the coast only about 8000 years ago during the Holocene, suggesting that this region was only recently colonized by forest dwelling-species (Mucina et al., 2006).

Due to the morphologically conservative nature of the genus, we used an integrative systematic approach by combining molecular and morphological analyses to answer three questions, one, how many cryptic lineages are present within *Afroedura pondolia*? Two, are there fixed morphological differences between the cryptic lineages? And three, to what extent does cladogenesis among these lineages coincide with forest habitat fragmentation due to past climatic ameliorations? The following two hypotheses are advanced, first, the long branch length in the phylogeny by Makhubo et al. (2015) between the *A. pondolia* sample from Mkambati and the remaining localities in the Eastern Cape Province would suggest that this locality is genetically isolated and therefore representative of a cryptic lineage. Following the general lineage concept, which identifies species as separately evolving metapopulation lineages that are recognizable using secondary criteria (de Queiroz, 1998), the sampling of additional localities throughout the distribution of the species in the Eastern Cape and KwaZulu-Natal provinces is likely to uncover additional cryptic species within *A. pondolia,* particularly from the most northern scarp forests in the MPA biodiversity hotspot. Second, divergence-time estimations will reveal that cladogenesis can be closely linked to forest fragmentation at the onset of the late Miocene and throughout the Plio/Pleistocene. The results of the present study may have further implications for the conservation status of *Afroedura pondolia* and emphasize the importance of documenting biodiversity patterning in the Maputaland-Pondoland-Albany biodiversity hotspot.

2.2 Materials and Methods

2.2.1 Sample collection

Specimens were hand collected from rock crevices on outcrops, crevices in tree trunks, under the bark of trees or human dwellings in forested regions of the Eastern Cape and the KwaZulu-Natal provinces of South Africa, yielding a total of 97 *A. pondolia* tissue samples, including 60 whole voucher specimens, and two *A. nivaria* to be employed as an outgroup in the phylogenetic analyses (Table 2.1; Fig. 2.1; Appendix 2.1). Where possible, five specimens per locality were collected, since Morando et al. (2003) demonstrated that five samples per locality were sufficient to detect population genetic structuring. However, due to permit restrictions, a maximum of three vouchers specimens per locality (two specimens in protected areas) were permitted to be collected in the KwaZulu-Natal Province. Tissue samples were obtained by removing the last 5 mm of the tail from live animals. In several instances, however, whole tails were collected due to tail autotomy. Tail tissue was preserved in absolute ethanol for molecular work. Live voucher specimens were humanely euthanized by injection with a tricaine methanesulfonate solution (Conroy et al., 2009), followed by a liver tissue biopsy and storage in absolute ethanol for further genetic analysis. The carcasses were either preserved in 70% ethanol or injected with 4% formalin and immersed in formalin solution for a week prior to being transferred to 50% isopropanol for permanent storage in the herpetological collection of the Port Elizabeth Museum (PEM), Eastern Cape Province, South Africa. Ethical clearance for the present study was obtained from Port Elizabeth Museum (Bayworld) ethics committee (Ethical Clearance no. 2017-2).
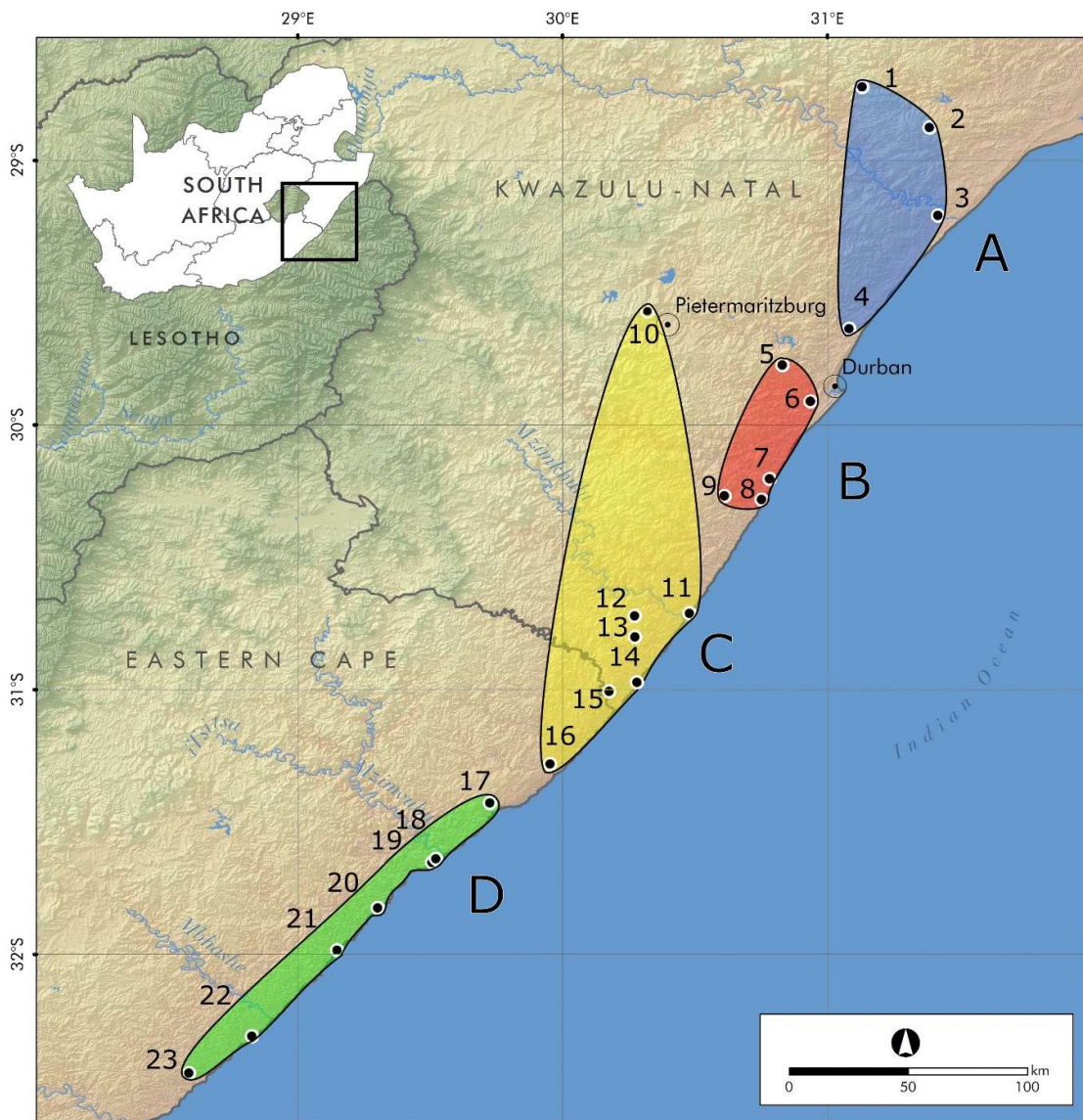
Figure 2.1. Map showing the sample localities where the Pondo flat gecko, *Afroedura pondolia,* was collected in the Eastern Cape and KwaZulu-Natal provinces of South Africa during the present study. Numbers on the map (1–23) correspond to the sample locality names in Table 2.1. Colored polygons and letters correspond to the four candidate species retrieved in the phylogenetic analysis (Fig. 2.2).

Table 2. 1. Localities where *Afroedura pondolia* specimens were sampled in the Eastern Cape and KwaZulu-Natal provinces of South Africa during the present study. The locality number (#) corresponds to the number on the map in Fig. 2.1. *N* = the number of specimens per locality.

#	Locality Name	Province	*N*	Longitude E	Latitude S
1	Nkandla Forest	KwaZulu-Natal	6	31.1320	-28.7224
2	Entumeni NR	KwaZulu-Natal	1	31.3858	-28.8765
3	Harold Johnson NR	KwaZulu-Natal	1	31.4186	-29.2085
4	Mount Moreland	KwaZulu-Natal	6	31.0831	-29.6359
5	Krantzkloof NR	KwaZulu-Natal	5	30.8307	-29.7730
6	Kenneth Stainbank NR	KwaZulu-Natal	1	30.9372	-29.9102
7	Umkomaas	KwaZulu-Natal	1	30.7827	-30.2031
8	Scotburgh	KwaZulu-Natal	1	30.7520	-30.2818
9	Vernon Crookes NR	KwaZulu-Natal	7	30.6120	-30.2681
10	Queen Elizabeth Park NR	KwaZulu-Natal	5	30.3219	-29.5713
11	Umtentweni	KwaZulu-Natal	1	30.4796	-30.7115
12	Oribi Gorge NR	KwaZulu-Natal	7	30.2731	-30.7214
13	Mbumbazi NR	KwaZulu-Natal	7	30.2746	-30.8010
14	Mpenjati NR	KwaZulu-Natal	7	30.2816	-30.9720
15	Umtamvuna NR	KwaZulu-Natal	5	30.1768	-31.0068
16	Mkambati NR	Eastern Cape	9	29.9541	-31.2815
17	Mbotyi	Eastern Cape	2	29.7261	-31.4280
18	Port St. Johns	Eastern Cape	1	29.5228	-31.6397
19	Silaka NR	Eastern Cape	3	29.5087	-31.6534
20	Hluleka NR	Eastern Cape	7	29.3028	-31.8246
21	Coffee Bay	Eastern Cape	5	29.1493	-31.9848
22	Dwesa NR	Eastern Cape	4	28.8274	-32.3096
23	Manubi Forest	Eastern Cape	5	28.5894	-32.4491

2.2.2 DNA sequencing

Total genomic DNA was extracted from either liver or tail tissue using a MacheryNagel DNA extraction kit, following the manufacturer's extraction protocol. Following extraction, DNA was stored at -20°C until required for the polymerase chain reaction (PCR). Two mitochondrial (mt) and two nuclear (nu) DNA markers were sequenced. For the two mtDNA loci all individuals (N = 97) were amplified and sequenced. However, for the two nuDNA loci a single sample per locality was sequenced (N = 23) since preliminary results revealed low intrapopulation variation for the two nuDNA markers. The two mtDNA markers selected were nicotinamide adenine dinucleotide dehydrogenase subunit 4 (*ND4*) and cytochrome b (*cyt b*). The primer pairs ND4 (5'-ACC TAT GAC TAC CAA AAG CTC ATG TAG-3') (Arévalo et al., 1994) and H12763V (5'-TTC TAT CAC TTG GAT TTG CAC CA-3') (Barlow et al., 2013) were used to amplify the *ND4* locus, while for the *cyt b* region the primer pairs used were WWF (5'-AAA YCA YCG TTG TWA TTC AAC TAC-3') and R2 (5'- GGG TGR AAK GGR ATT TTA TC-3') (Whiting et al., 2003). The latter two mtDNA loci are widely used in reptile phylogeograpic studies (Blair and Bryson, 2017; Díaz et al., 2017; Makhubo et al., 2015; Medina et al., 2016; Portillo et al., 2018; Vidal et al., 2008). The prolactin receptor (*PRLR*) and the recombination activating gene 1 (*RAG1*) were targeted as nuDNA sequence markers since they exhibit variation at the intraspecific levels and have been used extensively in the literature (Busschau et al., 2017; Diedericks and Daniels, 2013; Heinicke et al., 2017a,b; Medina et al., 2016). For *PRLR* the primers used were PRLR_f1 (5'-GAC ARY GAR GAC CAG CAA CTR ATG CC -3') and PRLR_r3 (5'-GAC YTT GTG RAC TTC YAC RTA ATC CAT -3') (Townsend et al., 2008) and primers L2408 (5'-TGC ACT GTG ACA TTG GCA A-3') and H2920 (5'-GCC ATT CAT TTT YCG AA-3') (Vidal and Hedges, 2004) were used to amplify the *RAG1* marker. For each PCR, a 25-µL reaction was performed that contained 14.9 µL of Millipore water, 3 µL of 25 mM MgCl$_2$, 2.5 µL of 10× Mg^{2+} free buffer, 0.5 µL of a 10 mM dNTP solution and 0.5 µL of the primer sets at 10 mM, 0.1 unit of *Taq* polymerase and 1–3 µL of template DNA. The PCR temperature regime for the two mt DNA markers was 94 °C for 4 min., 94 °C for 30 sec., 50 °C for 40 sec.,72 °C for 40 sec., and then 36-40 cycles of the last three steps, followed by a final extension of 10 min., at 72 °C. For the two nuDNA markers the temperature regime was 95 °C for 2 min., 95 °C for 35 sec., 48 °C for 35 sec., 72 °C for 60 sec., and then 36–40 cycles of the last three steps, followed by a final extension of 10 min., at 72 °C. The annealing temperature was optimized for each primer pair and ranged between 46°C and 50°C. PCR products were electrophoresed for 2–3 hours at 90V in a 1% regular agarose gel containing ethidium bromide, visualized under UV light and purified using a BIOFLUX gel purification kit. Purified PCR products were cycle sequenced using standard protocols (3 µL of the purified PCR product, 4 µL of the fluorescent-dye terminators with an ABI PRISM Dye Terminator Cycle Sequencing Reaction Kit, PerkinElmer, and 3 µL of a 10 µM primer solution for each

primer pair). Unincorporated dideoxynucleotides were removed by gel filtration using Sephadex G-25 (Sigma). Sequencing was performed on an ABI 3730 XL automated machine housed at the central analytical facility of Stellenbosch University.

2.2.3 Phylogenetic analyses

Sequences were aligned manually and checked for base ambiguity in Sequence Navigator (Applied Biosystems). Sequences were checked for the presence of stop codons using MEGA X (Kumar et al., 2018). Two species, *A. nivaria* and *A. tembulica* were used as outgroups. For the outgroups two *A. nivaria* specimens were sequenced for all markers and a single *A. tembulica ND4* locus was included from GenBank data (Makhuba et al., 2015) and aligned with the sequences generated during the present study; the remaining loci for this species were coded as absent. The phylogenetic analyses were performed on the concatenated *cyt b* and *ND4* mtDNA dataset and included all samples. A single sequence per locality for each nuDNA and mtDNA marker was used for the total-evidence topology. Maximum likelihood (ML) and Bayesian inference (BI) were used to infer phylogenetic relationships for the ingroup. jModeltest v2.1.10 (Posada, 2008) was used to identify the best-fitting substitution models for each of the individual marker datasets under the corrected Akaike information criterion (see Appendix 2.2 for substitution models used in each analysis). DAMBE v5 (Xia, 2013) was used to assess saturation and each dataset subsequently partitioned per gene. Bayesian inference (BI) was performed in MrBayes v3.2.2 (Ronquist et al., 2012), via the Cipres Science Gateway v3.3 available from http://www.phylo.org. For each analysis, four Markov chains were run, starting from a random tree and run for 20 x 10^6 generations, sampling each chain every 1000th tree. A 50% majority-rule tree was constructed with 20% of the sampled trees discarded as burn-in, and nodes with ≥0.95 posterior probability were considered supported. A partitioned maximum likelihood (ML) analysis was run in Garli v2.01 (Zwickl, 2006) on the Cipres Science Gateway with 1000 bootstrap replicates. A 50% majority rule bootstrap consensus tree was calculated in PAUP* v4.0a (Swofford, 2002). Bootstrap values ≥75% were regarded as well-supported. Sequence divergence values of each marker between observed clades were calculated in MEGA X.

2.2.4 Divergence-time estimates

Bayesian Evolutionary Analysis Sampling Trees (BEAST) v2.4.8 (Bouckaert et al. 2014) was used on the combined mitochondrial dataset to determine when cladogenic events occurred within *A. pondolia*. The mitochondrial dataset was chosen for the divergence-time estimation because of the larger sample size and known substitution rates for mitochondrial *cyt b* marker in squamate reptiles and specifically for geckos where it appears consistent in producing relatively accurate divergence estimates (e.g. Carranza and Arnold, 2012; Hawlitschek et al.,

2017; Šmíd et al., 2017). A substitution rate of 2.28% per million years for the *cyt b* locus was used in the dating analysis for *A. pondolia*, (0.0228 ± 0.00806: Carranza and Arnold, 2012). These calibrations were implemented in the Bayesian Evolutionary Analysis Utility (BEAUti) and executed in BEAST with a Yule prior, a relaxed uncorrelated molecular clock with a lognormal distribution on the *cyt b* locus and a strict clock for the *ND4* locus estimated from the *cyt b* clock rate. A Markov Chain Monte Carlo was run for 20 million generations, sampling every 1000th generation. Tracer v1.6 (Rambaut et al. 2014) was used to assess the chain convergence (ESS > 200) and TreeAnnotator, included in the BEAST package, was used to discard 20% of the sampled trees as burn-in and to determine the maximum clade credible tree. Trees were viewed and edited in FigTree (Rambaut, 2016) and TreeGraph2 (Stöver and Müller, 2010) and additional annotations made in Inkscape (www.inkscape.org).

2.2.5 Population genetic analyses

To examine genetic relationships between sample localities, haplotype networks were constructed in TCS 1.21 (Clement et al., 2000), using statistical parsimony with 95% for the *cyt b* locus since this was the fastest evolving marker. Hierarchical analysis of molecular variance (AMOVA) was performed on the total *cyt b* data as well as for each of the four candidate species observed during the preliminary phylogenetic analyses, using Arlequin v3.1 (Excoffier et al., 2005) to investigate the distribution of genetic variation among candidate species as well as among localities within candidate species.

2.2.6 Species delimitation

Analyses were employed on a single-locus mitochondrial dataset as well as the total-evidence dataset of all four loci to assess the validity of candidate species identified in the phylogenetic analyses. As the current study's focus is on *A. pondolia* and the analyses developed for single-locus datasets are threshold based (automatic barcode gap discovery (ABGD), Bayesian implementation of the generalized mixed Yule coalescent (bGMYC) and Poisson Tree Processes (PTP)), the inclusion of a greater number of taxa could possibly provide a more accurate estimation of putative species within the focal taxon and help to overcome some of the limitations in these methods (Ahrens et al., 2016). Only the mitochondrial *ND4* locus in present study aligns with the *Afroedura* sequences available on Genbank. Therefore, the *ND4* dataset which included sequences of all available *Afroedura* species was used in the single-locus species delimitation analyses (See Appendix 1 for sequences used in the analyses). This dataset largely comprised sequences of species within the *A. nivaria* complex that were generated by Makhubo et al. (2015). For species delimitation using the bGMYC and PTP models, the dataset was pruned to include only unique sequences, which removes zero branch lengths from the resulting gene trees. A single-gene phylogeny was estimated for the *ND4* mtDNA dataset by Bayesian Inference in BEAST (20 x 10^6 generations, sampling every

1000th generation). BEAST log files were examined in Tracer v1.6 to assess convergence (ESS > 200). A maximum clade credibility tree was estimated via TreeAnnotator v1.8.1 after discarding the first 20% as burn-in. Trees were viewed and converted to Newick format in TreeGraph2. In order to distinguish between cryptic species, molecular species delimitation tools were employed that do not require *a priori* assignment of specimens to groups or assumptions about relationships among specimens.

The automatic barcode gap discovery (ABGD) was performed via the ABGD web interface (http://wwwabi.snv.jussieu.fr/public/abgd/, web version 'October 25 2018'). ABGD is designed to infer species hypotheses based on automatized identification of a barcode gap between inter- and intraspecific pairwise distances. The method only requires a single locus alignment from which pairwise distances are computed either as simple p-distances, or as substitution-corrected distances via either JC69 (Jukes and Cantor, 1969) or K2P (Kimura, 1980) models. Simple p-distance metrics were selected, as this consistently produced more conservative species estimates. Default priors were used for minimum barcode gap width prior (1.5) and intraspecific divergence minima (0.001) and maxima (0.1).

Bayesian general mixed Yule-coalescent model (bGMYC) was implemented in R Studio Version 1.1.456 using the package bGMYC v. 1.0.2 (Reid and Carstens, 2012; R Core Team 2014). The traditional GMYC model aims to identify a time in a calibrated tree when the branching rate shifts from a Yule to a coalescent process. This method defines sets of species hypotheses to distinguish coalescent events from speciation events and searches for a single maximum likelihood model of species hypotheses that correspond to the phylogenetic species concept. The Bayesian implementation of the GMYC model provides flexible prior distributions and accounts for error in phylogenetic estimation and uncertainty in the model parameters by integrating uncertainty in tree topology and branch lengths in the parameters of the model via MCMC. bGMYC was applied to 500 posterior trees from the *ND4* BEAST runs, implementing 50,000 MCMC steps with 40,000 steps as burn-in and sampling every 100 steps.

The *ND4* gene-tree was also analyzed using the Poisson Tree Processes (PTP) model via the bPTP server (http://species.h-its.org/ptp/; Zhang et al., 2013) using the heuristic maximum likelihood and Bayesian implementations of the PTP algorithm. Like GMYC, the PTP model also aims to differentiate speciation processes among species from diversification processes within species but, differently from the GMYC model, examines numbers of substitutions between nodes instead of time. The algorithm heuristically infers species delimitations by searching for a delimitation pattern that maximizes likelihood of a mixed model describing speciation and diversification processes as two independent Poisson process classes. Default priors were used for this analysis as changing priors in the initial analyses did not affect delimitation results.

Species tree-estimation and species delimitation analysis was performed in Species Tree and Classification Estimation, Yarely - STACEY v.1.2.1 (Jones, 2017), in BEAST2, from all four loci (*cyt b, ND4, RAG1* and *PRLR*) with one representative sample from each locality where *A. pondolia* was sampled during the present study (*N*=23). In STACEY the possible number of putative species ranges from one to the number of minimal clusters specified. In this analysis each locality was defined as a taxon set or minimal cluster, i.e. without *a priori* species definition. The input files (.xml) were created using BEAUti, implementing a Yule Model prior to estimate the species tree [priors: Collapse Height=0.001, Collapse Weight=0.5 using a beta prior (1.1) around [0.1], bdcGrowthRate = log normal (M=4.6, S=1.5); popPriorScale = log normal(M=-7, S=2); relativeDeathRate = beta (alpha=1.0, beta=1.0)] and an uncorrelated Lognormal Model to describe the relaxed molecular clock. For the species delimitation analysis, we used equal ploidy settings for nuclear and mitochondrial loci to avoid overestimating the number of putative species. Equal ploidy settings for all loci represents a more robust approach by avoiding disproportionate influence of mitochondrial partial sequence data (Vitecek et al., 2017). The MCMC analysis was run for 100 million generations, saving the result every 10,000 generations. The obtained log files were analyzed with Tracer to verify convergence (ESS > 200) of the analysis and SpeciesDelimitationAnalyser (Jones et al., 2015) was used to process the log files and to examine the clusters of species assignments. Posterior probabilities of localities belonging in the same cluster were visualized in a similarity matrix constructed in R Studio Version 1.1.456. A second analysis was performed in STACEY where the clusters visualized in the similarity matrix were defined as minimal clusters.

2.2.7 Morphological analyses

A total of 59 sequenced *A. pondolia* specimens were adult and examined in the morphological analyses (See Appendix 2.1 for a list of specimens). Specimens were considered adults and regarded as sexually mature when they exhibited a snout to vent length (SVL) > 38 mm, (following Makhubo et al., 2015). Phenotypic variables included 28 morphometric measurements, measured with a digital caliper to an accuracy of 0.01 mm, and 10 meristic counts known to be taxonomically informative among gecko species (Jacobsen et al., 2014; Laver et al., 2018; Makhubo et al., 2015) (See Appendix 2.3 for a list of variables). All statistical analyses were performed in SPSS v25.0 (IBM Corp.). For the multivariate analyses the dataset was subdivided according to the four candidate species (A: *N* = 7; B: *N* = 9; C: *N* = 18; D: *N* = 25) to test whether they could be differentiated based on their morphology. All variables were log transformed to normalize the data. Sexual dimorphism was tested for using a multivariate analysis of covariance (MANCOVA) with sex as a fixed factor and log-SVL as a covariate. Sexually dimorphic characters were then removed from the analysis.

Differences in the morphometric measurements between species were tested using a MANCOVA on the log-transformed dataset, with species as a fixed factor and log-SVL as a covariate. Sets of morphometric variables that contribute to the overall morphological variation were then identified through a principal component analysis (PCA). To account for body size in the PCA, variables were regressed with log-SVL as a covariate and the unstandardized residuals were saved and used as input data. Only principal components with eigenvalues larger than 1.0 were considered. The number of variables with high loading on each principal component were minimized by using the varimax rotation with Kaiser Normalization. The saved principal component scores were used in an analysis of variance (ANOVA) to examine the differences between candidate species. For the post-hoc tests the Bonferroni correction was applied. The Bonferroni correction is more conservative in comparison to other post hoc-tests as it adjusts the significance levels for multiple tests, minimizing the possibility of Type I errors (Rice, 1989). Differences in meristic scale counts among the four candidate species were tested with a MANOVA, followed by univariate ANOVAs on each variable and the Bonferroni post-hoc test for the pairwise comparisons between candidate species.

Discriminant function analyses (DFA) were used to determine whether individuals could be assigned to the correct species based on the morphometric and meristic characters. For the morphometric characters, as with the PCA, the unstandardized residuals of the variables regressed against log-SVL were used as input data. For the meristic characters the log transformed characters were used as input data.

2.3 Results

2.3.1 Mitochondrial DNA tree topology and divergence-time estimation

The mtDNA dataset comprised 97 *A. pondolia* specimens and consisted of 1271 base pairs (bp), containing 609bp for *cyt b* and 662bp for *ND4*, and 486 variable sites across the entire alignment (See Appendix 2.1 for GenBank accession numbers). The concatenated mtDNA maximum likelihood (ML), Bayesian inference (BI) and BEAST analyses recovered congruent topologies; hence, only the BEAST topology is shown (Fig. 2.2). *Afroedura pondolia* was monophyletic and comprised four geographically discrete, statistically well-supported clades (A, B, C and D) (BI >0.95 Pp /BEAST >0.95 Pp /ML >75%). The four clades represent candidate species with levels of sequence divergence comparable to those observed between other species in the *A. nivaria* species complex (Figs. 2; Makhubo et al., 2015). The uncorrected 'p-distance' among the four species ranges between 12–19% for *cyt b* and between 10–17% for *ND4*. The within-species sequence divergences ranged from a minimum to a maximum of 2–7% and 1– 5% for the *cyt b* and *ND4* loci, respectively.

Species A was confined to the forest belt in the northeast of the KwaZulu-Natal Province coast and interior, where specimens inhabited scarp forest (Nkandla and Entumeni), and northern coastal forests (Harold Johnson and Mt. Moreland). Species B was confined to a narrow coastal forest strip of the KwaZulu-Natal Province, which is predominantly scarp forest (Vernon Crookes and Krantzkloof) and coastal forest (Umkomaas, Scotburgh and Stainbank), while Species C was present from the interior of the KwaZulu-Natal Province along the coastal belt into the Eastern Cape Province. Species C occupied both coastal forest and scarp forests, but only scarp forest is present at Mkambati and Queen Elizabeth Park. Species D was confined to the coastal belt of the Eastern Cape Province (including the type locality for *A. pondolia* at Mbotyi), which is dominated by scarp forest.

The divergence-time estimates from the BEAST analysis suggest the earliest divergence between the four *A. pondolia* species dates back to the late Miocene 8.6 Million years ago (95% HPD, 10.1 - 7.2 Mya), when species D diverged from the remaining three species. Subsequent diversification occurred in the early Pliocene when species A diverged 4.7 Mya (95% HPD, 5.5 - 3.97 Mya) and then species B and C, 4.2 Mya (95% HPD, 4.9 - 3.5 Mya). Basal divergence-time estimates within species A was 3.6 Mya (95% HPD, 4.3 - 2.9 Mya), in species B 1.7 Mya (95% HPD, 2.2 - 1.3 Mya), in species C 1.2 Mya (95% HPD, 1.5 – 0.93 Mya) and in species D 2.9 Mya (95% HPD, 2.4 – 3.5 Mya).
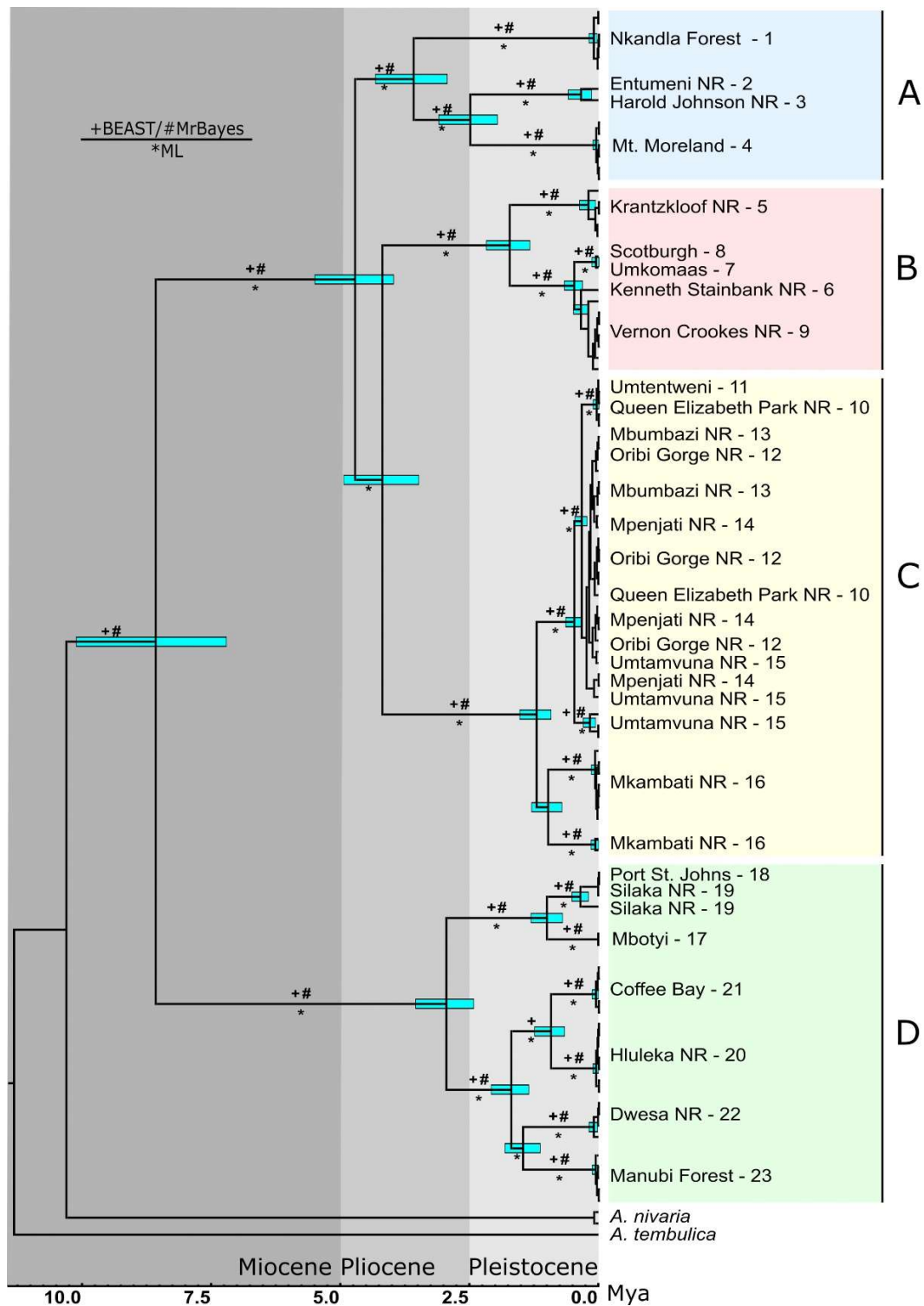
Figure 2.2. Bayesian phylogeny derived from the mtDNA loci, *cyt b + ND4,* together with the divergence-time estimation below the tree topology. Symbols represent support for maximum likelihood bootstrap > 75% (*) and posterior probabilities >0.95 from the BEAST (+) and MrBayes (#) analyses. Node bars show 95% highest posterior distributions for each estimated divergence date. Colored shading and letters denote the candidate species referenced throughout the present study. Numbers next to locality names correspond to the locality numbers on the map in Fig. 2.1.

2.3.2 Total DNA evidence tree topology

The total DNA evidence dataset consisted of 2233bp, the two mtDNA loci plus 481bp for the *RAG1* and 481bp for the *PRLR* with six and 33 variable positions, respectively (See Appendix 2.1 for GenBank accession numbers). The concatenated ML and BI analyses as well as the STACEY minimum cluster tree retrieved congruent topologies (Fig. 2.3). The relationships between sampling localities were congruent to those retrieved in the mtDNA topology (Fig. 2.2). The monophyly of *A. pondolia* was again well-supported and the identical four clades evident in the mtDNA topology were retrieved with varying nodal support. The uncorrected 'p-distance' for the nuclear markers between the candidate species ranged between 1.3–2.2% for the *PRLR* locus to < 0.4% for the *RAG1* locus. The within-clade sequence divergences were < 1% for *PRLR* and < 0.3% for *RAG1*.

Single-locus nuDNA tree topologies were largely unresolved (Appendix 2.4). The *RAG1* topology recovered one statistically supported clade comprising localities within species C but excluding Mkambati Nature Reserve. The *PRLR* topology retrieved species D as monophyletic comprising two statistically supported clades (BI >0.95 Pp / ML >75%). The *PRLR* topology also retrieved well-supported monophyly between three localities from species A and two localities from species C.
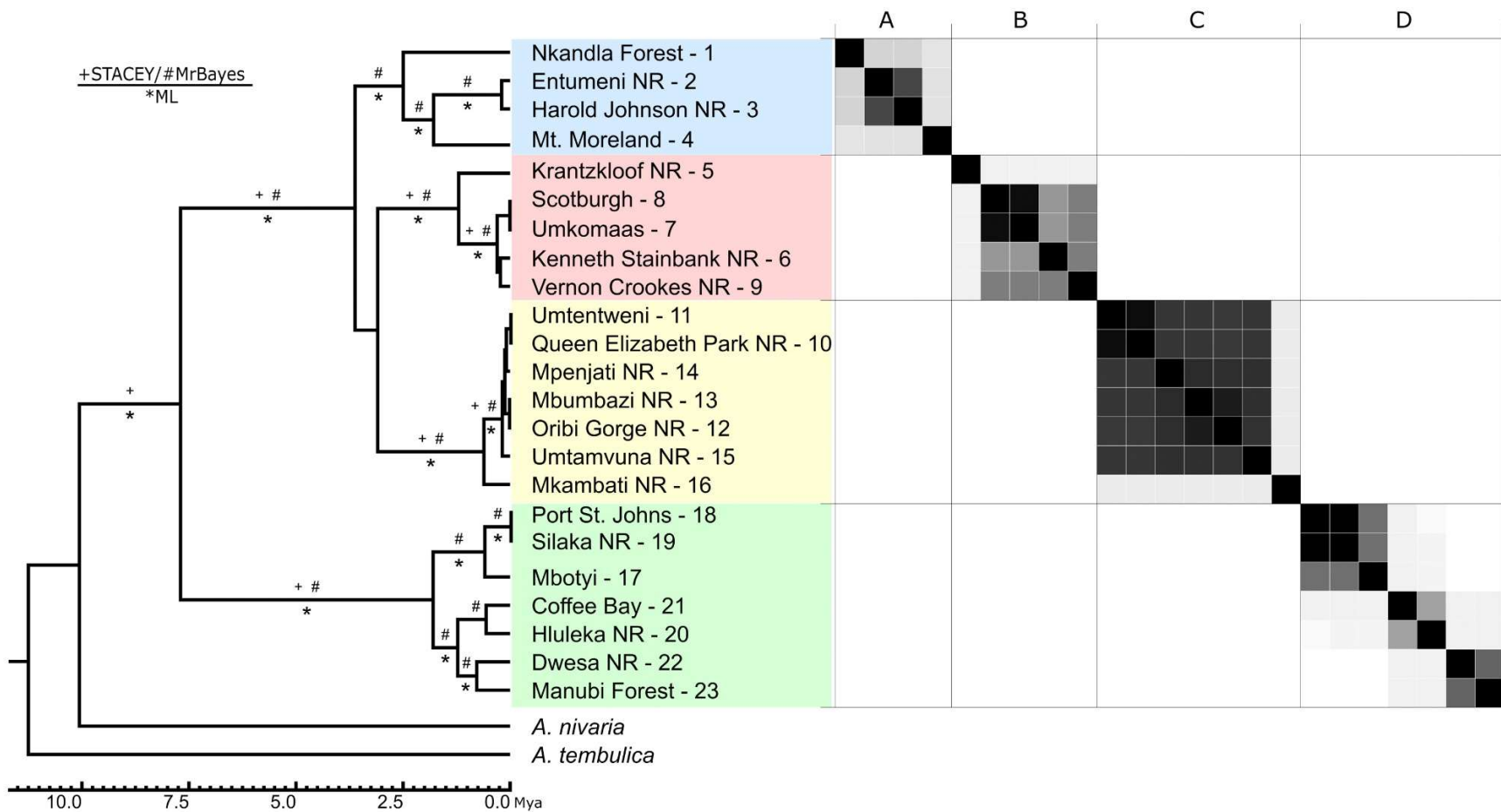
Figure 2.3. STACEY maximum clade credibility minimum cluster tree from the total-evidence dataset comprising four DNA loci (*cyt b, ND4, RAG1* and *PRLR*) with symbols representing posterior probabilities from STACEY (+) and MrBayes (#) analyses >0.95 and maximum likelihood (*) bootstrap values >75%. The squares in the similarity matrix represent posterior probabilities (white =0, black= 1) for pairs of individuals (localities) to belong to the same cluster. The lines in the matrix separate candidate species (named above matrix). Numbers next to locality names correspond to the locality numbers on the map in Fig. 2.1.

22

2.3.3 Population genetic analyses

From the 95 *cyt b* sequences (two samples from Krantzkloof failed to amplify, see Appendix 2.1) 44 haplotypes were retrieved in 17 haploclades using the 95% connection limit (Fig. 2.4). Species A comprised five haplotypes from four localities. In species B there are nine haplotypes, while in species C there are 20 haplotypes characterized by a large number of unsampled or missing haplotypes. Within species C there are several shared haplotypes, indicative of gene flow between localities. Species D comprised ten haplotypes.

The AMOVA results over all sample localities indicated marked genetic structure with 66.6% of the variation occurring among candidate species, 29.9% of the variation among localities within candidate species and 3.6% variation within localities (Table 2.2). Species A has the highest variation among sample localities (Va) followed by species D, B and C, respectively. Therefore, species C has the highest variation within sample localities (Vb) followed by species B, D and A respectively (Table 2.2). All fixation indices from the hierarchical analysis were high and statistically supported, indicating a high degree of genetic structuring. Apart from the localities in Clade C where there are shared haplotypes, the pairwise F_{ST} values between sample localities are generally high and statistically supported for comparisons where there are more than one sequence per locality (Appendix 2.5). High pairwise F_{ST} values and unconnected haplotypes among localities within candidate species suggest the presence of additional cryptic lineages (Fig 2.4; Appendix 2.5).

Table 2.2. Hierarchical AMOVA over all sample localities and among the four species detected in *Afroedura pondolia* based on the *cyt b* locus. All values are statistically significant ($p < 0.001$).

Source of variation	Variation	Variation (%)	Fixation index[a]
Among species	Va 29.2050	66.56	F_{CT} 0.6656
Among localities	Vb 13.1184	29.90	F_{SC} 0.8939
Within localities	Vc 1.5567	3.55	F_{ST} 0.9645

AMOVA on the four candidate species detected in *Afroedura pondolia.*

Species	Source of variation	Variation	Variation (%)	Fixation index
A	Among localities	Va 30.50383	99.13	F_{ST} 0.9913
	Within localities	Vb 0.2667	0.87	
B	Among localities	Va 9.2672	87.52	F_{ST} 0.8752
	Within localities	Vb 1.3214	12.48	
C	Among localities	Va 5.88231	69.76	F_{ST} 0.6976
	Within localities	Vb 2.5494	30.24	
D	Among localities	Va 19.07992	96.91	F_{ST} 0.9691
	Within localities	Vb 0.6083	3.09	

a F_{CT} = Va/VT, F_{SC} = Vb/(Vb + Vc), F_{ST} = (Va + Vb)/VT, where VT is the total of the variance components (Va + Vb + Vc).
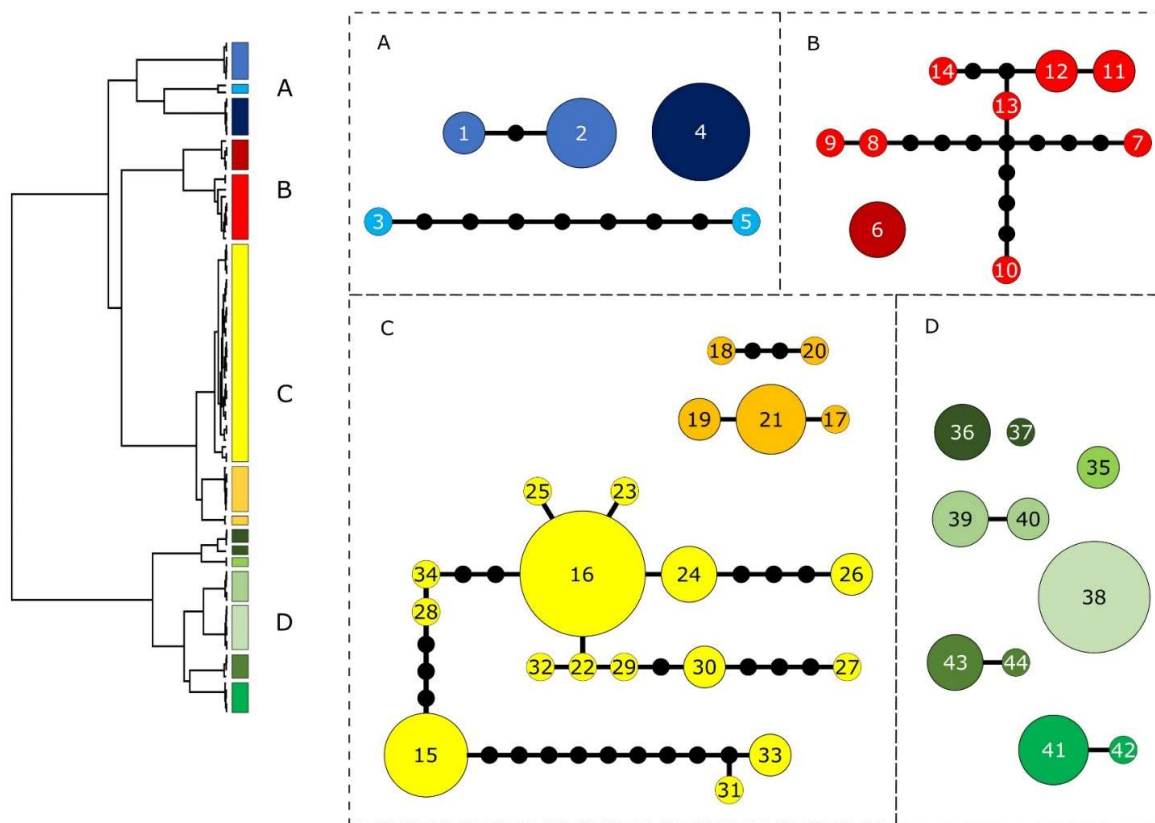
Figure 2.4. A 95% haplotype network based on the mtDNA *cyt b* sequences generated in this study. Colored bars represent the relative position of each cluster on the mtDNA phylogeny. Haplotype numbers correspond to the samples listed in Appendix 2.1.

2.3.4 Species delimitation

Results from the species delimitation methods were largely incongruent. Compared to the candidate species identified in the mtDNA phylogeny, most of the methods designed for single-locus datasets estimated more than four putative species in *A. pondolia*, particularly within candidate species characterized by deep divergence (Fig. 2.5). ABGD recognized two species within *A. pondolia* at an initial partition with intraspecific divergence of p<4%, grouping species A + B + C distinct from species D. This delimitation, however, also groups the highly divergent clades in *A. halli* (A+B) and *A.* cf. *nivaria* (C+D) that were regarded as separate species by Makhubo et al. (2015), suggesting an underestimation of species. At an initial partition with intraspecific divergence of p<2%, ABGD identified eight putative species within *A. pondolia;* three within species A, two within species B and D, and species C was identified as a single species. This delimitation recognizes the separate *A. halli* and *A.* cf. *nivaria* species while also identifying several putative species in the highly divergent *A. karroica*.

To delimit species based on the bGMYC output, a threshold needs to be established at which individuals could be considered conspecific. At a posterior probability of *p*>0.9, the bGMYC

24

identifies three putative species within species A, two in species B and four in species D while species C is recognized as a single species. This delimitation also identifies multiple species within *A. halli, A. karroica* and the *A. nivaria* clades, which could indicate a potential overestimation of putative species. At $p>0.5$, the bGMYC identified a pair of species within species A and recognizes species B, C and D as single species. This delimitation also recognizes the separate *A. halli* clades as putative species but fails to recognize the separate *A.* cf. *nivaria* clades as species.

The maximum likelihood PTP (PTP) and the Bayesian implementation of the PTP model (bPTP) retrieved the highest number of putative species within all taxa and most likely reflects intraspecific structure among the *Afroedura* and not putative species boundaries. 14 groups were identified within *A. pondolia,* three in species A, two in species B, three in species C and six in species D.

When defining localities as minimal clusters, the species delimitation analysis with STACEY retrieved a large number of possible delimitations with low posterior probabilities, ranging from seven to 19 clusters. The delimitation with the highest posterior probability (Pp = 0.044) retrieved 11 clusters. Upon visual inspection of the similarity matrix (Fig. 2.3), there are four broader clusters corresponding to the four candidate species with varying levels of support for pairs of localities belonging to the same cluster. There was absolute statistical support (Pp = 1.00) for four species in *A. pondolia* when defining the four candidate species as minimal clusters.
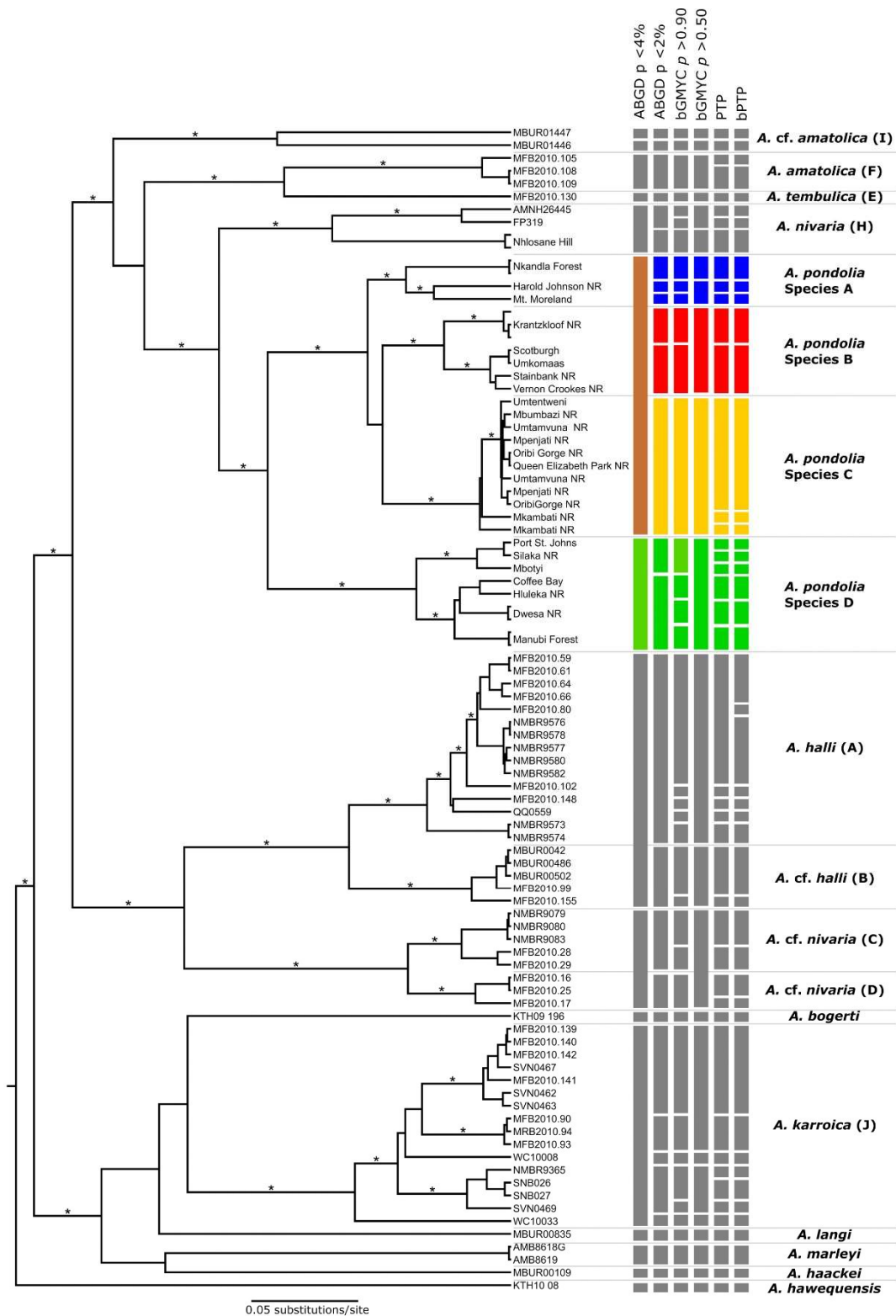
Figure 2.5. Bayesian phylogeny derived from the unique ND4 sequences for all available *Afroedura* species. Asterisks (*) represent posterior probabilities >0.95 from the BEAST analysis. Letters in brackets denote the clades as they were presented in Makhubo et al. (2015). Bars show putative species delimitation based on the various analyses. Colored bars show species delimitation within *Afroedura pondolia.*

2.3.5 Morphological analyses

Significant morphological differences were observed between sexes across all samples (MANCOVA: Wilks' λ 0.327, *P* 0.015). The sexually dimorphic characters included body width (BW), snout-coronoid distance (CT), snout-quadrate distance (QT), ear to eye distance (EE), interorbital distance (IO) and 4th toe width (4TW). Males were larger in all sexually dimorphic variables, except females had wider toes (4TW). These variables were excluded in subsequent analyses. A MANCOVA on the included morphometric data showed that there are significant morphological differences among the four candidate species (Wilks' λ = 0.056, *p* < 0.001). Homogeneity of slopes was accepted (Wilks' λ = 0.254, *p* = 0.829), suggesting that SVL was an appropriate covariate.

The principal component analysis (PCA) extracted five principal components (PCs) with eigen values greater than 1.0 and accounted for 66.1% of the variance across all samples (Table 2.3). From the extracted principal components, all variables were reliable contributors to the analysis (communalities > 0.5) and there was adequate sampling for the dataset (KMO = 0.763). ANOVA's on each principal component showed that there were significant differences between the group means of PC1 (head shape and limb length), PC2 (feet and toe lengths), PC3 (height and eye length), PC4 (carpal and tarsal length, and inversely trunk length) and PC5 (lower arm length and finger width) (Table 2.3, Fig. 2.6). Bonferroni post-hoc tests indicated in PC1 that species A and C had significantly larger heads and limbs than species D. In PC2 species A had significantly longer feet and toes than the other species. In PC3 species B had significantly higher bodies and larger eyes than species C. In PC4 species A had longer carpals and tarsals and a shorter trunk length in relation to SVL than species D. In PC5 species B and C had significantly longer forearms and wider fingers than species D.

For the meristic dataset, the MANOVA showed that there are significant differences among the four candidate species (Wilks' λ = 0.228, *p* < 0.001). The ANOVAs were significant for each variable (*p* < 0.05), except for the number of midbody scale rows and postmental scales (*p* > 0.05). Bonferroni post-hoc tests showed that species A had a significantly higher number of infralabial scales than species D. Species A and C had more scales between the eyes and nostrils than species D. Species D had more finger lamellae and internasal granules than species B and C. Species C had more scales between the eyes and ears than species D, but species D had more toe lamellae. There were no pairwise differences in the number of supralabial scales. There are no fixed/diagnostic meristic differences between the four candidate species, despite the statistical significance of this analysis, as the narrow ranges of these variables show considerable overlap among the four candidate species (see Appendix 2.6).

The DFA on the morphometric characters revealed three discriminant functions (DFs) that account for 56.9%, 28% and 15.1% of the total variance and significantly differentiate the four

candidate species (Wilks' λ = 0.061, $p < 0.001$). 94.9% of individuals were correctly classified from the morphometric characters (species A: 85.7%, B: 88.9%, C: 100%, D: 96%). A three-dimensional scatterplot of the three discriminant functions (Fig. 2.7A) corroborates these results, showing minimal overlap between groups. From the meristic data the DFA revealed three discriminant functions (DFs) that account for 79.6%, 14.9% and 5.4% of the total variance and also significantly differentiate the four species (Wilks' λ = 0.228, $p < 0.001$). However, only 86.4% of individuals were correctly classified based on the meristic characters (species A: 71.4%, B: 77.8%, C: 88.9%, D: 92%). The three-dimensional scatterplot of the discriminant functions from the meristic characters (Fig. 2.7B) shows substantial overlap between groups, but species D appears more separated from the remaining three species.

Table 2.3. Principal components analysis of size-corrected variables for *Afroedura pondolia*, with PC loadings for each variable of the five axes with eigenvalues >1.0. Characters that loaded most strongly for each principal component are in bold (rotated matrix). Percentage variation of each axes and significant ($p < 0.05$) F-values from the ANOVAs are also shown.

Residuals	1	2	3	4	5
Length of lower leg (Tibia)	**0.773**	0.114	-0.045	-0.087	0.040
Lower jaw length (LJL)	**0.766**	0.372	0.263	0.107	0.206
Eye-to-naris distance (EN)	**0.691**	0.079	0.269	0.209	0.255
Head length (HL)	**0.691**	0.405	0.278	0.075	0.195
Femur length (FM)	**0.643**	-0.101	-0.179	0.388	0.109
Internarial distance (IN)	**0.595**	-0.347	0.385	0.324	0.117
Humerus length (HM)	**0.589**	0.239	-0.018	-0.039	-0.544
Head width (HW)	**0.542**	0.423	0.336	0.161	0.210
4th toe length (4TL)	0.125	**0.805**	-0.055	-0.048	0.069
Hand length (Hand)	0.091	**0.763**	0.012	0.320	0.174
4th finger length (4FL)	0.243	**0.699**	0.244	0.167	0.127
Foot length (Foot)	0.512	**0.516**	0.285	0.173	0.346
Head height (HH)	0.110	0.138	**0.802**	0.080	-0.153
Rostral height (RH)	0.114	-0.173	**0.710**	-0.198	0.165
Body height (BH)	0.023	0.227	**0.636**	0.082	0.388
Transverse length of eye (EYE)	0.130	0.227	**0.524**	0.478	-0.114
Axilla to groin distance (Trunk)	-0.161	-0.008	0.070	**-0.725**	-0.072
Carpal length (CP)	-0.101	0.471	0.072	**0.618**	0.006
Tarsal length (TR)	0.304	0.320	0.191	**0.529**	0.315
Length of lower arm (Crus)	0.372	0.193	-0.038	0.060	**0.657**
4th finger width (4FW)	0.231	0.286	0.130	0.082	**0.608**
% Variance	20.258	15.566	12.144	9.485	8.596
F-value	5.526	4.698	3.213	4.848	5.720
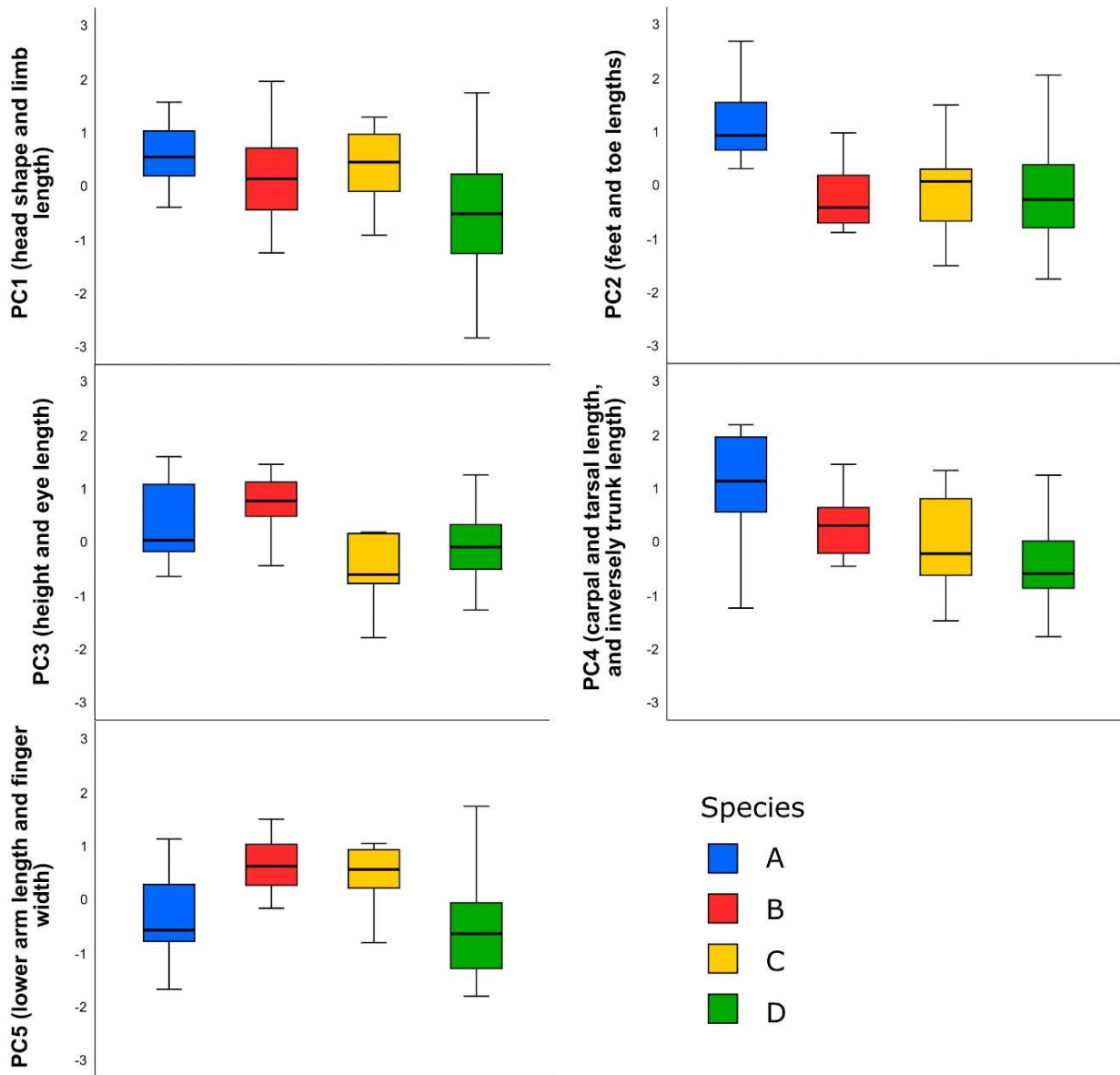
Figure 2.6. Boxplots of the principal component analysis (PCA) of *Afroedura pondolia* where the morphometric variables were assigned to five principal components. All principal components (PCs) were significantly different between candidate species. Axes show variation in PCs among candidate species. Boxes depict median, interquartile range, minimum and maximum values. Colors represent the different species.
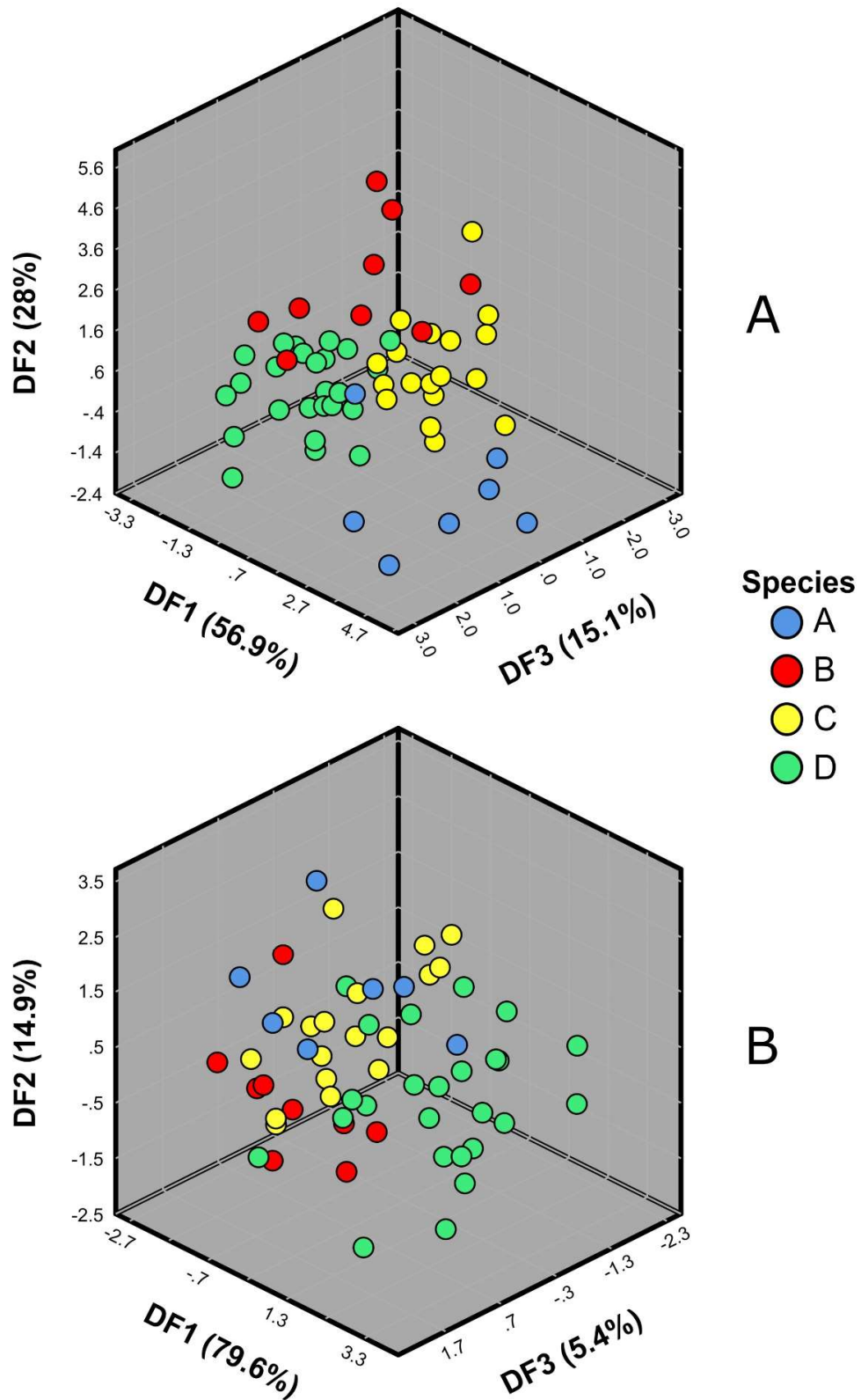
Figure 2.7. Discriminant function analysis (DFA) of the morphometric and meristic characters of *Afroedura pondolia*. Graphs A and B demonstrate morphometric and meristic characters for the three discriminant functions (DFs), respectively.

2.4 Discussion

Our phylogenetic results demonstrate that the forest-dwelling gecko, *Afroedura pondolia,* is a species complex comprising several possible lineages. Our preferred hypothesis is that four cryptic lineages are nested within *A. pondolia*, three of which potentially represent novel as yet undescribed species. These four species can be delineated, to a varying degree, by the phylogenetic analyses, the species delimitation methods and the morphometric analyses, satisfying the general lineage concept. However, it is noteworthy that there are several inconsistencies in the number of putative species retrieved using the various species delimitation platforms, a result that can be attributed to the underlying assumptions of these methods but may also indicate additional cryptic lineages within candidate species.

Divergence-time estimates indicate a late Miocene to early Pliocene cladogenesis within the *A. pondolia* species complex (Fig. 2.2). Cladogenesis during these periods corroborates the observations in several other lizard groups in southern Africa and along the Eastern Escarpment (Heinicke et al., 2017a; Medina et al., 2016; Stanley and Bates, 2014; Tolley et al., 2008; Weinell and Bauer, 2018). Within the *Bradypodion* chameleons, closed habitat species along the eastern escarpment and coastal region show comparatively similar timing of diversification where cladogenesis was initiated at the onset of the late Miocene through the Pliocene and some recent cladogenesis in the Pleistocene (Tolley et al., 2008). Although neither of the two previous phylogenies on *Afroedura* applied divergence-time estimations, the authors assumed that cladogenesis within their respective *Afroedura* groups was primarily driven by geomorphological changes and climatic oscillations during the same epochs (Jacobsen et al., 2014; Makhubo et al., 2015), an assumption that is broadly congruent to the observations made in other lizard groups from southern Africa (e.g. Jacobsen, 1994; Bauer and Lamb, 2002; Matthee and Flemming, 2002; Travers et al., 2014).

Among the South African chameleon species in the genus *Bradypodion*, it was demonstrated that, where the interior was more stable over multiple time periods, several lineages independently colonized the less stable eastern coastal regions, which produced several recent diversification events (da Silva and Tolley, 2017; Tolley et al., 2008). However, several closed-habitat *Bradypodion* species along the east coast also have long branch-lengths with no closely related sister taxa, which was suggested to be as a result of extinction filtering associated with forest fragmentation and isolation (Tolley et al., 2008). This observation is particularly evident in taxa from the northern MPA forests and scarp forests in the Eastern Cape Province (Tolley et al., 2008). The *A. pondolia* species largely corroborate these results, demonstrating congruent patterns of diversification, similar divergence-time estimates, and long branch-lengths in overlapping regions. There also appears to be a northward trend to the diversification within *A. pondolia*, corroborating the results presented by Makhubo et al., (2015) as well those presented by Tolley et al., (2018) in a phylogenetic study of the co-distributed

forest dwelling bush squeaker frog, *Arthroleptis wahlbergii*. Tolley et al., (2018) uncovered species-level divergence between their northern and southern clades that is (although shallower) largely congruent to the biogeographic break where the Pondoland grasslands may present a significant barrier between the *A. pondolia* species D and the remaining three species. Although the authors did not employ divergence estimates, they roughly estimated divergence between their clades to have been associated with global cooling and aridification at the start of the Pleistocene (Tolley et al., 2018).

In the *A. pondolia* species complex the most recent common ancestor would have occupied widespread Afrotemperate forests along the Eastern Escarpment. Fragmentation of these forests during the late Miocene likely initiated cladogenesis in the *A. pondolia* species complex (Fig. 2.2). Plio/Pleistocene climatic oscillations then led to further contraction of forests in the MPA, reinforcing isolation among lineages. As with the *Bradypodion* chameleons (Tolley et al., 2008), extinction filtering and isolation may have characterized the *A. pondolia* lineages where the long branch lengths suggest that several more vulnerable and closely related sister clades may have gone extinct as the forest biome contracted with Pleistocene climatic shifts. In the northern species (A, B and C) ancient forests would have persisted for longer and may have been more widespread, allowing several lineages to persist throughout the Plio/Pleistocene. The newly formed coastal forests were devoid of competition and as a result easily colonized by *A. pondolia* as this forest type expanded along the coast during the Holocene, further corroborating the observations by Tolley et al., (2018) in these regions.

The coastal region of the Eastern Cape Province is dominated by scarp forests, which had undergone major contraction during glacial periods but were able to recover from well-sheltered refugia (Mucina et al., 2006). This explains the isolation observed between localities in species D. Similarly, scarp forest refugia would have been vital for lineages in the northern species (A, B and C) to persist throughout the Plio/Pleistocene (Lawes et al., 2007). Subsequent expansion of forests and the recently formed continuous band of coastal forest permitted mixing of several lineages. This is particularly true for species C where gene flow between localities is evident from the number of shared haplotypes and relatively low genetic differentiation between localities as suggested by the low pairwise F_{ST} values compared to the F_{ST} values observed between localities in species A, B and D (Appendix 5). In species B dispersal through coastal forests can be deduced by the coastal forest locality at Stainbank having a closer affinity to the other coastal localities and the geographically distant Vernon Crookes locality rather than the scarp forest locality at Krantzkloof that is geographically the nearest sampled locality (Figs. 2.1, 2.2). Although there are several localities among species A, B and C that are in close geographic proximity to one another and within the band of continuous coastal forests, the lack of shared haplotypes and high F_{ST} values between localities of different species (Appendix 2.5) suggest an absence of gene flow among candidate species within *A. pondolia*;

Grasslands between scarp forest patches could present a formidable barrier to gene flow: however, there are no obvious biogeographic barriers along the coast to maintain lineage isolation between species A, B and C. There are several large rivers that could present dispersal barriers to small terrestrial taxa but do not appear to do so in the *A. pondolia* species complex as many of these rivers flow between localities within candidate species. The observed isolation in the coastal forests may reflect the recent colonization of coastal forests from scarp forests as suggested by Tolley et al., (2018) for *A. wahlbergii*. The latter hypothesis would suggest that scarp forests occupied by species C have higher interconnectivity, which allows for gene flow between localities. Alternatively, gene flow between even the most distant localities could indicate that individuals from species C have higher dispersal capabilities compared to other species. The lack of gene flow between candidate species at geographically proximate localities suggests that they are either reproductively isolated or occupy different microhabitats, maintaining lineage isolation.

In contrast, although the nuclear loci appear to be slow evolving and exhibit low variation in the dataset, the *PRLR* nuDNA topology retrieved a well-supported clade comprising localities from species A and C (Appendix 2.4). This observation is potentially indicative of secondary contact between these localities subsequent to the divergence of species A and C. However, since these localities are geographically the most distant from each other among the three northern species, the most likely explanation would be that these localities retained ancestral alleles since they last shared a common ancestor. Alternatively, this relationship could be an artifact attributed to the low informativeness of the nuclear loci and should be interpreted with caution. Species D is well-supported by the *PRLR* topology. The phylogenetic relationships retrieved by the *PRLR* topology among localities within species D are, however, inconsistent with the relationships retrieved by the mtDNA topology (Fig. 2.2, Appendix 2.4). In this case, the *PRLR* topology suggests admixture between geographically proximate localities that can be explained by secondary contact during forest expansion events.

In morphologically conservative reptiles where traditional taxonomy has proven to be problematic, molecular methods have widely been used to delineate species (e.g. Blair and Bryson, 2017; Kotsakiozi et al., 2018; Laver et al., 2018; Pinto et al., 2019; Šmíd et al., 2017; Travers et al., 2014). However, where several techniques are employed simultaneously, species delimitation results are often inconclusive (e.g. Blair and Bryson, 2017; Jacobs et al., 2018; Kornilios et al., 2018). Molecular delimitation analyses have been shown to be affected by the ratio of population sizes to species divergence times, gene flow, number of species involved, and number of sampling singletons and to a lesser degree sample size and number of loci (Luo et al. 2018; Esselstyn et al. 2012; Reid and Carstens 2012; Fujisawa and Barraclough, 2013; Dellicour and Flot, 2015; Ahrens et al. 2016). Among the single-locus delimitation methods ABGD is known to underestimate putative species while GMYC and PTP tend to over split species (e.g. Paz and Crawford 2012; Pentinsaari et al. 2017; Renner et al.,

2017; Luo et al., 2018). Results from the present study corroborate these observations with ABGD retrieving the lowest number of putative species in *A. pandolia* and PTP the highest (Fig. 2.4). The general consensus across the single-locus delimitation results, however, suggests that the four candidate species do in fact represent four lineages evolving independently of one another, but the question remains whether there are additional lineages within these species and how many.

Discordance between the single-locus delimitation analyses can successfully be resolved by multispecies coalescence models such as STACEY, and as a result it has widely been used to validate potential species (e.g. Jacobs et al., 2018; McKelvy and Burbrink, 2017; Pinto et al., 2019; Tomasello, 2018). It is, however, important to consider that the recognized operational taxonomic units (OTUs) from these analyses can represent species, populations, or even a combination of species and populations (Luo et al., 2018; Sukumaran and Knowles, 2017). Therefore, it is suggested that the results of molecular species delimitation should be interpreted alongside other lines of evidence, such as comparative morphology, population genetics, and ecology (Sukumaran and Knowles, 2017).

Interpreting the similarity matrix from the STACEY output (Fig. 2.3), alongside the single-locus delimitation results and tree topologies (Figs. 2.2 and 2.4), supports the four candidate species within *A. pondolia* as distinct evolutionary entities with varying degrees of intraspecific variation. For example, the localities in species A exhibit the highest degree of sequence divergence but species A also comprises pairs of localities with relatively high probability of belonging to the same cluster compared to localities in species B, C and D. It can with relative certainty be concluded, based on the low intraspecific divergence compared to other *Afroedura* species and single-locus delimitation results, that species C is representative of a single taxon. Species D exhibits the lowest probability of pairs of species belonging to the same cluster, but the probabilities are comparable to those seen in species C between Mkambati and the remaining localities. The phylogenetic relationships among localities within species D are also inconclusive with regard to the *PRLR* topology compared to the mtDNA topology. Therefore, it can be concluded from the currently available data that species D also represents a single taxon. It is, however, noteworthy that Species A, B and D exhibit relatively old divergence-time estimates as well as high genetic differentiation between localities (F_{ST} values) that are comparable to those observed between the candidate species (Fig. 2.2, Appendix 2.5). Therefore, additional sampling and perhaps the inclusion of more variable nuDNA loci could support further subdivision of species A, B and D in line with some of the single-locus species delimitation results.

Results of the morphological analyses indicate some, albeit limited, differentiation among the four observed *A. pondolia* species. These results are interpreted with caution due to the low sample sizes and the large differences in sample sizes among the four species, which may

have skewed results or produced random results with little biological significance. In the meristic data there are significant differences in the means of some characters between species D and the remaining species, but there are no diagnostic meristic characters present because of the large overlap in variables between species (see Appendix 2.6). Differences between the four *A. pondolia* species are limited to pairwise comparisons in morphometric characters, which corroborate the observations of Makhubo et al. (2015) for the *A. nivaria* complex. Results from the DFA do, however, strongly support the presence of four morphologically distinct species. Pairwise morphometric comparisons indicate differences in head, feet, and toe size as well as body depth and eye width. These traits are generally related to diet, locomotion, habitat specialization and habitat utilization in geckos and other lizards (Russell and Bauer, 1989, Johnson et al., 2005; Edwards et al., 2012, 2013).

In the *Hemidactylus* geckos, a genus notorious for their conservative morphology (Carranza and Arnold, 2012; Hosseinzadeh et al., 2015; Šmíd et al., 2017), morphological differences are generally associated with sympatry in accordance with the character-displacement hypothesis (Brown and Wilson, 1956). In some instances even distantly related sympatric *Hemidactylus* species are morphologically indistinguishable but appear to be separated by microhabitat selection (Šmíd et al., 2017). It can therefore be assumed that there would not necessarily be character shifts in allopatric species sharing similar habitat types, as is the case with the *A. pondolia* species complex.

Collectively, the results indicate that *A. pondolia* is a monophyletic group consisting of multiple cryptic species that resulted from extinction filtering and isolation associated with forest biome contraction. There are several lines of evidence, following the general lineage concept, along with morphology, in support of *A. pondolia* as a species complex comprising four morphologically similar but distinct species. The four species are geographically and genetically discrete and characterized by the absence of shared haplotypes, high fixation indices and marked sequence divergences. The sequence-divergence values observed between candidate species in the present study are comparable to those between known *Afroedura* species and candidate species as well as closely related species in other gecko groups (Bauer et al., 2006; Lajmi et al., 2016; Makhubo et al., 2015). Broader sampling could, however, uncover additional cryptic lineages within species characterized by high intraspecific sequence divergence. Since *A. pondolia* was described from three specimens collected at Mbotyi in the Eastern Cape Province (Hewitt, 1925), the species name should be restricted to species D, while species A,B and C represent novel taxa. Currently, the four species appear morphologically undiagnosable, although further investigation and closer examination with additional morphological characters could potentially diagnose closely related species within the *A. pondolia* complex.

Appendix 2.1. List of *Afroedura* samples used in this study with associated voucher and DNA numbers, locality name, and GenBank accession numbers for each gene. Voucher numbers in bold were used in the morphological analysis and Genbank accession numbers in bold indicate unique sequences from Makhubo et al. (2015). The *cyt b* haplotype numbers correspond to the haplotype network in Fig. 2.4.

Voucher Number	DNA Number	Taxon	Locality	cyt *b* Haplotype	Genbank accession number			
					cyt b	*ND4*	*PRLR*	*RAG1*
	TB-A087	*Afroedura pondolia*	Nkandla forest	1	MK540589	MK568712		
PEM R24420	TB-A023	*Afroedura pondolia*	Nkandla forest	1	MK540528	MK568653	MK568728	MK568751
	TB-A086	*Afroedura pondolia*	Nkandla forest	2	MK540588	MK568711		
	TB-A088	*Afroedura pondolia*	Nkandla forest	2	MK540590	MK568713		
PEM R24421	TB-A024	*Afroedura pondolia*	Nkandla forest	2	MK540529	MK568654		
PEM R24422	TB-A025	*Afroedura pondolia*	Nkandla forest	2	MK540530	MK568655		
PEM R24451	TB-A085	*Afroedura pondolia*	Entumeni NR	3	MK540587		MK568743	MK568766
	TB-A001	*Afroedura pondolia*	Mount Moreland	4	MK540512	MK568635	MK568723	MK568746
	TB-A002	*Afroedura pondolia*	Mount Moreland	4	MK540513	MK568636		
PEM R24406	TB-A003	*Afroedura pondolia*	Mount Moreland	4	MK540514	MK568637		
PEM R24407	TB-A004	*Afroedura pondolia*	Mount Moreland	4	MK540515	MK568638		
PEM R24408	TB-A005	*Afroedura pondolia*	Mount Moreland	4	MK540516	MK568639		
	TB-A014	*Afroedura pondolia*	Mount Moreland	4	MK540522	MK568645		
	TB-A022	*Afroedura pondolia*	Harold Johnson NR	5	MK540527	MK568652	MK568727	MK568750
PEM R24416	TB-A018	*Afroedura pondolia*	Krantzkloof NR	6	MK540524	MK568648	MK568726	MK568749
PEM R24417	TB-A019	*Afroedura pondolia*	Krantzkloof NR	6	MK540525	MK568649		
PEM R24419	TB-A021	*Afroedura pondolia*	Krantzkloof NR	6	MK540526	MK568651		
PEM R24415	TB-A016	*Afroedura pondolia*	Kenneth Stainbank NR	7	MK540523	MK568646	MK568725	MK568748
PEM R24447	TB-A076	*Afroedura pondolia*	Umkomaas	8	MK540578	MK568703		
PEM R24448	TB-A077	*Afroedura pondolia*	Scottburgh	9	MK540579	MK568704	MK568741	MK568764
PEM R24449	TB-A078	*Afroedura pondolia*	Vernon Crookes NR	10	MK540580	MK568705	MK568742	MK568765
PEM R24450	TB-A079	*Afroedura pondolia*	Vernon Crookes NR	11	MK540581	MK568706		
	TB-A080	*Afroedura pondolia*	Vernon Crookes NR	11	MK540582	MK568707		
	TB-A081	*Afroedura pondolia*	Vernon Crookes NR	12	MK540583	MK568708		
	TB-A083	*Afroedura pondolia*	Vernon Crookes NR	12	MK540585	MK568709		

	TB-A082	*Afroedura pondolia*	Vernon Crookes NR	13	MK540584			
	TB-A084	*Afroedura pondolia*	Vernon Crookes NR	14	MK540586	MK568710		
	TB-A006	*Afroedura pondolia*	Queen Elizabeth Park NR	15	MK540517	MK568640	MK568724	MK568747
PEM R24409	TB-A008	*Afroedura pondolia*	Queen Elizabeth Park NR	15	MK540519	MK568642		
PEM R24410	TB-A009	*Afroedura pondolia*	Queen Elizabeth Park NR	15	MK540520	MK568643		
PEM R24411	TB-A010	*Afroedura pondolia*	Queen Elizabeth Park NR	15	MK540521	MK568644		
PEM R24443	TB-A063	*Afroedura pondolia*	Umtentweni	15	MK540558	MK568683	MK568738	MK568761
PEM R24441	TB-A056	*Afroedura pondolia*	Mbumbazi NR	16	MK540559	MK568684	MK568737	MK568760
PEM R24442	TB-A058	*Afroedura pondolia*	Mbumbazi NR	16	MK540561	MK568686		
PEM R24440	TB-A050	*Afroedura pondolia*	Oribi Gorge	16	MK540552	MK568677		
	TB-A051	*Afroedura pondolia*	Oribi Gorge	16	MK540553	MK568678		
	TB-A053	*Afroedura pondolia*	Oribi Gorge	16	MK540555	MK568680		
	TB-A054	*Afroedura pondolia*	Oribi Gorge	16	MK540556	MK568681		
	TB-A055	*Afroedura pondolia*	Oribi Gorge	16	MK540557	MK568682		
	TB-A007	*Afroedura pondolia*	Queen Elizabeth Park NR	16	MK540518	MK568641		
PEM R19152	WC10-114	*Afroedura pondolia*	Mkambati NR	17	MK540503	MK568626		
PEM R22432	WC-4501	*Afroedura pondolia*	Mkambati NR	18	MK540511	MK568634		
	TB-A041	*Afroedura pondolia*	Mkambati NR	19	MK540544	MK568669	MK568735	MK568758
PEM R24434	TB-A042	*Afroedura pondolia*	Mkambati NR	19	MK540545	MK568670		
PEM R24435	TB-A043	*Afroedura pondolia*	Mkambati NR	20	MK540546	MK568671		
PEM R24436	TB-A044	*Afroedura pondolia*	Mkambati NR	21	MK540547	MK568672		
PEM R24437	TB-A045	*Afroedura pondolia*	Mkambati NR	21	MK540548	MK568673		
PEM R24438	TB-A046	*Afroedura pondolia*	Mkambati NR	21	MK540549	MK568674		
	TB-A047	*Afroedura pondolia*	Mkambati NR	21	MK540550	MK568675		
PEM R24439	TB-A049	*Afroedura pondolia*	Oribi Gorge	22	MK540551	MK568676	MK568736	MK568759
	TB-A052	*Afroedura pondolia*	Oribi Gorge	23	MK540554	MK568679		
	TB-A057	*Afroedura pondolia*	Mbumbazi NR	24	MK540560	MK568685		
	TB-A059	*Afroedura pondolia*	Mbumbazi NR	24	MK540562	MK568687		
	TB-A061	*Afroedura pondolia*	Mbumbazi NR	24	MK540564	MK568689		
	TB-A060	*Afroedura pondolia*	Mbumbazi NR	25	MK540563	MK568688		
	TB-A062	*Afroedura pondolia*	Mbumbazi NR	26	MK540565	MK568690		

	TB-A065	*Afroedura pondolia*	Mpenjati NR	26	MK540567	MK568692		
	TB-A064	*Afroedura pondolia*	Mpenjati NR	27	MK540566	MK568691		
	TB-A066	*Afroedura pondolia*	Mpenjati NR	28	MK540568	MK568693	MK568739	MK568762
PEM R24444	TB-A069	*Afroedura pondolia*	Mpenjati NR	28	MK540571	MK568696		
	TB-A067	*Afroedura pondolia*	Mpenjati NR	29	MK540569	MK568694		
	TB-A068	*Afroedura pondolia*	Mpenjati NR	30	MK540570	MK568695		
PEM R24445	TB-A070	*Afroedura pondolia*	Mpenjati NR	30	MK540572	MK568697		
	TB-A071	*Afroedura pondolia*	Umtamvuna NR	31	MK540573	MK568698	MK568740	MK568763
	TB-A072	*Afroedura pondolia*	Umtamvuna NR	32	MK540574	MK568699		
	TB-A073	*Afroedura pondolia*	Umtamvuna NR	33	MK540575	MK568700		
	TB-A074	*Afroedura pondolia*	Umtamvuna NR	33	MK540576	MK568701		
PEM R24446	TB-A075	*Afroedura pondolia*	Umtamvuna NR	34	MK540577	MK568702		
PEM R22430	WC-4404	*Afroedura pondolia*	Mbotyi	35	MK540509	MK568632		
PEM R22431	WC-4405	*Afroedura pondolia*	Mbotyi	35	MK540510	MK568633	MK568730	MK568753
PEM R24433	TB-A040	*Afroedura pondolia*	Port St. Johns	36	MK540543	MK568668	MK568734	MK568757
PEM R24430	TB-A037	*Afroedura pondolia*	Silaka NR	36	MK540540	MK568665	MK568733	MK568756
PEM R24431	TB-A038	*Afroedura pondolia*	Silaka NR	36	MK540541	MK568666		
PEM R24432	TB-A039	*Afroedura pondolia*	Silaka NR	37	MK540542	MK568667		
PEM R19427	WC-DNA 332	*Afroedura pondolia*	Hluleka NR	38	MK540506	MK568629		
PEM R19435	WC-DNA 371	*Afroedura pondolia*	Hluleka NR	38	MK540507	MK568630		
PEM R19436	WC-DNA 374	*Afroedura pondolia*	Hluleka NR	38	MK540508	MK568631		
PEM R24423	TB-A026	*Afroedura pondolia*	Hluleka NR	38	MK540531	MK568656	MK568731	MK568754
PEM R24424	TB-A027	*Afroedura pondolia*	Hluleka NR	38	MK540532	MK568657		
PEM R24425	TB-A028	*Afroedura pondolia*	Hluleka NR	38	MK540533	MK568658		
	TB-A031	*Afroedura pondolia*	Hluleka NR	38	MK540534	MK568659		
PEM R24426	TB-A032	*Afroedura pondolia*	Coffee Bay	39	MK540535	MK568660	MK568732	MK568755
PEM R24427	TB-A033	*Afroedura pondolia*	Coffee Bay	39	MK540536	MK568661		
	TB-A036	*Afroedura pondolia*	Coffee Bay	39	MK540539	MK568664		
PEM R24428	TB-A034	*Afroedura pondolia*	Coffee Bay	40	MK540537	MK568662		
PEM R24429	TB-A035	*Afroedura pondolia*	Coffee Bay	40	MK540538	MK568663		
PEM R22940	WC-5434	*Afroedura pondolia*	Manubi forest	41	MK540591	MK568714	MK568744	MK568767

PEM R22942	WC-5436	*Afroedura pondolia*	Manubi forest	41	MK540593	MK568716		
PEM R22938	WC-5432	*Afroedura pondolia*	Manubi forest	41	MK540596	MK568719		
PEM R22939	WC-5433	*Afroedura pondolia*	Manubi forest	41	MK540597	MK568720		
PEM R22941	WC-5435	*Afroedura pondolia*	Manubi forest	42	MK540592	MK568715		
PEM R19799	WC-DNA 398	*Afroedura pondolia*	Dwesa NR	43	MK540504	MK568627	MK568729	MK568752
PEM R19803	WC-DNA 592	*Afroedura pondolia*	Dwesa NR	43	MK540505	MK568628		
PEM R23161	WC-5347	*Afroedura pondolia*	Dwesa NR	43	MK540595	MK568718		
PEM R22937	WC-5335	*Afroedura pondolia*	Dwesa NR	44	MK540594	MK568717		
	TB-A017	*Afroedura pondolia*	Krantzkloof NR			MK568647		
PEM R24418	TB-A020	*Afroedura pondolia*	Krantzkloof NR			MK568650		
PEM R24412	TB-A011	*Afroedura nivaria*	Inhlosane hill, Midlands		MK540598	MK568721	MK568745	MK568768
PEM R24413	TB-A012	*Afroedura nivaria*	Inhlosane hill, Midlands		MK540599	MK568722		
NMB R9311	MFB 2010.105	*Afroedura amatolica*	Zingcuka, Amatole MTNS			**LM654522.1**		
NMB R9314	MFB 2010.108	*Afroedura amatolica*	Farm No. 18, Amatole MTNS			**LM654523.1**		
NMB R9315	MFB 2010.109	*Afroedura amatolica*	Farm No. 18, Amatole MTNS			**LM654524.1**		
	MBUR01446	*Afroedura amatolica*	Double Drift Game Reserve			**LM654520.1**		
	MBUR01447	*Afroedura amatolica*	Double Drift Game Reserve			**LM654521.1**		
PEM R17936	KTH09-196	*Afroedura bogerti*	Omuha Lodge			**LM654622.1**		
NMB R9106	MFB 2010.59	*Afroedura halli*	Aasvoelberg, Zastron District			**LM654533.1**		
NMB R9107	MFB 2010.61	*Afroedura halli*	Farm No. 147, Wodehouse District			**LM654534.1**		
NMB R9109	MFB 2010.64	*Afroedura halli*	Koesberg, Zastron District			**LM654536.1**		
NMB R9111	MFB 2010.66	*Afroedura halli*	Koesberg, Zastron District			**LM654538.1**		
NMB R9116	MFB 2010.80	*Afroedura halli*	Elandsberg, Zastron District			**LM654543.1**		
NMB R9301	MFB 2010.99	*Afroedura halli*	Penhoek Pass, Wodehouse District			**LM654545.1**		
NMB R9303	MFB 2010.102	*Afroedura halli*	Thaba Phatshwa, Ladybrand District			**LM654546.1**		
NMB R9353	MFB 2010.155	*Afroedura halli*	Farm: Kruis Fontein, Hofmeyr District			**LM654548.1**		
NMB R9354	MFB 2010.148	*Afroedura halli*	Farm No. 147, Wodehouse District			**LM654549.1**		
NMB R9573		*Afroedura halli*	Jobert's Pass, Lady Grey District			**LM654553.1**		
NMB R9574		*Afroedura halli*	Jobert's Pass, Lady Grey District			**LM654554.1**		
NMB R9576		*Afroedura halli*	Witteberg MTNS, Herschel District			**LM654556.1**		
NMB R9577		*Afroedura halli*	Witteberg MTNS, Herschel District			**LM654557.1**		

NMB R9578		*Afroedura halli*	Witteberg MTNS, Herschel District	**LM654558.1**	
NMB R9580		*Afroedura halli*	Witteberg MTNS, Herschel District	**LM654560.1**	
NMB R9582		*Afroedura halli*	Mfinci, Witteberg MTNS, Herschel	**LM654562.1**	
	MBUR00429	*Afroedura halli*	Farm	**LM654528.1**	
	MBUR00486	*Afroedura halli*		**LM654529.1**	
	MBUR00502	*Afroedura halli*	Farm	**LM654530.1**	
	QQ0559	*Afroedura halli*	Jamestown Rd near Streepfontein	**LM654563.1**	
	KTH10-08	*Afroedura hawequensis*	Limietberg	**LM654624.1**	
NMB R9293	MFB 2010.90	*Afroedura karroica*	Buffelskop, Cradock District	**LM654570.1**	
NMB R9296	MRB 2010.94	*Afroedura karroica*	Buffelskop, Cradock District	**LM654573.1**	
NMB R9344	MFB 2010.139	*Afroedura karroica*	Farm No. 124, Tarkastad District	**LM654576.1**	
NMB R9345	MFB 2010.140	*Afroedura karroica*	Farm No. 124, Tarkastad District	**LM654577.1**	
NMB R9346	MFB 2010.141	*Afroedura karroica*	Farm No. 124, Tarkastad District	**LM654578.1**	
NMB R9347	MFB 2010.142	*Afroedura karroica*	Farm No. 124, Tarkastad District	**LM654579.1**	
NMB R9365		*Afroedura karroica*	Lootsberg Pass, Graaf Reinet District	**LM654582.1**	
	MFB 2010-93	*Afroedura karroica*	Buffelskop, Cradock District	**LM654569.1**	
PEM R18690	SNB026	*Afroedura karroica*	Hartbeesfontein, Sneeuberge	**LM654583.1**	
PEM R 18691	SNB027	*Afroedura karroica*	Hartbeesfontein, Sneeuberge	**LM654584.1**	
PEM R19579	SVN0462	*Afroedura karroica*	~20km NE Cradock	**LM654589.1**	
PEM R19568	SVN0463	*Afroedura karroica*	~20km NE Cradock	**LM654590.1**	
PEM R19576	SVN0467	*Afroedura karroica*	rd btw Tarkastad & Commando Drift	**LM654591.1**	
PEM R19513	SVN0469	*Afroedura karroica*	~5km N of Middelburg	**LM654593.1**	
	WC10-008	*Afroedura karroica*	Zuurkloof, Asante Sanna	**LM654565.1**	
	WC10-033	*Afroedura karroica*	Top of Waterkloof	**LM654568.1**	
	MBUR00835	*Afroedura langi*	Cleveland NR	**LM654634.1**	
	AMB8618	*Afroedura marleyi*	The Hippos	**LM654631.1**	
	AMB8619	*Afroedura marleyi*	The Hippos	**LM654632.1**	
	MBUR00109	*Afroedura haackei*		**LM654633.1**	
NMB R10196	AMNH26445	*Afroedura nivaria*	Top of Mnweni cutback	**LM654614.1**	
NMB R9079		*Afroedura nivaria*	Korannaberg, Excelsior District	**LM654594.1**	
NMB R9080		*Afroedura nivaria*	Korannaberg, Excelsior District	**LM654595.1**	

40

NMB R9083		*Afroedura nivaria*	Korannaberg, Excelsior District		**LM654597.1**
NMB R9090	MFB 2010.16	*Afroedura nivaria*	Platberg, Ladybrand District		**LM654598.1**
NMB R9091	MFB 2010.17	*Afroedura nivaria*	Platberg, Ladybrand District		**LM654599.1**
NMB R9096	MFB 2010.25	*Afroedura nivaria*	Platberg, Ladybrand District		**LM654604.1**
NMB R9099	MFB 2010.28	*Afroedura nivaria*	Ribboksberg, Clocolan District		**LM654607.1**
NMB R9100	MFB 2010.29	*Afroedura nivaria*	Ribboksberg, Clocolan District		**LM654608.1**
	FP319	*Afroedura nivaria*	The Sentinel		**LM654613.1**
NMB R9338	MFB 2010.133	*Afroedura tembulica*	Tshangana, Cofimvaba District		**LM654618.1**

Appendix 2.2. Substitution models used for each dataset in the various molecular analyses.

Dataset	Garli	MrBayes	BEAST	STACEY
mtDNA Concatenated	*ND4* (TPM1uf+I+G) *cyt b* (TPM1uf+I+G)	*ND4* (TPM1uf+I+G) *cyt b* (TPM1uf+I+G)	*ND4* (HKY+I+G) cyt *b* (HKY+I+G)	
ND4 Afroedura gene tree			HKY+I+G	
Total-evidence	*ND4* (TPM1uf+I+G) *cyt b* (TPM1uf+I+G) *PRLR* (TPM1+I) *RAG1* (TPM1uf)	*ND4* (TPM1uf+I+G) *cyt b* (TPM1uf+I+G) *PRLR* (TPM1+I) *RAG1* (TPM1uf)		*ND4* (HKY+I+G) *cyt b* (HKY+I+G) *PRLR* (HKY+I) *RAG1* (HKY)

41

Appendix 2.3. Morphological variables measured for voucher specimens of *Afroedura pondolia*.

Morphological variables	Definition
Morphometric measures	
Snout to vent length (SVL)	Measured from the tip of the snout to the cloaca
Body width (BW)	Body width measured across the shoulders
Body height (BH)	Body height measured at the shoulders
Head width (HW)	Maximum width of head
Head height (HH)	Maximum height of head just posterior to orbitals
Head length (HL)	Length from anterior edge of ear to tip of snout
Lower jaw length (LJL)	Tip of the snout to the back of the lower jaw
Snout-coronoid distance (CT)	Tip of snout to coronoid process of mandible (corner of the mouth)
Snout-quadrate distance (QT)	Tip of snout to quadrate
Eye-to-naris distance (EN)	Length from anterior corner of eye to posterior edge of naris
Rostral height (RH)	Height of the rostral scale
Internarial distance (IN)	Distance between inner edges of nares
Interorbital distance (IO)	Distance between anterior-dorsal edges of eyes
Transverse length of eye (EYE)	Transverse length of eye
Ear-to-eye distance (EE)	Length from anterior edge of ear to posterior corner of eye
Axilla to groin distance (Trunk)	Length from posterior edge of forelimb insertion to anterior edge of hindlimb insertion
Humerus length (HM)	Length from intersection with body to elbow
Length of lower arm (Crus)	Length from posterior edge of bent elbow to wrist
Hand length (Hand)	Length from wrist to tip of longest finger
Femur length (FM)	Length from intersection with body to knee
Length of lower leg (Tibia)	Length from anterior edge of bent knee to heel
Carpal length (CP)	From wrist to base of longest toe
Foot length (Foot)	From ankle to tip of longest toe
Tarsal length (TR)	From ankle to base of longest toe
4th finger length (4FL)	Maximum length of the 4th finger
4th finger width (4FW)	Maximum width of the 4th finger
4th toe length (4TL)	Maximum length of the 4th toe
4th toe width (4TW)	Maximum width of the 4th toe
Meristic Characters	
Supralabial scales (SuL)	Number of supralabial scales
Infralabial scales (InL)	Number of infralabial scales
4th finger lamellae (4FLam)	Number of enlarged lamellae more than twice the width of surrounding scales under the 4th finger
4th toe lamellae (4TLam)	Number of enlarged lamellae more than twice the width of surrounding scales under the 4th toe
Internasal granules (InNG)	Number of scales between the nasal scales
Post mental scales (PM)	Number of postmental scales
Scales between eye and ear (SEE)	Number of scales between the eye and ear
Midbody scales (MBS)	Number of midbody scale rows counted halfway from axila to groin
Scales between eye and nostril (SEN)	Number of scales between the eye and nostril
Scales between eyes (SBE)	Number of scales counted between the anterior-dorsal edges of eyes
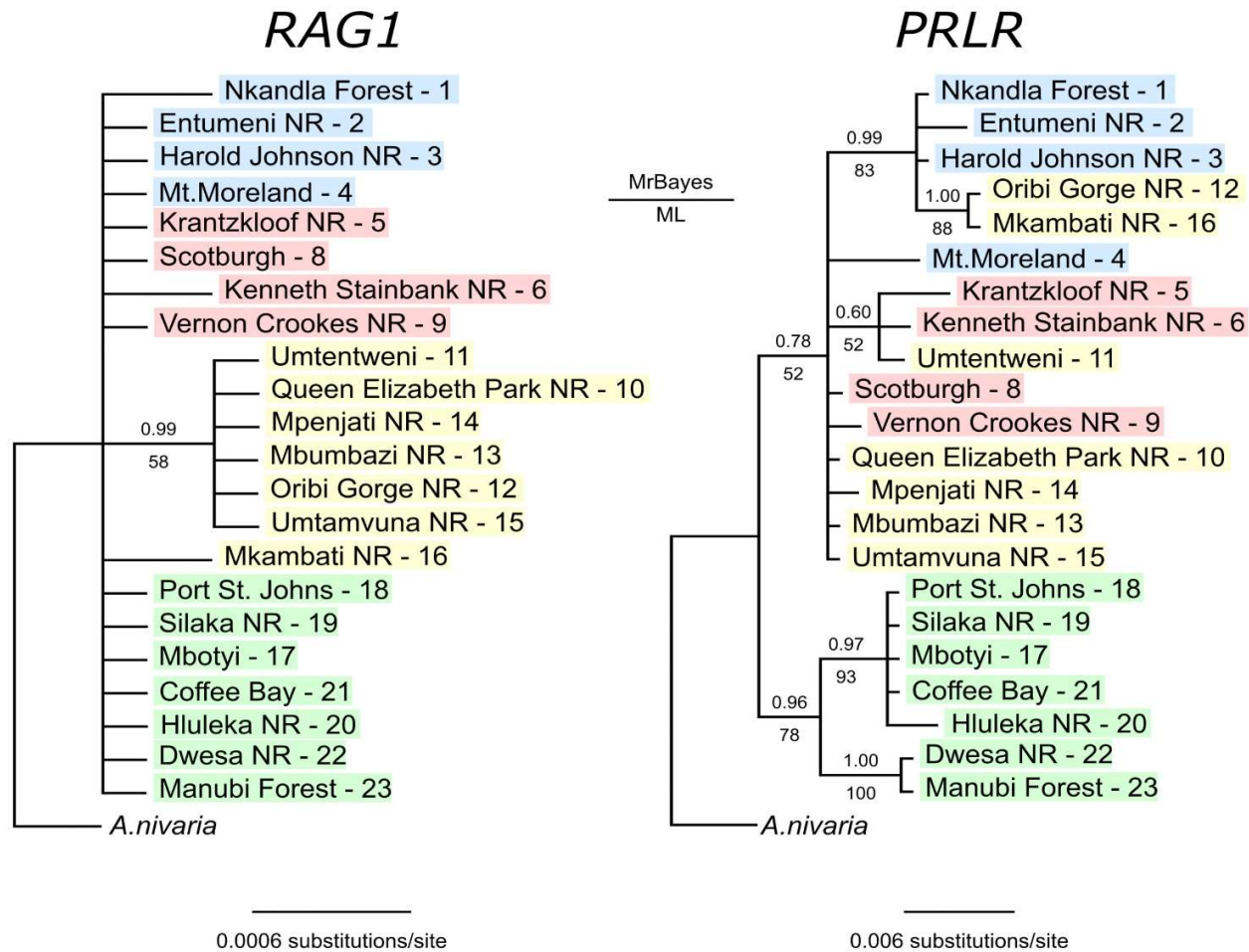
Appendix 2.4. Bayesian topologies for the individual nuDNA loci, *RAG1* and *PRLR*, with posterior probabilities from the MrBayes analysis above branches and maximum likelihood bootstrap values below branches. Locality colors correspond to the four candidate species identified within *Afroedura pondolia* in the mtDNA phylogeny, A = blue, B = red, C = yellow and D = green.

43

Appendix 2.5. Pairwise F_{ST} values between *Afroedura pondolia* sample localities for the *cyt b* locus. Bold values are statistically significant (P < 0.05). Borders in the matrix outline pairwise F_{ST} values within each candidate species.

Sp.		Locality	1	2	3	4	5	6	7	8	9	10	11	12
A	1	Nkandla Forest	0.00000											
	2	Entumeni NR	0.98447	0.00000										
	3	Harold Johnson NR	0.98424	1.00000	0.00000									
	4	Mt.Moreland	**0.99184**	1.00000	1.00000	0.00000								
B	5	Krantzkloof NR	**0.99021**	1.00000	1.00000	**1.00000**	0.00000							
	6	Stainbank NR	0.98571	1.00000	1.00000	1.00000	1.00000	0.00000						
	7	Umkomaas	0.98609	1.00000	1.00000	1.00000	1.00000	1.00000	0.00000					
	8	Scotburgh	0.98627	1.00000	1.00000	1.00000	1.00000	1.00000	1.00000	0.00000				
	9	Vernon Crookes NR	**0.96792**	0.94807	0.94956	**0.97386**	**0.91760**	0.51634	0.50667	0.56725	0.00000			
C	10	Queen E. P. NR	**0.97178**	0.95122	0.95335	**0.97935**	**0.96982**	0.95543	0.95415	0.95480	**0.95246**	0.00000		
	11	Umtentweni	0.98512	1.00000	1.00000	1.00000	1.00000	1.00000	1.00000	1.00000	0.95077	0.00000	0.00000	
	12	Oribi Gorge NR	**0.98877**	0.99111	0.99151	**0.99550**	**0.99373**	0.99198	0.99175	0.99187	**0.97110**	**0.74146**	0.92857	0.00000
	13	Mbumbazi NR	**0.97807**	0.96903	0.97040	**0.98443**	**0.97835**	0.97217	0.97131	0.97172	**0.96140**	**0.67383**	0.78462	0.18182
	14	Mpenjati NR	**0.94650**	0.90557	0.90958	**0.95122**	**0.93345**	0.91344	0.91067	0.91190	**0.93265**	**0.38479**	0.29101	**0.23617**
	15	Umtamvuna NR	**0.93884**	0.86604	0.87202	**0.94319**	**0.91966**	0.88122	0.87784	0.87955	**0.92245**	0.32028	0.00000	**0.55530**
	16	Mkambati NR	**0.91806**	0.85801	0.86348	**0.91352**	**0.89424**	0.87186	0.86507	0.86705	**0.90310**	**0.76636**	0.69245	**0.82809**
D	17	Mbotyi	**0.99046**	1.00000	1.00000	**1.00000**	1.00000	1.00000	1.00000	1.00000	**0.97087**	**0.97344**	1.00000	**0.99492**
	18	Port St. Johns	0.98900	1.00000	1.00000	1.00000	1.00000	1.00000	1.00000	1.00000	0.96742	0.96869	1.00000	0.99424
	19	Silaka NR	**0.96630**	0.92192	0.92121	**0.97692**	0.96000	0.92145	0.92375	0.92442	**0.95554**	**0.95010**	0.91475	**0.97355**
	20	Hluleka nR	**0.99529**	1.00000	1.00000	**1.00000**	**1.00000**	1.00000	1.00000	1.00000	**0.98404**	**0.98664**	1.00000	**0.99703**
	21	Coffee Bay	**0.99090**	0.99441	0.99420	**0.99752**	**0.99647**	0.99471	0.99489	0.99493	**0.97917**	**0.98049**	0.99384	**0.99403**
	22	Dwesa NR	**0.98907**	0.99065	0.99048	**0.99659**	**0.99452**	0.99078	0.99095	0.99103	**0.97513**	**0.97614**	0.98942	**0.99246**
	23	Manubi Forest	**0.99246**	0.99640	0.99627	**0.99834**	**0.99765**	0.99643	0.99656	0.99659	**0.98002**	**0.98211**	0.99601	**0.99508**

44

Appendix 2.5 continued.

Sp.		Locality	13	14	15	16	17	18	19	20	21	22	23
C	13	Mbumbazi NR	0.00000										
	14	Mpenjati NR	**0.19792**	0.00000									
	15	Umtamvuna NR	**0.52813**	**0.35867**	0.00000								
	16	Mkambati NR	**0.81246**	**0.76080**	**0.69142**	0.00000							
D	17	Mbotyi	**0.98243**	**0.94450**	**0.92939**	**0.91731**	0.00000						
	18	Port St. Johns	0.98003	0.93673	0.91585	0.91034	1.00000	0.00000					
	19	Silaka NR	**0.96305**	**0.93078**	**0.91485**	**0.91071**	**0.73913**	0.00000	0.00000				
	20	Hluleka NR	**0.98968**	**0.96787**	**0.96454**	**0.94716**	**1.00000**	1.00000	**0.95399**	0.00000			
	21	Coffee Bay	**0.98536**	**0.95975**	**0.95354**	**0.93829**	**0.98896**	0.98897	**0.93595**	**0.98329**	0.00000		
	22	Dwesa NR	**0.98259**	**0.95336**	**0.94442**	**0.92969**	0.98709	0.98462	**0.93608**	**0.98987**	**0.97689**	0.00000	
	23	Manubi Forest	**0.98682**	**0.96150**	**0.95545**	**0.93857**	**0.99421**	0.99396	**0.94948**	**0.99545**	**0.98366**	**0.98270**	0.00000

Appendix 2.6. Means and ranges of the meristic characters for the four candidate species in *A. pondolia*.

	A	B	C	D
Infralabial scales (InL)	9.71 (9-11)	8.89 (8-11)	9.22 (8-11)	8.68 (7-10)
Scales between eye and nostril (SEN)	12.29 (10-13)	12 (10-14)	12.17 (9-15)	10.88 (10-13)
Scales between eyes (SBE)	23.33 (20-25)	25.11 (22-27)	23.5 (20-26)	22.04 (18-26)
4th finger lamellae (4FLam)	7.71 (7-9)	6.89 (5-9)	6.61 (5-8)	8.04 (6-10)
Internasal granules (InNG)	1.14 (1-2)	1.11 (1-2)	1	1.56 (1-3)
Scales between eye and ear (SEE)	24.86 (23-27)	25.33 (22-28)	25.28 (23-30)	22.88 (18-30)
4th toe lamellae (4TLam)	8 (7-9)	6.78 (6-10)	6.83 (5-10)	8.2 (6-11)
Supralabial scales (SuL)	10.43 (10-11)	9.44 (9-11)	9.89 (9-11)	9.64 (8-11)
Post mental scales (PM)	2.29 (2-3)	2.11 (2-3)	2	2.2 (1-3)
Midbody scales (MBS)	97.14 (84-108)	101.33 (94-111)	98.72 (91-106)	98.56 (86-110)

Chapter 3

Phylogeographic patterning of two co-distributed fossorial forest-living snake species reveals hidden diversity

3.1 Introduction

Climatic variables are critical in sculpting the distribution and cladogenetics of reptiles, largely due to the physiological constraints imposed by an ectothermic lifestyle (Aragón et al., 2010; Moura et al., 2016). This would imply that terrestrial ectothermic vertebrates, such as reptiles, are ideal non model organisms with which to test biogeographic hypotheses related to ancient temporal and spatial climatic shifts associated with habitat fragmentation. For example, the modelling of climatic variables have indicated that both climatic oscillations and climatic variation across the landscape drove cladogenesis and phylogeographic structuring in several southern African reptile taxa (Barlow et al., 2013; da Silva and Tolley, 2017; Diedericks and Daniels, 2013; Engelbrecht et al., 2013; Stanley and Bates, 2014). In addition, divergence-time estimates have demonstrated that cladogenesis within southern African reptile taxa closely correlate with periods characterized by climatic ameliorations throughout the Mio/Plio/Pleistocene (Kullenkampf et al., 2019; Medina et al., 2016; Tolley et al., 2008; Weinell and Bauer, 2018).

South Africa experienced several dramatic episodic climatic ameliorations as a consequence of global climatic shifts (Deacon, 1983; Tyson, 1986). These paleoclimatic oscillations had a significant impact on biome structure and composition that resulted in repeated contractions, extinction and expansion episodes for organisms occurring within these biomes, creating a complex biogeographic mosaic (Barlow et al., 2013; Lawes et al., 2007; Tolley et al., 2008). One of the South African biomes most affected by paleoclimatic shifts is the highly fragmented indigenous forest biome, primarily as a consequence of aridification since the onset of the late Miocene (Mucina et al., 2006). During more xeric periods the distribution of forest habitats contracted to areas with suitable climatic conditions while the more arid adapted grassland habitats expand (Feakins and Demenocal, 2010; Deacon, 1983). Continuous uplift throughout the late Tertiary contributed to the formation of South Africa's great escarpment and, along with the warm Aghulhas current, created a rain shadow effect which maintained a subtropical climate along the escarpment's eastern slopes (Clark et al., 2011; Neumann and Bamford, 2015; Sepulchre et al., 2006). Higher precipitation and the high elevation of the Eastern Escarpment resulted in many deep valleys that would've allowed forest patches to persist during glacial periods throughout the Plio/Pleistocene (Eeley et al., 1999; Mucina and Geldenhuys, 2006; Neumann and Bamford, 2015). The contraction of forests and the expansion of grasslands during these periods is thought to be the main driver of cladogenesis

46

in forest living species (White, 1978; Lawes, 1990; Tolley et al., 2008, 2018). While a select group of southern African forest living fauna have been studied to understand the impact of forest fragmentation and cladogenesis (see: Lawes, 1990; Lawes et al., 2000a,b, 2007; Tolley et al., 2008, 2018; Daniels et al., 2016), the evolutionary and biogeographic history of forest dwelling reptiles remain poorly studied.

South African forests are broadly divided into two major types, the inland Afrotemperate forest and Indian Ocean coastal belt (IOCB) forest types (Midgley et al, 1997; Von Maltitz et al., 2003; Mucina and Rutherford, 2006). Afrotemperate forests are ancient and have been in South Africa since at least prior to the Miocene while the IOCB forests recently expanded along the Mozambique coast southwards into South Africa, following the last glacial maximum about 8000 years ago (Lawes, 1990; Eeley et al., 1999). Afrotemperate forests are generally fragmented, discontinuous and restricted to higher elevations, sheltered valleys or gorges where they are separated by dry low-lying areas that present dispersal barriers for forest specialist species (Mucina and Geldenhuys, 2006). The younger IOCB forests occurs along the coastal margins of the Eastern Cape and KwaZulu-Natal provinces in areas that were formerly submerged and became exposed during recent marine regressions (Mucina et al., 2006).

Two recent phylogeographic studies of near co-distributed forest dwelling ectotherms along the coast of the Eastern Cape and KwaZulu-Natal provinces revealed marked phylogenetic structuring and deep genetic divergence in the northeastern portion of Eastern Cape Province, suggesting the presence of an ancient gene flow barrier (Tolley et al., 2018; Busschau et al., 2019). However, no visible contemporaneous physical barrier exist in the region apart from the intrusion of grasslands that appears to be the main factor causal to the observed break (Mucina and Geldenhuys, 2006; Von Maltitz et al., 2003). Busschau et al. (2019) demonstrated late Miocene cladogenesis in the Pondo flat gecko, *Afroedura pondolia*, while Tolley et al. (2018) proposed a younger Pleistocene divergence in the bush squeaker frog, *Arthroleptis wahlbergii*. This would imply the possible oscillating nature of the assumed biogeographic break, most likely attributed to the contraction and expansion cycles of forests during climatic oscillations affecting taxa to varying degrees. Congruent phylogeographic breaks for the aforementioned taxa coupled with the fact that biogeographic breaks for forest dwelling taxa along the IOCB have not explicitly been tested warrant further investigation among other co-distributed taxa, in an attempt to understand spatial and temporal factors causal to the observed break.

Forest living reptiles in South Africa exhibit proportionately lower diversity in comparison to the high diversity of reptile fauna in other biomes (Branch 1998; Bates et al., 2014). This may be due to the relatively recent establishment of forests along the IOCB (Lawes, 2007). The ancient Afrotemperate forests, on the other hand, are generally only occupied by species that

are either highly vagile and able to disperse among geographically isolated forest patches, generalist species from the surrounding habitat that occupy vacant niches or, in some cases, resilient taxa that survived extinction filtering events during cooler more arid periods (Lawes, 2007). Reptiles would be removed during extinction filtering events, resulting in communities that are therefore generally species-poor but ecologically robust and persistent (Balmford, 1996). Because of their limited dispersal abilities compared to other terrestrial vertebrates such as birds and mammals (Bonnet et al., 1999; Massot et al., 2008), reptiles are less likely to track climatic change, rendering them particularly susceptible to extinction filtering and range contraction or fragmentation (Araújo et al., 2006, 2008). This is particularly true for forest specialists during periods of unfavorable climatic conditions. In the present study we will, therefore, focus on two co-distributed forest dwelling fossorial snake species, the Natal black snake, *Macrelaps microlepidotus,* and the forest thread snake, *Leptotyphlops sylvicolus*, distributed in forest fragments along the Eastern Cape and KwaZulu-Natal provinces of South Africa.

The monotypic *Macrelaps microlepidotus* is a medium sized fossorial snake with a maximum snout to vent length (SVL) of 938 mm (Branch, 1998). The species has a strong affinity to forest habitats where it burrows in loamy soils and is generally active on the surface on warm humid evenings (Branch, 1998; Bates et al., 2014). It occurs along the Eastern Cape Province coastal belt and adjacent interior from East London to the northern KwaZulu-Natal Province (Bates et al., 2014). The latter species is co-distributed with *Leptotyphlops sylvicolus*, a small (SVL) 105 mm fossorial snake species (Broadley and Wallach, 1997) initially reported from three isolated forest habitats along the east coast by Broadley and Broadley (1999). However, there are recent collection records of *L. sylvicolus* specimens from grassland habitats that appear morphologically dubious (Bates et al., 2014). Adalsteinsson et al. (2009) observed deep genetic divergence within the *L. sylvicolus* species complex, alluding to the presence of cryptic species.

Thread snakes are small primitive snakes adapted to subterranean life with highly polished scales, a blunt head and blind with eyes reduced to black spots beneath the head shields (Branch, 1998). In such well adapted fossorial reptile taxa it is well documented that species boundaries have been widely obscured by the conservation of morphological characters, rendering molecular tools imperative in delineating operational taxonomic units (e.g. Daniels et al., 2006, 2009; Parham and Papenfuss, 2009; Siler et al., 2011; Valente et al., 2014). Increased alpha taxonomic diversity has been observed among South African fossorial reptiles, particularly among skinks that have been subjected to molecular systematic endeavors (Busschau et al., 2017, Engelbrecht et al., 2013; Lamb et al., 2010). The latter observation is especially true for taxa characterized by disjunct populations (often defined as subspecies) and taxa devoid of fine scale sampling and lacking recent molecular scrutiny,

suggesting that fossorial snakes may exhibiting high levels of genetic differentiation between assumed conspecific populations, as well as possibly exhibiting increased taxonomic diversity.

We aim to document and compare the phylogeographic diversity in the two co-distributed forest-dwelling snake species and examine the species boundaries in *L. sylvicolus* by incorporating both morphological and molecular data. Since both focal taxa are fossorial, forest-living, and largely co-distributed along the east coast of South Africa, they are expected to reveal congruent phylogeographic patterns in response to historic climatic oscillation. Because of its small size, *L. sylvicolus* is likely incapable of dispersing large geographic distances and is expected to exhibit higher genetic structure in comparison to the larger and presumably more vagile *M. microlepidotus*. Divergence time estimates are likely to reveal different evolutionary histories of the two taxa since we expect both deep and shallow divergences among the two snake species, while levels of cladogenesis are likely to coincide with habitat fragmentation due to past climatic events. Our hypotheses are twofold, first, the two focal snake taxa will show phylogeographic breaks congruent to those observed in other forest living reptile taxa, in the northeastern portions of Eastern Cape Province. Second, *L. sylvicolus* species complex will harbor several cryptic species in line with the general lineage concept, which identifies species as separately evolving metapopulation lineages that are recognizable using secondary criteria (de Queiroz, 1998), and demonstrate ancient cladogenesis in contrast to *M. microlepidotus* that will demonstrate both shallower and more recent population level differentiation.

3.2 Materials and Methods

3.2.1 Sample collection

Specimens of the two snake species were collected from forest and grassland habitat in the Eastern Cape and KwaZulu-Natal provinces of South Africa. A total of 41 *M. microlepidotus* tissue samples were acquired from predominantly forested habitat, while 94 *L. sylvicolus* specimens were collected from both forests and grasslands (Table 3.1; Fig. 3.1; Appendix 3.1). An additional 18 *Leptotyphlops* specimens were sampled from localities that are geographically proximate to known localities for *L. sylvicolus,* including topotypic localities (Broadley and Wallach, 1997). Where possible, at least five random specimens were collected per locality to optimize the probability of obtaining representative genetic variation (Morando et al., 2003). However, due to the reclusive nature of these two fossorial snake species, low sample numbers were collected in several localities despite exhaustive collection efforts. Voucher specimens of both taxa were humanely euthanized by injection with a tricaine methanesulfonate solution (Conroy et al., 2009), followed by a liver tissue biopsy and storage in absolute ethanol for further genetic analysis. For *M. microlepidotus* additional tissue

samples were obtained from live specimens by removing < 5 mm of the tail tip, taking belly scale clippings or from recently shed skin. Biopsied tissue was preserved in absolute ethanol for molecular work. Ethical clearance for the present study was obtained from the Port Elizabeth Museum (Bayworld) ethics committee (Ethical Clearance no. 2017-2). Carcasses were either preserved directly in 70% ethanol or injected with 4% formalin and immersed in formalin solution for a week prior to being transferred to 50% isopropanol for permanent storage in the herpetological collection of the Port Elizabeth Museum (PEM), Eastern Cape Province, South Africa (see Appendix 3.1 for accession numbers).
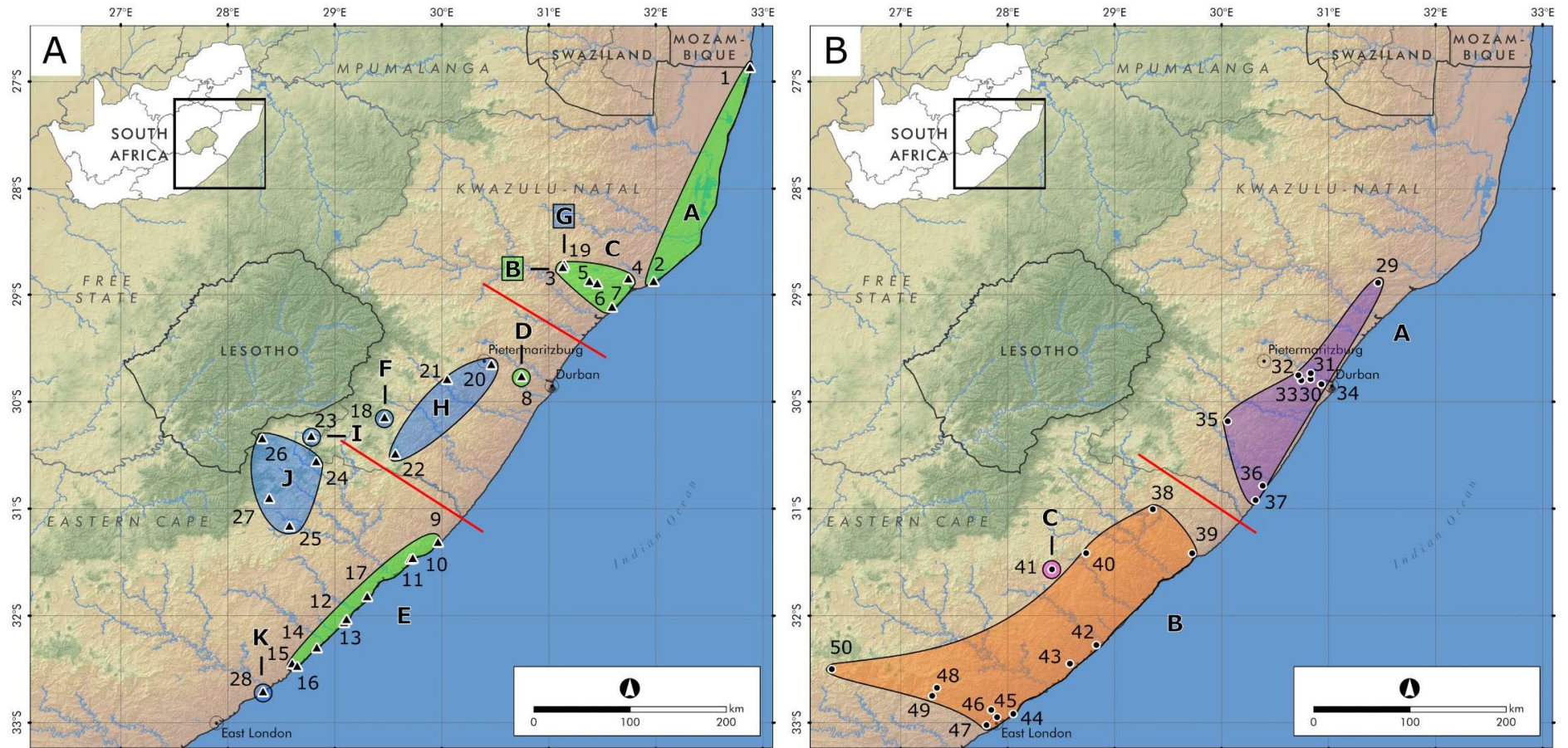
Figure 3.1. Maps showing localities in the Eastern Cape and the KwaZulu-Natal provinces of South Africa where the forest thread snake, *Leptotyphlops sylvicolus,* (Map A - triangles) and the Natal black snake, *Macrelaps microlepidotus,* (Map B - circles) were sampled during the present study. Numbers correspond to the sample locality numbers in Table 3.1. On Map A green polygons depict *L. sylvicolus* lineages sampled from forest localities and blue polygons depict lineages sampled from grassland habitats. On Map B coloured polygons depict the relative distribution of lineages in *M. microlepidotus*. Red lines depict the inferred biogeographic breaks referred to in the text.

51

Table 3.1. Localities where *Leptotyphlops sylvicolus* and *Macrelaps microlepidotus* specimens were collected for the present study. The locality number (#) corresponds to the number on the map in Fig. 3.1. *N* = the number of samples per locality. Locality 1 – 17 represent forest localities and 18 – 28 grassland localities within *L. sylvicolus*.

#	Locality Name	Province	*N*	Longitude E	Latitude S
	Leptotyphlops sylvicolus				
1	Xilonde	KwaZulu-Natal	2	-26.8683	32.8819
2	Empembeni	KwaZulu-Natal	2	-28.8732	31.9811
3	Nkandla Forest	KwaZulu-Natal	2	-28.7457	31.1368
4	Ngoye Forest	KwaZulu-Natal	10	-28.8518	31.7440
5	Dlinza Forest	KwaZulu-Natal	2	-28.8973	31.4550
6	Entumeni NR	KwaZulu-Natal	3	-28.8781	31.3833
7	Amatikulu NR	KwaZulu-Natal	2	-29.1126	31.5920
8	Hillcrest	KwaZulu-Natal	1	-29.7707	30.7509
9	Mkambati NR	Eastern Cape	9	-31.3153	29.9658
10	Njombela	Eastern Cape	2	-31.4712	29.7082
11	Mbotyi	Eastern Cape	6	-31.4652	29.7303
12	Hole In The Wall	Eastern Cape	6	-32.0375	29.1083
13	Lubanzi	Eastern Cape	5	-32.0650	29.0871
14	Dwesa NR	Eastern Cape	6	-32.3002	28.8321
15	Manubi Forest	Eastern Cape	3	-32.4501	28.6024
16	Mazzepa Bay	Eastern Cape	3	-32.4756	28.6503
17	Hluleka NR	Eastern Cape	2	-31.8232	29.3024
18	Ntsikeni NR	KwaZulu-Natal	2	-30.1468	29.4642
19	Nkandla Grassland	KwaZulu-Natal	2	-28,7067	31,1529
20	Ashburton	KwaZulu-Natal	1	-29.6524	30.4656
21	Ncwadi	KwaZulu-Natal	1	-29.7923	30.0502
22	Elandskuil	KwaZulu-Natal	5	-30.4839	29.5657
23	Matatiele	Eastern Cape	6	-30.3234	28.7782
24	Fever Village	Eastern Cape	3	-30.5591	28.8297
25	Ntywenka	Eastern Cape	1	-31.1625	28.5780
26	Ongeluksnek NR	Eastern Cape	3	-30.3456	28.3195
27	Upper Tsitsana	Eastern Cape	3	-30.9036	28.3885
28	Morgan's Bay	Eastern Cape	1	-32.7147	28.3304

Table 3.1 continued.

	Macrelaps microlepidotus				
29	Eshowe	KwaZulu-Natal	2	-28.8880	31.4599
30	Kloof	KwaZulu-Natal	3	-29.7899	30.8313
31	Waterfall	KwaZulu-Natal	1	-29.7384	30.8325
32	Assagay	KwaZulu-Natal	1	-29.7530	30.7211
33	Hillcrest	KwaZulu-Natal	3	-29.7968	30.7423
34	Westville	KwaZulu-Natal	3	-29.8375	30.9331
35	Ixopo	KwaZulu-Natal	1	-30.1873	30.0601
36	Shelley Beach	KwaZulu-Natal	1	-30.7860	30.3852
37	Southbroom	KwaZulu-Natal	2	-30.9220	30.3151
38	Gomo Forest	Eastern Cape	2	-31.0095	29.3578
39	Mbotyi	Eastern Cape	1	-31.4198	29.7238
40	Nqadu	Eastern Cape	1	-31.4208	28.7354
41	Baziya	Eastern Cape	1	-31.5684	28.4138
42	Dwesa NR	Eastern Cape	2	-32.2763	28.8271
43	Manubi Forest	Eastern Cape	5	-32.4491	28.5894
44	Sunrise on Sea	Eastern Cape	2	-32.9188	28.0499
45	Dorchester Heights	Eastern Cape	2	-32.9508	27.9009
46	Thorn Park	Eastern Cape	2	-32.8828	27.8506
47	East London	Eastern Cape	1	-33.0260	27.8052
48	Isedenge	Eastern Cape	1	-32.6767	27.3403
49	Pirie	Eastern Cape	1	-32.7521	27.2950
50	Hogsback	Eastern Cape	3	-32.5031	26.3583

3.2.2 DNA sequencing

Total genomic DNA was extracted from tissue samples (either liver, muscle or skin) using a MacheryNagel DNA extraction kit, following the manufacturer's extraction protocol. Following extraction, DNA was stored at -20°C until required for the polymerase chain reaction (PCR). Two mitochondrial (mt) and two nuclear (nu) DNA markers were sequenced for all specimens from both taxa. However, for the two nuDNA loci we only sequenced a single sample per locality in *L. sylvicolus* since preliminary results revealed low intrapopulation variation in *L. sylvicolus* and overall low variation for *M. microlepidotus* for the nuDNA loci. Noticeable exceptions were made for *L. sylvicolus* where two divergent clades were present at a site as observed with the mtDNA data, resulting in additional nuDNA sequences at these sites. The two mtDNA loci selected were cytochrome b (*cyt b*) and nicotinamide adenine dinucleotide dehydrogenase subunit 4 (*ND4*). The latter two mtDNA loci are widely used in reptile phylogeograpic studies (Blair and Bryson, 2017; Díaz et al., 2017; Makhubo et al., 2015; Medina et al., 2016; Portillo et al., 2018; Vidal et al., 2008; Kullenkampf et al., 2019).The primer pairs *ND4* (5'-ACC TAT GAC TAC CAA AAG CTC ATG TAG-3') (Arévalo et al., 1994) and H12763V (5'-TTC TAT CAC TTG GAT TTG CAC CA-3') (Barlow et al., 2013) were used to amplify the *ND4* locus, while for the *cyt b* region the primer pairs used were WWF (5'-AAA YCA YCG TTG TWA TTC AAC TAC-3') and R2 (5'- GGG TGR AAK GGR ATT TTA TC-3') (Whiting et al., 2003). The prolactin receptor (*PRLR*) and the recombination activating gene 1 (*RAG1*) were targeted as nuDNA sequence markers since they exhibit variation at the intraspecific levels and have been used extensively in the literature (Busschau et al., 2017; Diedericks and Daniels, 2013; Heinicke et al., 2017a,b; Medina et al., 2016). For *PRLR* the primers used were *PRLR*_f1 (5'-GAC ARY GAR GAC CAG CAA CTR ATG CC -3') and *PRLR*_r3 (5'-GAC YTT GTG RAC TTC YAC RTA ATC CAT -3') (Townsend et al., 2008), while for the *RAG1* locus the primers L2408 (5'-TGC ACT GTG ACA TTG GCA A-3') and H2920 (5'-GCC ATT CAT TTT YCG AA-3') (Vidal and Hedges, 2004) were used. For each PCR, a 25-μL reaction was performed that contained 14.9 μL of Millipore water, 3 μL of 25 mM $MgCl_2$, 2.5 μL of 10× Mg^{2+} free buffer, 0.5 μL of a 10 mM dNTP solution and 0.5 μL of the primer sets at 10 mM, 0.1 unit of *Taq* polymerase and 1–3 μL of template DNA. The PCR temperature regime for the two mt DNA markers was 94 °C for 4 min., 94 °C for 30 sec., 50 °C for 40 sec.,72 °C for 40 sec., and then 36–40 cycles of the last three steps, followed by a final extension of 10 min., at 72 °C. For the two nuDNA markers the temperature regime was 95 °C for 2 min., 95 °C for 35 sec., 48 °C for 35 sec., 72 °C for 60 sec., and then 36–40 cycles of the last three steps, followed by a final extension of 10 min., at 72 °C. The annealing temperature was optimized for each primer pair and ranged between 46°C and 50°C. PCR products were electrophoresed for 2–3 hours at 90V in a 1% regular agarose gel containing ethidium bromide, visualized under UV light and purified using a BIOFLUX gel purification kit. Purified PCR products were cycle sequenced using standard protocols (3 μL of the purified

PCR product, 4 µL of the fluorescent-dye terminators with an ABI PRISM Dye Terminator Cycle Sequencing Reaction Kit, PerkinElmer, and 3 µL of a 10 µM primer solution for each primer pair). Unincorporated dideoxynucleotides were removed by gel filtration using Sephadex G-25 (Sigma). Sequencing was performed on an ABI 3730 XL automated machine housed at the central analytical facility of Stellenbosch University.

3.2.3 Phylogenetic analysis

Sequences were aligned manually and checked for base ambiguity in Sequence Navigator (Applied Biosystems), while the presence of stop codons in all four protein coding loci were checked using MEGA X (Kumar et al., 2016). Due to the morphological conservation and paraphyly observed within *Leptotyphlops*, all available *Leptotyphlops* sequences (*cyt b*) from GenBank (Adalsteinsson et al., 2009) were downloaded and aligned with sequences generated during the present study. The three most basal species, *L. nigroteminus*, *L. merkeri* and *L. pitmani*, were employed as outgroups. For the *M. microlepidotus* phylogeny ten sequences (*ND4* and *cyt b*) for the closest sister species, *Amblyodipsas concolor*, were included to compare the results from the divergence time estimates in the present study to those observed by Portillo et al. (2018). Sequences for *Amblyodipsas ventrimaculata, A. microphthalma, A. unicolor, A. dimidiata, A. polylepis, Xenocalamus michelli, X. mechowii, X. transvaalensis* and *X. bicolor* for both *cyt b* and *ND4* were included as outgroups. The phylogenetic analyses were performed on the concatenated *cyt b* and *ND4* mtDNA dataset and included all samples. A single sequence per locality for each nuDNA and mtDNA marker was used for the total-evidence topology in *L. sylvicolus.* The total-evidence topology included *L. sylvicolus* along with the additional *Leptotyphlops* specimens collected in the present study. Maximum likelihood (ML) and Bayesian inference (BI) were used to infer phylogenetic relationships. jModeltest v2.1.10 (Posada, 2008) was used to identify the best fitting substitution models for each of the individual marker datasets under the corrected Akaike information criterion (see Appendix 2 for substitution models used in each analysis). DAMBE v5 (Xia, 2013) was used to assess saturation and each dataset subsequently partitioned per gene. Bayesian inference (BI) was performed in MrBayes v3.2.2 (Ronquist et al., 2012), via the Cipres Science Gateway v3.3 available from http://www.phylo.org. For each analysis, four Markov chains were run, starting from a random tree and run for 20×10^6 generations, sampling each chain every 1000th tree. A 50% majority rule tree was constructed with 20% of the sampled trees discarded as burn-in and nodes with ≥0.95 posterior probability were considered supported. A partitioned maximum likelihood (ML) analysis was run in Garli v2.01 (Zwickl, 2006) on the Cipres Science Gateway with 1000 bootstrap replicates. A 50% majority rule bootstrap consensus tree was calculated in PAUP* v4.0a (Swofford, 2002). Bootstrap values ≥75% were regarded as well supported. Sequence divergence values of each marker between observed clades were calculated in MEGA X.

Automatic barcode gap discovery (ABGD) was employed to identify candidate lineages for further analyses. ABGD was performed on the *cyt b* datasets for each taxon via the ABGD web interface (http://wwwabi.snv.jussieu.fr/public/abgd/, web version 'May 19 2019'). ABGD is designed to infer species hypotheses based on automatized identification of a barcode gap between inter- and intraspecific pairwise distances. Simple p-distance metrics were selected along with default priors for minimum barcode gap width prior (1.5) and intraspecific divergence minima (0.001) and maxima (0.1).

3.2.4 Divergence-time estimates

Bayesian Evolutionary Analysis Sampling Trees (BEAST) v2.4.8 (Bouckaert et al. 2014) was used on the combined mitochondrial dataset to determine when cladogenic events occurred in each species. The mitochondrial dataset was chosen for the divergence time estimation because of known substitution rates for the mtDNA markers. Adalsteinsson et al. (2009) made use of distant fossil calibrations to date the Leptotyphlopidae phylogeny, however, the divergence time estimates within *Leptotyphlops* and specifically *L. sylvicolus* were ancient and retrieved broad confidence intervals. Therefore, we assumed a mitochondrial mutation rate of 0.65% per million years as proposed by Macey et al. (1998) and used in several recent publications to date squamate phylogenies (e.g. Lavin et al., 2018; Stanley and Bates, 2014). Recent publications on the more modern Caenophidians also use a rate of 0.65% per million years (e.g. Guo et al., 2019), however, others employed a rate of 1.34% per million years (e.g. Myers et al., 2017). The latter rate was based on fossil calibrated divergence time estimates for *cyt b* and *ND4* in colubroid snakes (Daza et al., 2009), and was recently used to date divergence times in *Duberria lutrix lutrix* which, like *M. microlepidotus*, is a lamprophiid (Kullenkampff et al., 2019). Therefore, we assumed the mean of these rates (0.995% per million years) to date the *M. microlepidotus* phylogeny while implementing 0.65% and 1.34% as the lower and upper limits, respectively. These calibrations were implemented in the Bayesian Evolutionary Analysis Utility (BEAUti) and executed in BEAST with a Yule prior and a strict molecular clock with a lognormal distribution. A Markov Chain Monte Carlo was run for 20 million generations, sampling every 1000th generation. Tracer v1.6 (Rambaut et al. 2014) was used to assess the chain convergence (ESS > 200) and TreeAnnotator, included in the BEAST package, was used to discard 20% of the sampled trees as burn-in and determine the maximum clade credible tree. Trees were viewed and edited in FigTree (Rambaut, 2016) and TreeGraph2 (Stöver and Müller, 2010) and additional annotations made in Inkscape (www.inkscape.org).

3.2.5 Population genetic analyses

To examine genetic relationships among sample localities in each of the focal taxa, haplotype networks were constructed in TCS 1.21 (Clement et al., 2000) using statistical parsimony with

95%. For *L. sylvicolus* the *cyt b* dataset was selected as this was the most complete dataset with regard to the number of missing sequences. For *M. microlepidotus* a concatenated mtDNA dataset was possible due to the lack of missing sequences for both *cyt b* and *ND4* locus. Hierarchical analysis of molecular variance (AMOVA) was performed in Arlequin v3.1 (Excoffier et al., 2005) to investigate the distribution of genetic variation among lineages.

3.2.6 Species tree and species delimitation in L. sylvicolus

Species tree and species delimitation analyses were performed for *L. sylvicolus* because there are known taxonomic inconsistencies in this species. To delineate species boundaries in *L. sylvicolus,* the Bayesian implementation of the general mixed yule coalescent model (bGMYC) was employed on the mtDNA dataset and the combined species tree estimation and species delimitation analysis was performed in Species Tree and Classification Estimation, Yarely - STACEY v.1.2.1 (Jones, 2017), in BEAST2, from all four loci (*cyt b*, *ND4*, *RAG1* and Prolactin). The bGMYC analysis was applied to 500 posterior trees from the mtDNA BEAST runs, implementing 50,000 MCMC steps with 40,000 steps as burn-in and sampling every 100 steps, in R Studio Version 1.1.456 using the package bGMYC v. 1.0.2 (Reid and Carstens, 2012; R Core Team 2014).

The STACEY analysis was employed with a representative sample from each *L. sylvicolus* locality (*N*=29) as well as a representative sample from the *L. conjunctus* and *L. nigricans* localities sequenced in the present study (N=15). In STACEY the possible number of putative species range from one to the number of minimal clusters specified. In this analysis each locality was defined as a taxon set or minimal cluster, i.e. without a priori species definition. The input files (.xml) were created using BEAUti, implementing a Yule Model prior to estimate the species tree [priors: Collapse Height=0.001, Collapse Weight=0.5 using a beta prior (1.1) around [0.1], bdcGrowthRate = log normal (M=4.6, S=1.5); popPriorScale = log normal (M=-7, S=2); relativeDeathRate = beta (alpha=1.0, beta=1.0); Ploidy: equal 2 for nuDNA loci and 0.5 for mtDNA loci], a strict molecular clock with a clock rate of 0.65% per million years was defined for the two mtDNA loci and the rate for the two nuDNA loci estimated from the mtDNA rate. The MCMC analysis was set to run for 1 billion generations, saving the result every 50,000 generations. The obtained log files were analyzed with Tracer to verify convergence of the analysis. Convergence was reached for all traces after 300 million generations (ESS > 200). SpeciesDelimitationAnalyser (Jones et al., 2015) was used to process the log files and examine the clusters of species assignments. Posterior probabilities of localities belonging in the same cluster were visualized in a similarity matrix constructed in R Studio Version 1.1.456 (R Core Team 2014). A second analysis was performed in STACEY where the clusters visualized in the similarity matrix were defined as minimal clusters.

3.2.7 Morphological analyses of L. sylvicolus

A total of 71 sequenced adult specimens of *L. sylvicolus* were examined (see Appendix 1 for a list of specimens)*.* Specimens were considered adults when they exhibited a total length within the 40% range of the maximum total length reported in Broadley and Wallach (1997). Phenotypic variables included 20 morphometric measurements and five meristic counts known to be taxonomically informative among Leptotyphlopidae (Adalsteinsson et al., 2009; Broadley and Wallach, 1997; Hedges, 2008) (See Appendix 3.3 for a list of variables). Body measurements were measured with a digital caliper to an accuracy of 0.01 mm. For the scalation measurements images were taken using an Image Source DFK 72AUC02 camera attached to a Nikon SMZ1270 binocular stereo microscope and characters measured in NIS-Elements Microscope Imaging Software (Nikon) to an accuracy of 0.01mm. All statistical analyses were carried out in SPSS v25.0 (IBM Corp.).

For the univariate and multivariate statistical analyses, the datasets were subdivided into putative species as they were identified by STACEY. For comparison all putative species were included in the meristic analysis (N=71), despite the low sample sizes in several groups. However, to obtain statistically meaningful results in the morphometric analyses only the three putative species with adequate sample sizes were included (Total, N=59; species C, N=15; species E, N=31; species I+J=13). From the meristic scale counts, the number of midbody scale rows (MBS=14), Supralabial scales (SLS=2) and mid-tail scale rows (MTS=10) were constant across all specimens. Therefore, these variables were excluded from the analyses. A non-parametric Kruskal Wallis test was used to compare the number of middorsal scale rows and subcaudal scales between putative species. For the post-hoc tests the Bonferroni correction was applied as it adjusts the significance levels for multiple tests, reducing the possibility of Type I errors (Rice, 1989).

For the morphometric analysis 21 ratios of morphometric measurements were used as input data (see Table 3.3 for the ratios used). The dataset was tested for multivariate outliers using Mahalanobis distance. Subsequently, a multivariate analysis of variance (MANOVA) was used to test whether there are differences in the morphometric ratios between the three putative species. Sets of morphometric ratios that contribute to the overall morphological differences were then identified through a principal component analysis (PCA). Only principal components with eigenvalues larger than 1.0 were considered. The number of variables with high loadings on each principle component were minimized by using the varimax rotation with Kaiser normalization. The saved principal component scores were used in an analysis of variance (ANOVA) followed by Bonferroni post hoc tests to examine the differences between clades. A discriminant function analysis (DFA) was used to explore structuring of the data in a morphometric space and determine whether individuals could be assigned to the correct groups based on the morphometric characters.

3.2.8 Alternative phylogenetic hypotheses

The combined total-evidence dataset was used to test alternative phylogenetic hypotheses based on the results of the molecular and morphological analyses of the present study. A ML phylogeny was estimated with the online version of IQ-TREE 1.4.3 (Trifinopoulos et al., 2016). The best-fit substitution model for each gene-partition was determined by selecting the "auto" option. To evaluate alternative hypotheses, seven constrained topologies were compared to the unconstrained ML tree using the Shimodaira–Hasegawa (SH) and approximately unbiased (AU) tests with 10,000 replicates (Shimodaira and Hasegawa, 1999; Shimodaira, 2002).

3.3 Results

3.3.1 Mitochondrial DNA tree topology and divergence-time estimation

The *Leptotyphlops* mtDNA dataset consisted of 1194 base pairs (bp), containing 588 bp and 606 bp for the *cyt b* and *ND4* loci, respectively, and 331 variable sites among the *L. sylvicolus* sequences across the entire alignment (see Appendix 3.1 for GenBank accession numbers). The dataset comprises 139 samples of which 94 samples belong to *L. sylvicolus*. The concatenated mtDNA maximum likelihood (ML), Bayesian inference (BI) and BEAST analyses recovered congruent topologies, hence only the BEAST topologies are shown (Fig. 3.2, Appendix 3). *Leptotyphlops sylvicolus* was monophyletic and comprised two statistically well-supported clades (clades 1 and 2) (BI >0.95 Pp /BEAST >0.95 Pp /ML >75%) (Fig. 3.2). The remaining 18 *Leptotyphlops* specimens sequenced in the present study grouped with *L. nigricans* (one sample) and *L. conjunctus* (17 samples) sequences from Adalsteinson et al. (2009) in four clades (see Appendix 3.2). Within *L. sylvicolus,* clade 1 comprises localities along the Eastern Cape and KwaZulu-Natal coast and adjacent interior of KwaZulu-Natal where specimens were sampled from forest habitats, along the forest edge and the adjacent grasslands (Fig. 3.3), with the exception of the Ntsikeni Nature Reserve (F) being a predominantly grassland habitat. In contrast, clade 2 is comprised entirely of specimens collected from grassland habitats in the interior of the Eastern Cape and KwaZulu-Natal provinces, and Morgan's bay along the Eastern Cape coast (Fig. 3.3). Clade 1 and 2 are near sympatric at Nkandla, KwaZulu-Natal.

The ABGD identified six and five lineages within clades 1 and 2, respectively, with a prior intraspecific divergence of 1% (Fig. 3.2). Lineages in both clades were statistically well-supported by the mtDNA phylogenetic analyses and generally characterized by long branch lengths between lineages. The average uncorrected 'p-distance' between clades 1 and 2 is 7% for *cyt b* and 12% for *ND4* and <5% and <6% within clades for *cyt b* and *ND4*, respectively. Uncorrected 'p-distance' between lineages in clade 1 range between 4–5% for *cyt b* and 5–

8% for *ND4* and in clade 2 between 4-8% for *cyt b* and 3–11% for *ND4*. Within lineages the uncorrected 'p-distance' is <2% for both *cyt b* and *ND4*.

Divergence-time estimates suggest the two *L. sylvicolus* clades diverged during the middle Miocene 13.8 Million years ago (95% HDP, 12.1–15.8 Mya) (Fig. 3.2). Subsequent divergences among lineages in clade 1 occurred from the late Miocene 8.2 Mya (95% HDP, 6.9-9.5 Mya) to the early Pleistocene 4.6 Mya (95% HDP, 3.3-5.9 Mya). Divergence times among lineages in clade 2 date from the late Miocene 11.7 Mya (95% HDP, 9.9-13.5 Mya) to the early Pleistocene 4.6 Mya (95% HDP, 3.6-5.7 Mya).

The *M. microlepidotus* mtDNA dataset consisted of 1294 bp containing 610 bp and 684 bp for the *cyt b* and *ND4* loci, respectively, with 49 variable sites within *M. microlepidotus* across the entire alignment (see Appendix 3.1 for GenBank accession numbers). The concatenated mtDNA maximum likelihood (ML), Bayesian inference (BI) and BEAST analyses recovered congruent topologies, hence only the BEAST topology is shown (Fig. 3.3). *Macrelaps microlepidotus* was monophyletic (BI >0.95 Pp /BEAST >0.95 Pp /ML >75%) (Fig. 3.2). The specimen from Baziya was basal and the remaining samples comprise two statistically well-supported sister clades, A and B. Samples in clade A were collected from the coastal and fragmented inland forest patches in the KwaZulu-Natal Province, while samples in clade B were collected from the coastal and adjacent forested interior of the Eastern Cape Province. Within M. *microlepidotus*, ABGD identified two lineages (A+B, C) at an intraspecific divergence prior of 1% and three lineages (A, B, C) at 0.5% (Fig. 3.3).The average uncorrected 'p-distance' between lineages was 1–3% for *cyt b* and 0.4–1% for *ND4*. The uncorrected 'p-distance' within lineages was <0.3% for *cyt b* and <0.1% for *ND4*.

The divergence-time estimates suggest *M. microlepidotus* and its sister species, *A. concolor,* diverged during the middle Miocene 15.3 Mya (95% HDP, 10.7–20.3 Mya). Within *M. microlepidotus*, the initial divergence occurred during the Pleistocene 1.35 Mya (95% HDP, 0.87-1.93 Mya) when Baziya (lineage C) diverged from the remaining two lineages, followed by the divergence between lineage A and B 0.65 Mya (95% HDP, 0.39-0.95 Mya).
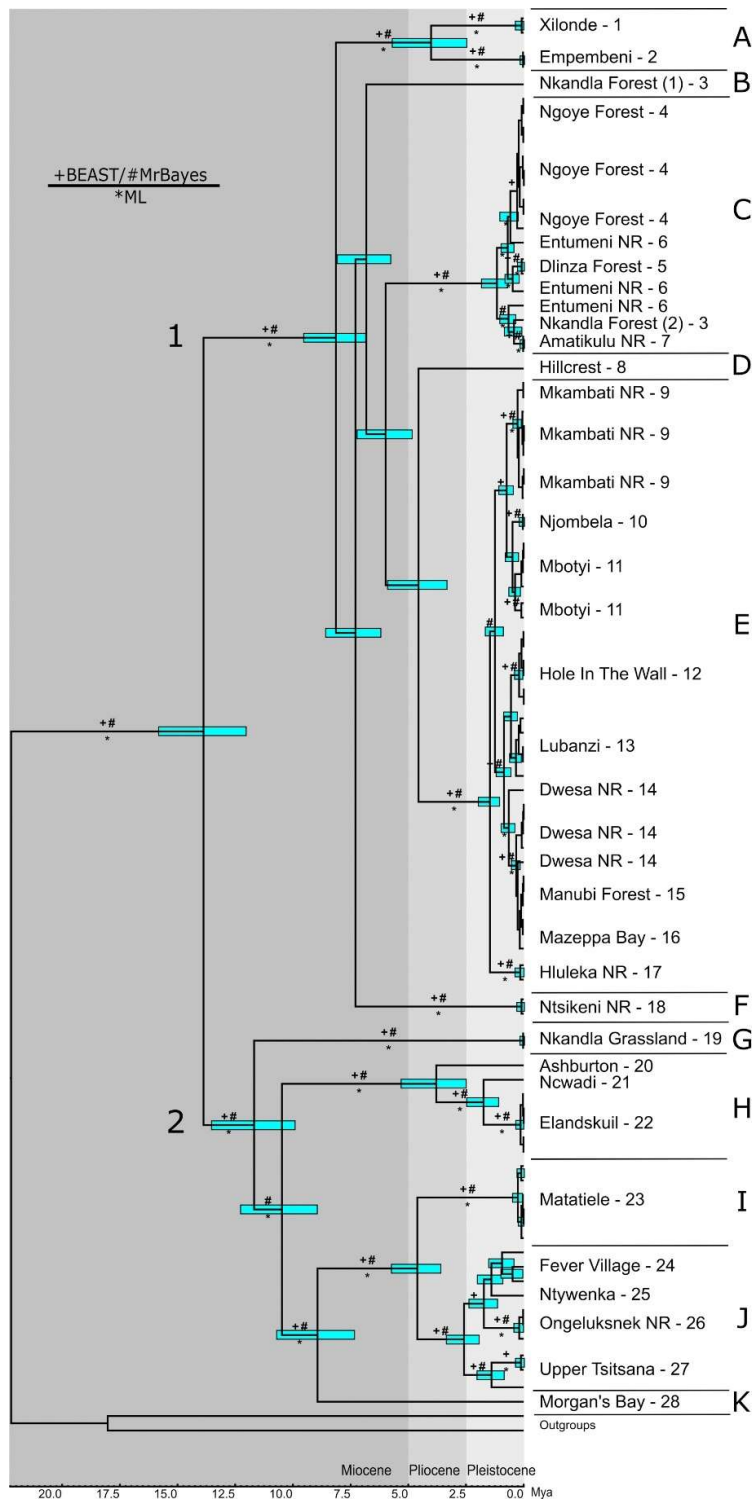
Figure 3.2. Bayesian phylogeny derived from the two mtDNA loci, *cyt b + ND4* for the *Leptotyphlops sylvicolus* species complex. Symbols represent support for maximum likelihood bootstrap > 75% (*) and posterior probabilities >0.95 from the BEAST (+) and MrBayes (#) analyses. Node bars show 95% highest posterior distributions for each estimated divergence date. Numbers show clades 1 and 2. Letters (A – K) denote the candidate lineages identified by the ABGD analysis. Numbers next to locality names correspond to the locality numbers on the map in Fig. 3.1.

61
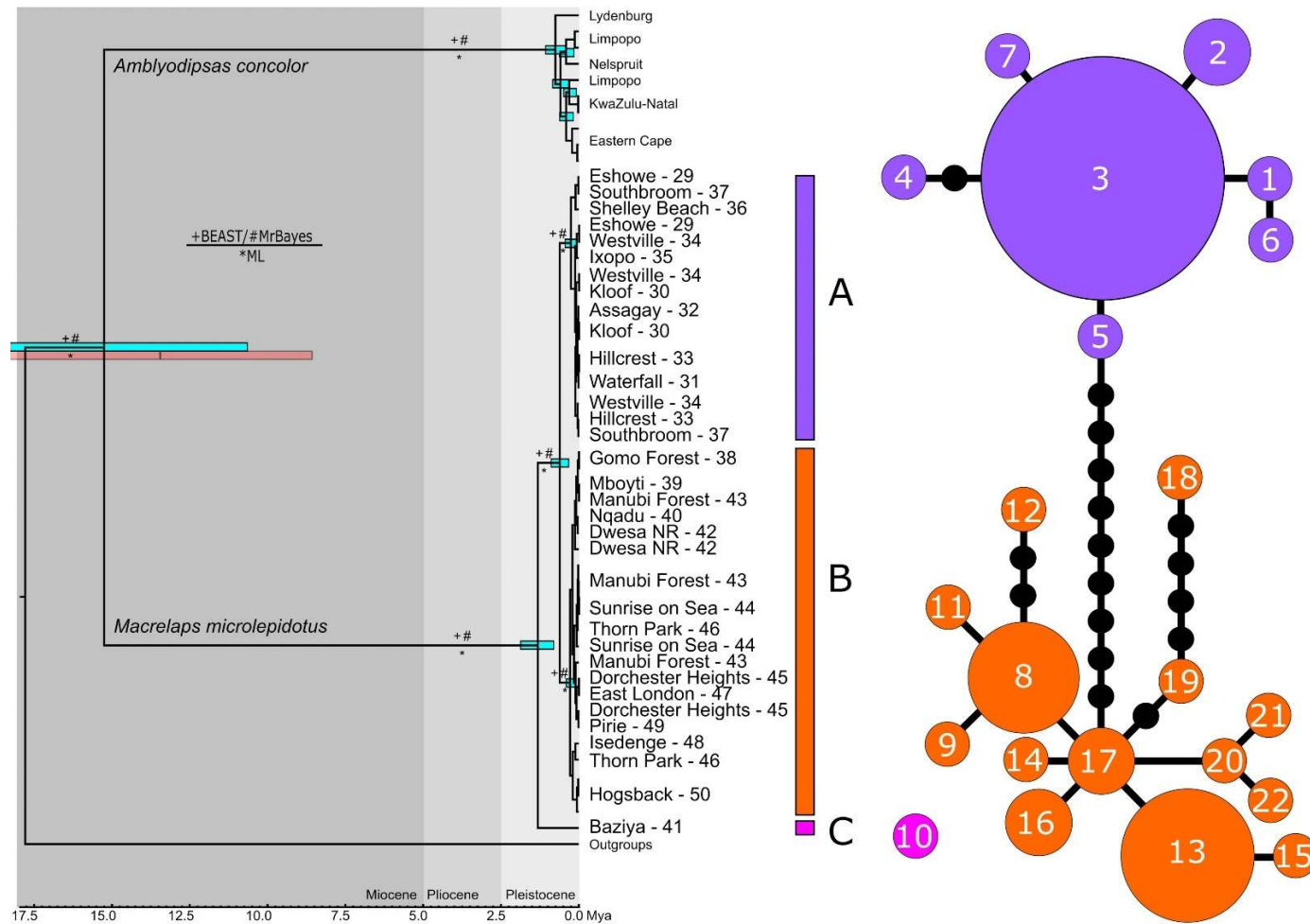
Figure 3.3. Results from the molecular analyses for *M. microlepidotus*. Bayesian phylogeny derived from the two mt DNA loci, *cyt b + ND4* with symbols representing support for maximum likelihood bootstrap > 75% (*) and posterior probabilities >0.95 from the BEAST (+) and MrBayes (#) analyses. Blue node bars show 95% highest posterior distributions for each estimated divergence date from the present study. The red node bar shows the mean and 95% highest posterior distributions for the estimated divergence date between *M. microlepidotus* and *A. concolor* from Portillo et al. (2018). Colored bars next to the tree represent the relative position of each lineage on the mtDNA phylogeny which correspond with the colors of the 95% haplotype network based on the concatenated mtDNA dataset. Haplotype numbers correspond to the samples listed in Appendix 3.1. Numbers next to locality names correspond to the locality numbers on the map in Fig. 3.1.

62

3.3.2 Total DNA evidence tree topology for L. sylvicolus

The total DNA evidence dataset consisted of 2180 bp (485 bp for the *RAG1* locus and 501 bp for the *PRLR* locus plus the two mtDNA loci) with 12 and 35 variables sites for *PRLR* and *RAG1*, respectively, among *L. sylvicolus* sequences (see Appendix 3.1 for GenBank accession numbers). The concatenated ML and BI analyses as well as the STACEY minimum cluster tree retrieved congruent topologies hence only the STACEY tree is shown (Fig. 3.4). The relationships among sampling localities were congruent with those retrieved in the mtDNA topology (Fig. 3.2). *Leptotyphlops sylvicolus* was again monophyletic and statistically well-supported with identical relationships to those retrieved in the mtDNA dataset with marginally greater nodal support.

The uncorrected 'p-distance' for the two nuclear loci between clades 1 and 2 was 1% for both *PRLR* and *RAG1*. The within clade sequence divergences were <0.6% for *PRLR* and <0.5% for *RAG1*. In clade 1 the uncorrected 'p-distance' between lineages ranged between 0.4–0.9% for the *PRLR* locus to 0.1–0.9% for the *RAG1* locus. In clade 2 the uncorrected 'p-distance' between lineages ranged between 0.1–1% for the *PRLR* locus to 0.1–0.4% for the *RAG1* locus. The uncorrected 'p-distance' within lineages was 0.1–0.8% for *PRLR* and <0.2% for *RAG1*.

The *RAG1* topology was largely unresolved yet lineage C and E were well-supported (Appendix 3.4). The *RAG1* topology also retrieved supported monophyly for Matatiele (lineage I) and Upper Tsitsana (lineage J). The *PRLR* topology corroborates the *RAG1* and mtDNA topologies with statistical support for lineage C and E. In contrast, the *PRLR* topology supports Nkandla Forest 1 (lineage B) within lineage C. The majority of grassland localities in Clade 2 comprise a well-supported clade with the exclusion of Nkandla Grassland (lineage G) and Ncwadi (lineage H). In contrast to the mtDNA topology, the *PRLR* topology retrieved Hillcrest (lineage D in clade 1) as part of this clade comprising grassland localities from clade 2.
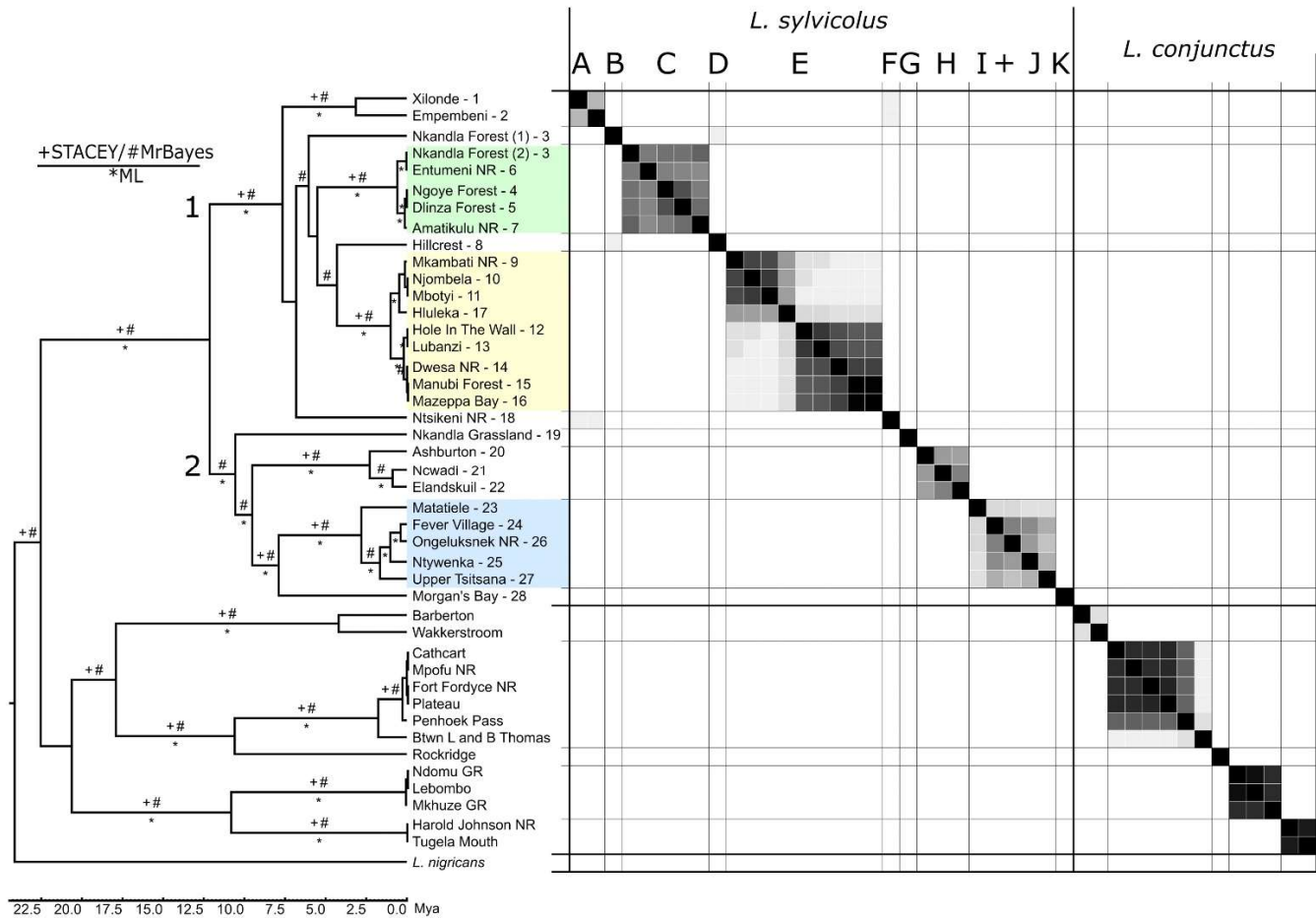
Figure 3.4. STACEY maximum clade credibility minimum cluster tree from the total-evidence dataset comprising four loci (*cyt b*, *ND4*, *RAG1* and *PRLR*) with symbols representing posterior probabilities from STACEY (+) and MrBayes (#) analyses >0.95 and maximum likelihood (*) bootstrap values > 75%. Numbers next to locality names correspond to the numbers on the map in Fig. 3.1. The squares in the similarity matrix represent posterior probabilities (white = 0, black = 1) for pairs of individuals (sample localities) to belong to the same cluster. The lines in the matrix separate putative species boundaries based on the observed clusters. Bold lines separate species complexes. Colored shading denotes the putative species tested for morphometric differences.

64

3.3.3 Population genetic analyses

From the 89 *L. sylvicolus cyt b* sequences (see Appendix 3.1 for samples that failed to amplify) 43 haplotypes were retrieved using the 95% connection limit (Fig. 3.5). In lineages C, E and J there are six, 18 and eight haplotypes, respectively, that are characterized by several unsampled or missing haplotypes. Lineage I comprises two haplotypes from one locality while the remaining lineages comprise a single unconnected haplotype at each locality.

The AMOVA results over all *L. sylvicolus* sample localities indicate marked genetic structure with 83.1% of the variation occurring among lineages, 14.8% of the variation among localities within lineages and 2.1% variation within localities (Table 3.2A). All fixation indices from the hierarchical analysis were high and statistically supported. Pairwise F_{ST} values between sample localities in different lineages are generally high and statistically supported for comparisons where there are more than one sequence (See Appendix 3.4A).

The combined mtDNA dataset for *M. microlepidotus* yielded 22 haplotypes. Baziya (lineage C) is separate from the two main clades, while lineages A and B are separated by nine mutational steps. Lineage A comprised seven haplotypes while lineage B comprised 14 haplotypes. The results from the hierarchical AMOVA indicated marked genetic structure with 85.76% of the variation among lineages (Table 3.2B). Variation among sample localities within lineages was low, 3.99%, compared to the variation within sample localities, 10.25%. The fixation index among lineages is high while the fixation index among localities within lineages is relatively low. These results are corroborated by high pairwise F_{ST} values between lineages and low significant pairwise F_{ST} values between localities within lineages (See appendix 3.5B).

3.3.4 Species tree and species delimitation for L. sylvicolus

Results from the bGMYC analysis largely corroborate lineages from the ABGD analysis on the mtDNA datasets, identifying all lineages in *L. sylvicolus* as putative species. The two localities in lineage A are, however, recognized as two putative species. When defining localities as minimal clusters, STACEY retrieved a large number of possible delimitations with low posterior probabilities, ranging from 15 to 29 clusters. Upon visual inspection of the similarity matrix (Fig. 3.4), it is however clear that there are ten broader clusters with high posterior support for individuals belonging to each cluster (Pp > 0.95). Clusters in the similarity matrix largely correspond to the lineages identified in the mtDNA phylogenetic analysis, however, lineages I and J were grouped together. There was also low posterior support for lineages A and F and lineages B and D belonging to the same cluster. When defining ten minimal clusters as they were visualized from the first delimitation analysis in STACEY, there was high statistical support (Pp = 0.99) for ten putative species.
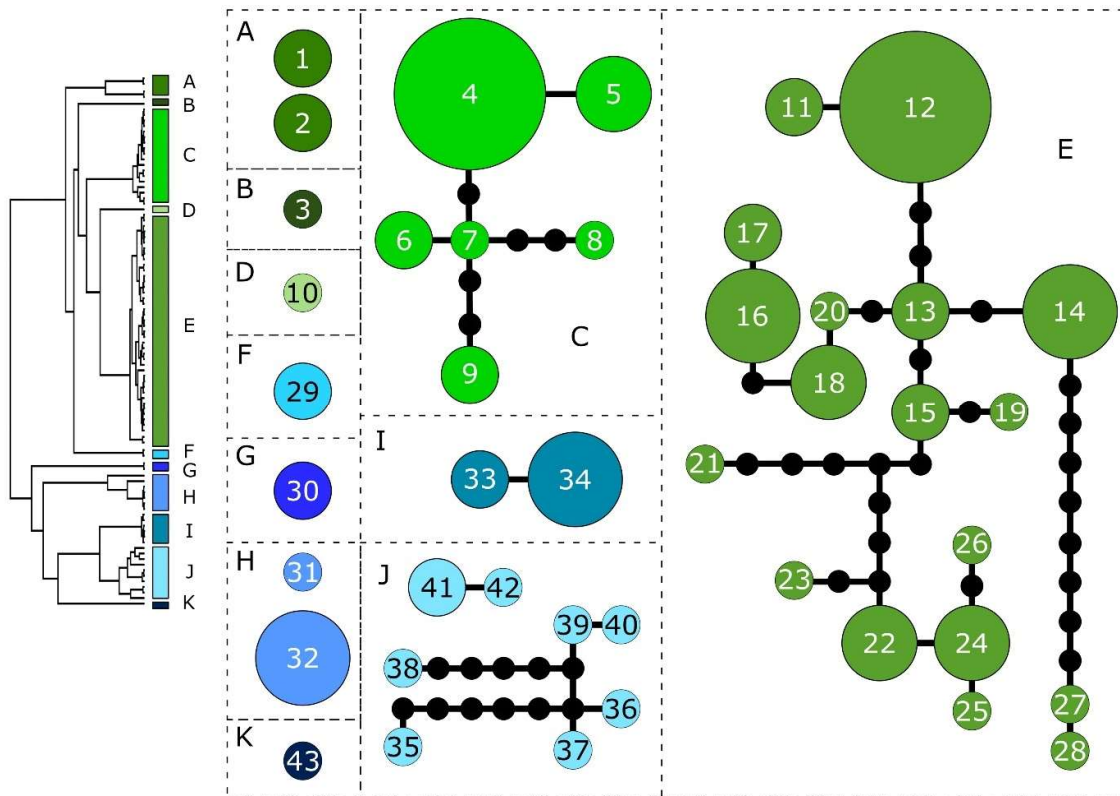
Figure 3.5. 95% haplotype network based on the mtDNA *cyt b* sequences for *Leptotyphlops sylvicolus*. Colored bars represent the relative position of each lineage on the mtDNA phylogeny. Haplotype numbers correspond to the samples listed in Appendix 3.1.

Table 3.2.

A. Hierarchical AMOVA on the *L. sylvicolus cyt b* dataset for 28 sampling localities. All values are statistically significant ($p < 0.001$).

Source of variation	Variation	Variation (%)	Fixation index[a]
Among lineages	Va 19.40128	83.09	F_{CT} 0.83089
Among localities	Vb 3.45062	14.78	F_{SC} 0.87383
Within localities	Vc 0.49821	2.13	F_{ST} 0.97866

B. Hierarchical AMOVA on the combined mtDNA dataset for *M. microlepidotus* from 22 sampling localities. All values are statistically significant ($p < 0.001$).

Among lineages	Va 6.29928	85.76	F_{CT} 0.85763
Among localities	Vb 0.29331	3.99	F_{SC} 0.28029
Within localities	Vc 0.75263	10.25	F_{ST} 0.89753

a F_{CT} = Va/VT, F_{SC} = Vb/(Vb + Vc), F_{ST} = (Va + Vb)/VT, where VT is the total of the variance components (Va + Vb + Vc).

66

3.3.5 Morphological analyses of L. sylvicolus

The Kruskal Wallis test indicated that there was a significant difference in the number of middorsal scale rows (MDS) among putative species (H = 47.31, p < 0.001; Fig. 3.6). Pairwise comparisons with the Bonferroni correction indicated that species C (MDS: 170 – 196) and E (MDS: 176 – 206) each had a significantly lower number of mid-dorsal scale rows than species I+J (MDS: 209 – 235). Furthermore, there was also a significant difference in the number of subcaudal scales (SCS) among putative species (Kruskal Wallis: H = 28.22, p = 0.001; Fig. 3.6). Pairwise comparisons with the Bonferroni correction indicated that species C (SCS: 18 – 23) had a significantly lower number of subcaudal scales than species I+J (SCS: 21 – 29).

The MANOVA on the morphometric data indicated that there are significant morphological differences among the three putative species - C, E and I+J (Wilks' λ = 0.127, p < 0.001). The principle component analysis (PCA) extracted seven principle components (PCs) with eigen values greater than 1.0 and accounted for 78.1% of the variance across all samples (Table 5). From the extracted principle components, all variables were reliable contributors to the analysis (communalities > 0.5) and there was adequate sampling for the dataset (KMO = 0.652). ANOVAs on each principle component showed that there were significant differences among the group means of PC1 (Head scales and body proportions relative to length), PC2 (Head scale shapes), PC3 (Middorsal scale length) and PC7 (Tail length relative to BWCl) (Table 3.4, Fig. 3.7). Bonferroni post-hoc tests indicated in PC1 that species C and species E have larger body proportions relative to length than species I+J. In PC2, Species C has larger SO-RO relative to SO-PN, RW relative to HW and PAW relative to PAL than Species E. In PC3 Species C has larger middorsal scales relative to both SVL and SO than species E. In PC7 Species E has a shorter tail relative to BWCl than Species I+J.

The DFA on the morphometric ratios revealed two discriminant functions (DFs) that account for 61.2% and 38.8% of the total variance and significantly differentiate the three putative species (Wilks' λ = 0.127, p < 0.001). 93.2% of individuals were correctly classified from the morphometric characters (species C: 93.3%, E: 93.5%, I+J: 92.3%). A visual inspection of the two discriminant functions (Fig. 3.8) corroborate these results and display minimal overlap among the three putative species.
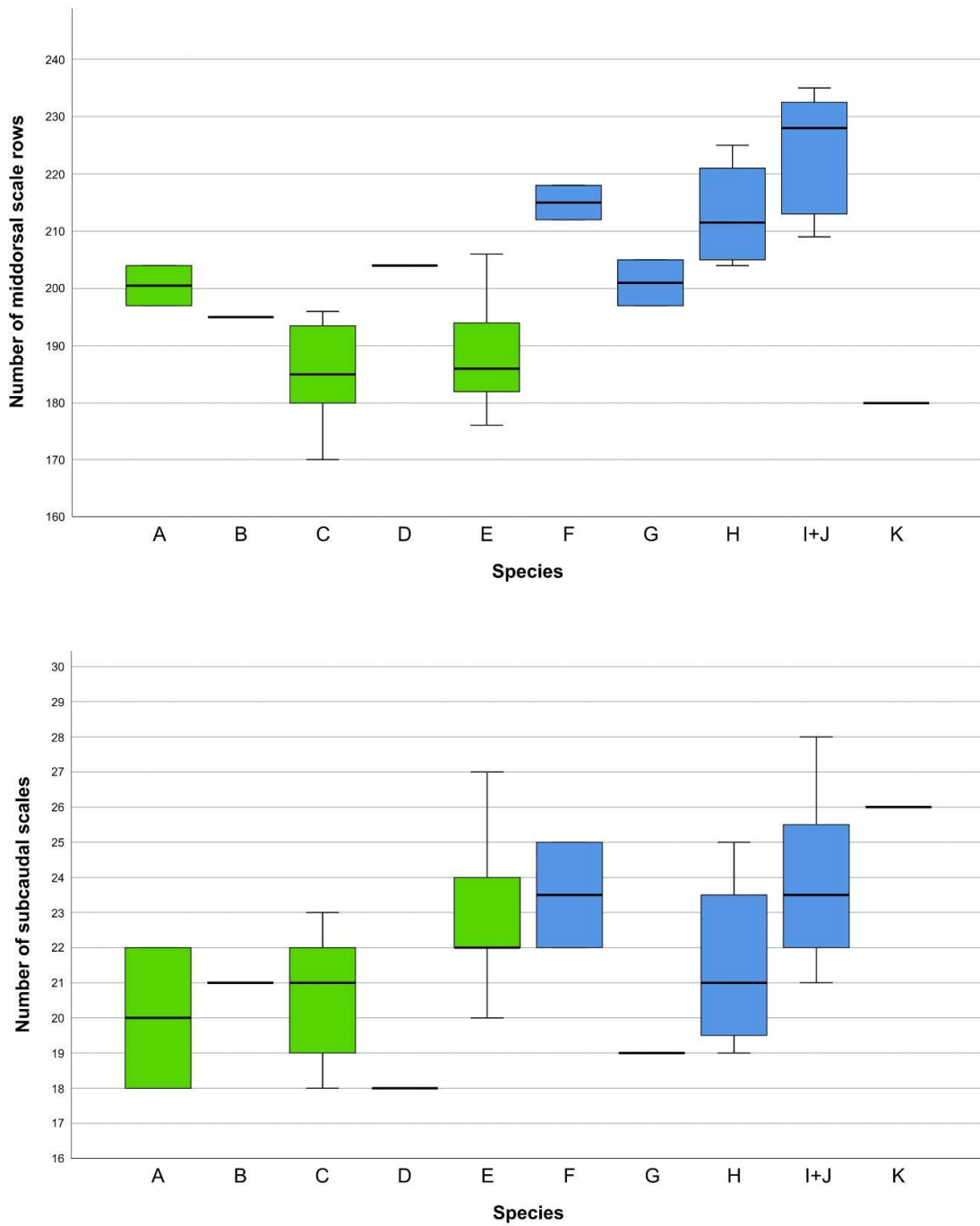
Figure 3. 6. Boxplots showing variation in the number of middorsal scale rows and number of subcaudal scales among putative species within the *Leptotyphlops sylvicolus* species complex. Boxes depict median, interquartile range, minimum and maximum values. Green boxes depict species sampled from forest habitat and blue boxes depict species from grassland habitat.

68

Table 3.3. Principal component analysis of morphometric ratios for *Leptotyphlops sylvicolus*, with PC loadings for each variable of the seven axes with eigenvalues >1.0. Characters that loaded most strongly for each principal component are in bold (rotated matrix). Percentage variation of each axes is shown and significant ($p < 0.05$) F-values from the ANOVAs are shown in bold.

Ratio	1	2	3	4	5	6	7
HW (% SVL)	**0.881**	-0.163	0.141	-0.035	0.047	-0.184	-0.171
OC L (% SVL)	**0.874**	-0.153	-0.005	-0.207	0.066	-0.039	-0.096
BWCl (%SVL)	**0.868**	0.005	0.010	0.025	-0.014	-0.181	-0.266
PF+FR+IP L (% SVL)	**0.845**	-0.031	0.283	0.033	0.019	-0.095	0.179
SO L (% SVL)	**0.780**	0.369	-0.025	0.109	-0.143	-0.067	0.230
PA-OCC (% SVL)	**0.727**	-0.198	-0.176	-0.015	0.123	0.153	-0.217
TaL (% ToL)	**0.687**	-0.337	-0.249	0.117	0.125	-0.190	0.137
SO-RO/SO-PN	-0.064	**0.908**	-0.105	-0.061	-0.114	-0.061	0.010
RW/HW	-0.338	**0.787**	-0.034	0.049	0.180	0.045	0.025
PA W/L	0.116	**0.538**	0.234	0.064	-0.031	-0.195	0.476
MDS L (%SVL)	-0.030	-0.048	**0.909**	-0.001	-0.013	0.052	-0.111
SO L/MDS L	-0.066	0.001	**-0.839**	-0.042	-0.114	-0.010	0.001
EL/OC L	0.020	0.009	-0.016	**-0.868**	0.024	0.022	0.066
UL-OC/EL	0.132	-0.056	0.132	**0.829**	0.081	-0.245	-0.137
OC-SO/OC-PN	-0.230	0.142	-0.146	**0.595**	-0.242	0.286	0.228
PF-RO/PF-SO	0.005	0.260	0.013	-0.091	**0.921**	-0.020	-0.120
PF-RO/RW	0.105	-0.221	0.106	0.028	**0.905**	-0.046	0.017
Cl W/L	-0.164	-0.013	0.087	-0.070	-0.098	**0.868**	-0.029
Cl W/BWCl	-0.415	-0.151	0.037	0.017	0.215	**0.606**	0.460
OCC W/L	-0.096	0.358	0.340	0.280	0.088	**-0.407**	0.253
BWCl/TaL	0.118	-0.067	0.152	0.108	0.101	-0.051	**-0.768**
% Variance	24.091	11.301	9.470	9.438	9.159	7.724	6.936
F-value	**8.096**	**5.054**	**7.980**	0.264	0.802	0.936	**3.904**
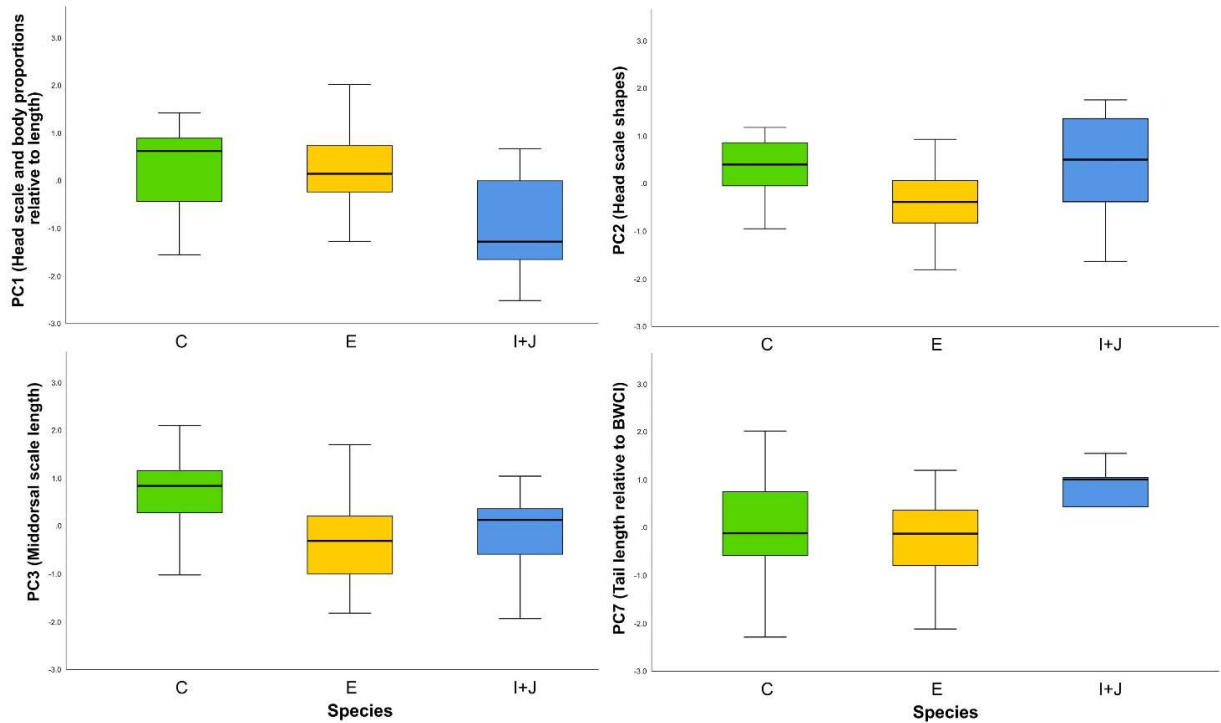
Figure 3.7. Boxplots of the principal component analysis (PCA) on three putative species within *Leptotyphlops sylvicolus* where the morphometric variables were assigned to seven principal components (PCs). Only the four PCs shown were significantly different among putative species. Axes show variation in PCs among species with median, interquartile range, minimum and maximum values.
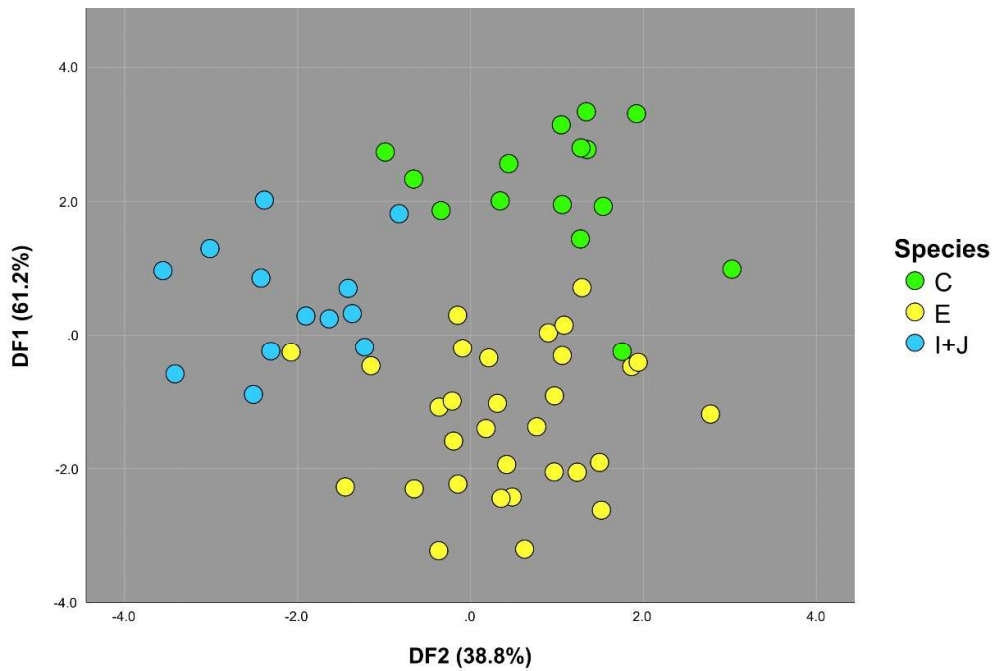
Figure 3.8. Discriminant function analysis (DFA) of the morphometric ratios from three putative species within the *Leptotyphlops sylvicolus* species complex.

3.3.6 Alternative phylogenetic hypotheses

Seven alternative phylogenetic hypotheses were tested based on the preceding results using the total-evidence dataset (Table 3.4). Due to similar habitat and morphology, we tested the monophyly of Ntsikeni (lineage F) and clade 2 (Fig.3.1A and Fig. 3.7). We assessed the monophyly of lineages D and E due to the well-supported monophyly on the Bayesian total-evidence topology (Fig. 3.4). Due to the topological incongruence between the mtDNA and nuDNA topologies, we tested whether lineage B could be monophyletic with lineage C or lineage E and also tested whether lineage D could be monophyletic with clade 2 (Fig. 3.2; Appendix 3.6). Based on the similarity matrix retrieved in the STACEY analyses, we tested the monophyly of lineages A and F and lineages B and D (Fig. 3.4). Both the SH and AU tests rejected the monophyly of lineage F and clade 2 as well as the monophyly of lineage B and C. Only the AU test rejected the monophyly of lineages D and E, monophyly of lineages B and E as well as the monophyly of lineages D and clade 2. The latter two scenarios were, however, on the cusp of the $p = 0.05$ significance threshold in the SH test. Both tests failed to reject the monophyly of lineages A and F and the monophyly of lineages B and D.

Table 3.4. Results of topology tests for the concatenated total-evidence data using the likelihood-based Shimodaira–Hasegawa (SH) and approximately unbiased (AU) tests. Significant p-values for each test are in bold.

Tree	logL	deltaL	p-SH	p-AU
ML tree	-9427.0713	-	-	-
Monophyly of Ntsikeni (F) and clade 2	-9483.2485	57.557	**0.0098**	**0.0003**
Monophyly of Ntsikeni (F) and lineage A	-9429.6356	3.945	0.8870	0.1150
Monophyly of Nkandla Forest 1(B) and lineage C	-9481.5361	55.845	**0.0061**	**0.0004**
Monophyly of Nkandla Forest 1(B) and lineage E	-9464.3667	38.676	0.0512	**0.0017**
Monophyly of Hillcrest (D) and lineage E	-9437.3911	11.700	0.5740	**0.0162**
Monophyly of Hillcrest (D) and clade 2	-9462.3042	36.613	0.0538	**0.0003**
Monophyly of Hillcrest (D) and Nkandla Forest 1 (B)	-9433.3770	7.686	0.7200	0.0685

3.4 Discussion

Our phylogenetic results revealed broadly congruent phylogeographic breaks within the two study taxa along the north-eastern portions of the Eastern Cape Province while additional breaks were observed within *L. sylvicolus* in the KwaZulu-Natal Province. Cladogenesis in *M. microlepidotus* occurred recently during the Pleistocene while in *L. sylvicolus* much older mid- to late Miocene cladogenesis is observed. Phylogenetic analyses suggest that *L. sylvicolus* is a species complex comprising ten putative species. Within the *L. sylvicolus* species complex,

putative species can be delineated using the phylogenetic framework, the species delimitation results, discrete distributions, habitat preferences and to some degree by the morphological analyses to satisfy the general lineage species concept (de Queiroz, 1998).

The *Leptotyphlops* phylogeny generated in the present study was largely congruent to the phylogeny retrieved by Adalsteinsson et al. (2009), with the exception of the relationships among lineages in the *L. scutifrons*/*L. distanti* clade (Appendix 3.4). Compared to Adalsteinsson et al. (2009), the mean divergence-time estimates retrieved in the present study were marginally younger with considerably narrower confidence intervals (95% HPD) (Appendix 3.4). Within the *L. sylvicolus* species complex cladogenesis occurred from the mid- to late Miocene (Fig. 3.2, Appendix 3.4). Recent studies on fossorial Lamprophids throughout Africa retrieved similar trends of diversification with major divergences between species occurring during the mid- to late Miocene (Portillo et al., 2019, 2018). These divergence-times further corroborate the timing of cladogenesis seen in several other reptile species throughout southern Africa (e.g. Busschau et al., 2019; Heinicke et al., 2017a; Medina et al., 2016; Stanley and Bates, 2014; Tolley et al., 2008). The late Miocene was characterized by global cooling and widespread aridification (Sepulchre et al., 2006) and the resulting contraction of mesic habitats such as forests and the expansion of xeric open habitats is thought to have facilitated diversification among both mesic and xeric adapted fossorial Lamprophids (Portillo et al., 2019, 2018). Diversification within the *L. sylvicolus* species complex corroborated these observations. After an initial divergence between clades 1 and 2 and a shift to forest habitat in clade 1, cladogenesis among forest-living lineages in clade 1 would have been driven by forest fragmentation and the subsequent isolation of populations/lineages. Diversification among grassland lineages could have been facilitated by the expansion of grassland habitat which permitted range expansion and the invasion of novel habitats (Portillo et al., 2019, 2018).

The estimated divergence-time between *A. concolor* and *M. microlepidotus* in the present study is comparable to the divergence-time retrieved by Portillo et al. (2018). Although the mean divergence time in the present study is marginally older, the confidence intervals are well within the 95% HDP retrieved by Portillo et al. (2018), 15.3 Mya (95% HDP, 10.7–20.3 Mya) versus 13.4 Mya (95% HDP, 8.3–22.3 Mya), respectively (Fig. 3.3). Divergence-time estimates among *M. microlepidotus* lineages occurred during the Pleistocene which was characterized by repeated glacial-interglacial cycles with periodicity of about 100 000 years (Deacon, 1983; Tyson, 1986). These Interglacial periods were characterized by warmer and wetter climatic conditions which permitted the expansion of more mesic habitats like forests while glacial periods were characterized by cooler and more arid conditions which resulted in the contraction of forest habitats (Deacon, 1983). In South Africa repeated glacial-interglacial cycles during the Pleistocene and the contraction of suitable habitat is thought to have been causal to the diversification among clades in the puff adder, *Bitis arietans* (Barlow et al., 2013),

and the slug eating snake, *Duberria lutrix lutrix* (Kullenkampff et al., 2019)*,* as well as the dwarf chameleons, *Bradypodion* sp*.* (da Silva and Tolley, 2017; Tolley et al., 2008), and the forest-dwelling bush squeaker frogs, *A. wahlbergii* and *A. wageri* (Tolley et al., 2018), along the east coast.

Although the recent divergence in *M. microlepidotus* does not constitute species level differences, the absence of shared haplotypes and high fixation indices among lineages possibly suggest that these lineages could be genetically isolated, alternatively this could also reflect the low samples sizes per locality (Fig. 3.3, Table 3.2, Appendix 3.5). The single specimen from Baziya possibly represents an isolated maternal lineage in the interior of the Eastern Cape Province (Fig. 3.1B). The subsequent divergence between lineages A and B along the border of the Eastern Cape and KwaZulu-Natal provinces appears congruent with the phylogeographic break among lineages in the forest clade (clade 1) of the *L. sylvicolus* species complex where the lineage from the Eastern Cape Province (lineage E) diverged from the lineages in the KwaZulu-Natal Province during the Miocene-Pliocene transition (Figs. 3.1 – 3.3). Similarly, although grassland lineages occur more inland, there appear to be congruent latitudinal breaks in both grassland- and forest-dwelling *L. sylvicolus* lineages (Fig. 3.1A). At a glance these biogeographic breaks appear congruent to the break between *A. wahlbergii* and *A. wageri* (Tolley et al., 2018) as well as the break between the southern and northern *A. pondolia* species (Busschau et al., 2019).

In *M. microlepidotus*, *A. pondolia* and *A. wageri* (Kushata, 2018) the most northern coastal locality occupied by the Eastern Cape lineages is Mbotyi. However, in *L. sylvicolus* the Eastern Cape lineage (lineage E) extends approximately 30 km further north along the coast to Mkambati Nature Reserve which is also the southernmost locality among the northern species in *A. pondolia* (Busschau et al., 2019)*.* The northern forest lineages C and D of *L. sylvicolus* do, however, show similar breaks around Durban in the KwaZulu-Natal province compared to *A. pondolia* species A and B (Fig. 3.1A; Busschau et al., 2019). Furthermore, lineages within the aforementioned taxa exhibit strikingly similar distributions to the forest-dwelling *Bradypodion* species along the east coast of South Africa (Bates et al., 2014), reinforcing the inferred biogeographic breaks as possible dispersal barriers maintaining lineage isolation.

Discordance among the inferred biogeographic breaks and the timing of cladogenesis in the aforementioned taxa can most likely be attributed to lineages specific characters such as habitat specificity, range size and dispersal capabilities in conjunction with the dynamic history of forest distribution along the east coast of South Africa (see Lawson, 2010; Myers et al., 2017; Ornelas et al., 2013; Tolley et al., 2018). However, similar resultant biogeographic patterns may reflect both ancient and contemporary climatic gradients acting, to varying degrees, on the distribution of suitable habitat or directly on the physiology of these taxa or both (Aragón et al., 2010; Moura et al., 2016). Smaller ectotherms like *L. sylvicolus* would be

more susceptible to climatic fluctuations because of their limited dispersal capabilities, smaller range sizes and inability to track changes in their environment, which would inevitably drive diversification (Araújo et al., 2008; Gaston and Blackburn, 2006; Turner et al., 1969; Wollenberg et al., 2011). The inverse would be true for larger taxa like *M. microlepidotus* that would be able to disperse greater distances and generally have larger ranges, therefore being able to mitigate change in their environment and exhibit lower rates of diversification (Araújo et al., 2008; Gaston and Blackburn, 2006). These observations are reflected in the AMOVA results where the larger *M. microlepidotus* exhibits low variation and generally low fixation indices among localities within lineages compared to *L. sylvicolus* exhibiting higher variation and generally high fixation indices among localities, suggesting lower gene flow and higher genetic differentiation (Table 3.2, Appendix 3.5).

The low sample sizes per locality for the study taxa, however, resulted in most of the pairwise F_{ST} values between localities not being statistically significant (Appendix 3.5) and reduced the probability of detecting shared haplotypes, therefore limiting the inferences made with regard to the gene flow among localities. Furthermore, the inferred breaks in the present study are somewhat arbitrarily based on the currently available data. Increasing the number of samples for the current sampling localities as well as including additional samples from within these breaks would reveal whether the inferred breaks represent true barriers to gene flow or simply reflect sampling gaps. Future studies should therefore focus on sampling within these breaks and possibly include additional species to statistically test the congruence among several taxa across these breaks. The present study does, however, emphasize the inferred breaks as possible centers of diversification among forest-living taxa.

In addition to their small size, adaptations to a fossorial lifestyle would have restricted the dispersal of *L. sylvicolus* lineages to areas of suitable substrata, therefore imposing additional dispersal barriers (Albert et al., 2007; Martín et al., 2013). Similar to the forest-living *Bradypodion* and *A. pondolia* that have high habitat specificity (Tolley et al., 2008; Busschau et al., 2019), the dispersal limitations imposed on *L. sylvicolus* lineages would have made them vulnerable to extinction filtering where the inability to track climatic oscillations since the late Miocene could have resulted in the extinction of populations that were unable to adapt to less suitable environments. The long branch lengths observed among clades in the *L. sylvicolus* species complex corroborates this hypothesis. However, considering the number of novel lineages identified among *Leptotyphlops* species in the present study and by Adalsteinsson et al. (2009), the long branch lengths may also allude to the existence of unsampled point endemic lineages that are missed during sampling. Additionally, the genetically distant lineages around Nkandla suggest that multiple *Leptotyphlops* lineages may occur in near sympatry and that fine scale sampling would be essential to quantifying the true diversity of *Leptotyphlops* (Fig. 3.2). This observation is corroborated by distantly related *L. conjunctus* lineages cooccurring at Mkuze Game Reserve, KwaZulu-Natal, and *L. conjunctus*

being sampled from the type locality of *L. sylvicolus*, Hlogwene Forest at Tugela Mouth (Adalsteinsson et al., 2009; Broadley and Wallach, 1997; Appendix 3.4).

The lineages within *L. sylvicolus* are separated by mitochondrial sequence divergence values comparable to the divergence values seen among recognized Scolecophidian species, suggesting species level divergence among the *L. sylvicolus* species complex (Thomas and Hedges, 2007; Hedges, 2008; Kornilios, 2017). Although mitochondrial sequence divergence values are not absolute indicators of taxonomic distinctiveness, they can be used as a guideline alongside other lines of evidence to support taxonomic inferences (Ferguson, 2002). The *L. sylvicolus* lineages are further separated by high fixation indices and the lack of shared haplotypes, suggesting that there is a lack of gene flow and that they are evolving independently of one another (Fig. 3.5, Table 3.2, Appendix 3.5). The species delimitation analyses on the mtDNA dataset further support the distinctiveness of these lineages with ABGD and bGMYC retrieving 11 and 12 putative species, respectively.

Inferences from the slow evolving nuDNA loci are more conservative. In both nuDNA topologies the relatively large forest lineages, lineages C and E, are well-supported and lineages F and G, although only represented by a single sample, are always separate from the remaining lineages, suggesting that these four lineages are genetically distinct (Appendix 3.6). The phylogenetic relationships among the remaining lineages are somewhat dubious, most likely attributed to the slow evolution of the nuDNA loci and the fact that not all localities were successfully sequenced for both nuDNA loci. Lineage B exhibited well-supported monophyly with localities from lineage C on the *PRLR* topology, suggesting admixture between these geographically proximate lineages, but was sister to lineage E on the *RAG1* topology. Similarly, the grassland lineages exhibited low resolution on the nuclear topologies (Appendix 3.6). On the *PRLR* topology several grassland localities comprise a well-supported clade, suggesting that the grassland habitats could potentially have exhibited a higher degree of interconnectivity among localities throughout their evolutionary history compared to the forest lineages, which allowed for gene flow and facilitated admixture among lineages. This clade, however, included the specimen sampled from forest habitat in Hillcrest (lineage D) that is distantly related to the grassland clade (clade 2) on the mtDNA topology (Fig. 3.2). The alternative topology tests on the total-evidence dataset rejected the alternative hypotheses deduced from the nuDNA topologies (Table 3.4), suggesting that these observations could be attributed to the low variability of the nuDNA markers and possibly the retention of ancestral alleles in these lineages.

Multispecies coalescent models such as STACEY on multi-locus datasets have been proven to out-perform single-locus delimitation methods, such as ABGD and bGMYC, and as a result it has widely been used to validate potential species (e.g. Jacobs et al., 2018; McKelvy and Burbrink, 2017; Pinto et al., 2019; Tomasello, 2018). Within *L. sylvicolus* delimitation results

from the STACEY analyses retrieved ten putative species (retrieving lineages I and J as a single species) with well-supported monophyly (Fig. 3.4). These results also retrieved additional similarity between lineages A and F as well as between lineages B and D. The alternative topology tests also failed to reject the monophyly among these lineages (Table 3.4). It is, however, noteworthy that lineages A and D were only sequenced for a single mtDNA locus and a single nuDNA locus which may have influenced the delimitation results. Although the results from the current data would suggest that these lineages share similar evolutionary histories and could therefor represent species, high sequence divergence and geographic segregation differentiate these lineages. Including additional sequences and possibly additional samples for lineages A, B, D and F could resolve their taxonomic affinities in the future.

Delineating the ten putative species, identified in the STACEY delimitation analyses, based on the meristic data is problematic. Not only because of the low sample sizes for the majority of the species, but there appear to be substantial overlap in both middorsal and subcaudal scale counts among species within the *L. sylvicolus* species complex. Despite this, specimens from forest localities are more similar and exhibit lower scale counts compared to grassland localities (Fig. 3.6). Even Ntsikeni (lineage F) in clade 1 is more similar to the lineages in clade 2 both in morphology (Fig. 3.6) and habitat, however, the alternative topology tests rejected the monophyly of Ntsikeni and clade 2 (Table 3.4), supporting the hypothesis that forest colonization occurred in clade 1.These results corroborate the results presented by Broadley and Wallach (1997) where the forest-living *L. sylvicolus* could be differentiated from the savanna-living *L. conjunctus* by lower middorsal and subcaudal counts. The grassland *L. sylvicolus* lineages are morphologically more similar to *L. conjunctus* and share considerable overlap in the number of middorsal scale rows (Broadley and Broadley, 1999; Fig. 3.6). This observation suggests that additional morphological analyses would be required to differentiate the grassland *L. sylvicolus* species from the genetically diverse *L. conjunctus* species complex. Considering that the *L. conjunctus* species complex and *L. sylvicolus* share a common ancestor and *L. conjunctus* generally inhabit similar open habitat to the grassland *L. sylvicolus* species in the present study, the results here suggest that a reduction of middorsal scale rows is a more derived state that can be associated with the shift towards forest habitat in clade 1 (Broadley and Broadley, 1999; Fig. 3.4; Appendix 3.4).

The morphometric results for three of the species further indicate that the two forest species (species C and E) have larger body proportions relative to their length compared to the grassland species (species I+J) (Fig. 3.7). The grassland species also tend to have longer tails relative to their body width at the cloaca (Fig. 3.7). These results could potentially indicate subtle morphological adaptations to the substrate in different habitats; forest species exhibit a shorter more robust body plan in comparison to a slender more elongated body plan in the grassland species, corroborating the observations by Broadley and Broadley (1999) for the

forest-living *L. sylvicolus* compared to other *Leptotyphlops* species. Furthermore, differences in scalation proportions differentiate the two forest species (Fig. 3.7). Although the differences in morphology are subtle and exhibit overlap among the three species, the results from the DFA strongly support the presence of morphologically distinct species (Fig. 3.8).

The morphological conservativeness and lack of taxonomically informative characters have widely obscured diversity among Scolecophidians, resulting in species often being diagnosed by subtle, sometimes non-traditional, morphological differences (e.g. Hedges, 2008; Thomas and Hedges, 2007). Several *Leptotyphlops* species currently recognized in Southern Africa are differentiated by such subtle differences (Broadley and Broadley, 1999). However, Adalsteinsson et al. (2009) postulated that there are at least 12 cryptic species among *L. conjunctus*, *L. nigricans*, *L. scutifrons*, and *L. sylvicolus*. The results presented here indicate that the number of cryptic species among the *L. sylvicolus* and *L. conjunctus* species complexes are significantly higher, suggesting that a taxonomic revision of the genus is required to quantify the total diversity. In *L. sylvicolus*, the molecular analyses support the species status of ten isolated populations, three of which were statistically differentiated by the morphological analyses. Although currently assessed as least concern (Alexander, 2018), *L. sylvicolus* was previously assessed as data deficient due to the uncertain taxonomic status of several isolated populations that had areas of occupancy lower than the endangered threshold (Bates et al., 2014). Therefore, the supporting evidence in the present study for several cryptic species within *L. sylvicolus* that exhibit significantly reduced ranges warrants the reassessment of their conservation status. Furthermore, Marked genetic differentiation, at both the inter- and intraspecific level, among the study taxa emphasize the importance of forest habitat conservation along the east coast of South Africa as these forests possibly harbor significantly higher levels of diversity than currently recognized.

Appendix 3.1. List of samples used in this study with associated voucher and DNA numbers, locality name, and GenBank accession numbers for each gene. Voucher numbers in bold were used in the morphological analyses and Genbank accession numbers in bold indicate sequences from Adalsteinsson et al. (2009) and bold underlined indicate sequences from Portillo et al. (2018). The *cyt b* haplotype numbers for *Leptotyphlops sylvicolus* correspond to the haplotype network in Fig. 3.5 and the concatenated mtDNA haplotype numbers for *Macrelaps microlepidotus* correspond to the haplotype network in Fig. 3.3.

Voucher Number	DNA Number	Taxon	Locality	Cytb Haplotype	mtDNA Haplotype	Cyt b	ND4	PRLR	RAG1
PEM R17343a	SBH267158	*Leptotyphlops sylvicolus*	Xilonde	1		**GQ469101**			
PEM R17343b	SBH268079	*Leptotyphlops sylvicolus*	Xilonde	1		**GQ469150**			**GQ469054**
PEM R20928		*Leptotyphlops sylvicolus*	Empembeni	2		MN250570	MN250655		MN250718
PEM R20934		*Leptotyphlops sylvicolus*	Embembeni	2		MN250571	MN250656		
PEM R24482	TB-L032	*Leptotyphlops sylvicolus*	Nkandla Forest 1	3		MN250552	MN250637	MN250689	MN250712
PEM R24481	TB-L029	*Leptotyphlops sylvicolus*	Nkandla Forest 2				MN250636	MN250688	MN250711
PEM R24466	TB-L016	*Leptotyphlops sylvicolus*	Ngoye Forest	4		MN250537	MN250621		
PEM R24467	TB-L017	*Leptotyphlops sylvicolus*	Ngoye Forest	4		MN250538	MN250622		
PEM R24470	TB-L020	*Leptotyphlops sylvicolus*	Ngoye Forest	4		MN250541	MN250625		
PEM R24472	TB-L022	*Leptotyphlops sylvicolus*	Ngoye Forest	4		MN250543	MN250627		
PEM R24473	TB-L023	*Leptotyphlops sylvicolus*	Ngoye Forest	4		MN250544	MN250628		
PEM R24474	TB-L024	*Leptotyphlops sylvicolus*	Ngoye Forest	4		MN250545	MN250629		
PEM R24475	TB-L025	*Leptotyphlops sylvicolus*	Ngoye Forest	4		MN250546	MN250630		
PEM R24468	TB-L018	*Leptotyphlops sylvicolus*	Ngoye Forest	5		MN250539	MN250623		
PEM R24469	TB-L019	*Leptotyphlops sylvicolus*	Ngoye Forest	5		MN250540	MN250624	MN250701	MN250724
PEM R24471	TB-L021	*Leptotyphlops sylvicolus*	Ngoye Forest	5		MN250542	MN250626		
PEM R24476	TB-L026	*Leptotyphlops sylvicolus*	Dlinza Forest	6		MN250547	MN250631	MN250685	MN250708
PEM R24477	TB-L027	*Leptotyphlops sylvicolus*	Dlinza Forest	6		MN250548	MN250632		
PEM R20933		*Leptotyphlops sylvicolus*	Entumeni NR	7		MN250572	MN250658		
PEM R20931		*Leptotyphlops sylvicolus*	Entumeni NR				MN250657		
PEM R24478	TB-L028	*Leptotyphlops sylvicolus*	Entumeni NR	8		MN250549	MN250633	MN250686	MN250709
PEM R24483	TB-L033	*Leptotyphlops sylvicolus*	Amatikulu NR	9		MN250553	MN250638	MN250690	MN250713
PEM R25204	TB-L053	*Leptotyphlops sylvicolus*	Amatikulu NR	9		MN250586	MN250673		
PEM R25206	TB-L057	*Leptotyphlops sylvicolus*	Hillcrest	10		MN250590		MN250700	
PEM R22463	WC-4445	*Leptotyphlops sylvicolus*	Mkambati NR	11		MN250517	MN250601		

78

PEM R22464	WC-4464	*Leptotyphlops sylvicolus*	Mkambati NR	11		MN250518	MN250602	MN250681	MN250704
PEM R22466	WC-4477	*Leptotyphlops sylvicolus*	Mkambati NR	12		MN250520	MN250604		
PEM R22465	WC-4479	*Leptotyphlops sylvicolus*	Mkambati NR	12		MN250519	MN250603		
PEM R22468	WC-4480	*Leptotyphlops sylvicolus*	Mkambati NR	12		MN250522	MN250606		
PEM R22467	WC-4481	*Leptotyphlops sylvicolus*	Mkambati NR	12		MN250521	MN250605		
PEM R22469	WC-4482	*Leptotyphlops sylvicolus*	Mkambati NR	12		MN250523	MN250607		
PEM R22470	WC-4483	*Leptotyphlops sylvicolus*	Mkambati NR	12		MN250524	MN250608		
PEM R22471	WC-4484	*Leptotyphlops sylvicolus*	Mkambati NR	12		MN250525	MN250609		
PEM R22461	WC-4438	*Leptotyphlops sylvicolus*	Njombela	13		MN250515	MN250599		
PEM R22462	WC-4439	*Leptotyphlops sylvicolus*	Njombela	13		MN250516	MN250600	MN250680	MN250703
PEM R22455	WC-4422	*Leptotyphlops sylvicolus*	Mbotyi	14		MN250509	MN250593	MN250679	MN250702
PEM R22456	WC-4423	*Leptotyphlops sylvicolus*	Mbotyi	14		MN250510	MN250594		
PEM R22457	WC-4424	*Leptotyphlops sylvicolus*	Mbotyi	14		MN250511	MN250595		
PEM R22458	WC-4431	*Leptotyphlops sylvicolus*	Mbotyi	14		MN250512	MN250596		
PEM R22459	WC-4433	*Leptotyphlops sylvicolus*	Mbotyi	15		MN250513	MN250597		
PEM R22460	WC-4434	*Leptotyphlops sylvicolus*	Mbotyi	15		MN250514	MN250598		
PEM R24461	TB-L011	*Leptotyphlops sylvicolus*	Hole In The Wall	16		MN250532	MN250616	MN250684	MN250707
PEM R24462	TB-L012	*Leptotyphlops sylvicolus*	Hole In The Wall	16		MN250533	MN250617		
PEM R24463	TB-L013	*Leptotyphlops sylvicolus*	Hole In The Wall	16		MN250534	MN250618		
PEM R20232	WC-DNA-924	*Leptotyphlops sylvicolus*	Hole In The Wall	16		MN250507	MN250591		
PEM R24464	TB-L014	*Leptotyphlops sylvicolus*	Hole In The Wall	17		MN250535	MN250619		
PEM R24465	TB-L015	*Leptotyphlops sylvicolus*	Hole In The Wall	17		MN250536	MN250620		
PEM R24456	TB-L006	*Leptotyphlops sylvicolus*	Lubanzi	18		MN250527	MN250611	MN250683	MN250706
PEM R24458	TB-L008	*Leptotyphlops sylvicolus*	Lubanzi	18		MN250529	MN250613		
PEM R24459	TB-L009	*Leptotyphlops sylvicolus*	Lubanzi	18		MN250530	MN250614		
PEM R24457	TB-L007	*Leptotyphlops sylvicolus*	Lubanzi	19		MN250528	MN250612		
PEM R24460	TB-L010	*Leptotyphlops sylvicolus*	Lubanzi	20		MN250531	MN250615		
PEM R22979	WC-5304	*Leptotyphlops sylvicolus*	Dwesa NR	21		MN250558	MN250643	MN250693	MN250716
PEM R22981	WC-5308	*Leptotyphlops sylvicolus*	Dwesa NR	22		MN250560	MN250645		
PEM R22293	WC-5309	*Leptotyphlops sylvicolus*	Dwesa NR	22		MN250561	MN250646		
PEM R22983	WC-5327	*Leptotyphlops sylvicolus*	Dwesa NR	22		MN250562	MN250647		
PEM R22984	WC-5328	*Leptotyphlops sylvicolus*	Dwesa NR	22		MN250563	MN250648		
PEM R22301	WC-5305	*Leptotyphlops sylvicolus*	Dwesa NR	23		MN250559	MN250644		

PEM R22985	WC-5382	*Leptotyphlops sylvicolus*	Mazeppa Bay	24		MN250564	MN250649	MN250694	MN250717
PEM R22988	WC-5391	*Leptotyphlops sylvicolus*	Manubi Forest	24		MN250567	MN250652		
PEM R22989	WC-5392	*Leptotyphlops sylvicolus*	Manubi Forest	24		MN250568	MN250653		
PEM R22990	WC-5438	*Leptotyphlops sylvicolus*	Manubi Forest	24		MN250569	MN250654		
PEM R22987	WC-5385	*Leptotyphlops sylvicolus*	Mazeppa Bay	25		MN250566	MN250651		
PEM R22986	WC-5383	*Leptotyphlops sylvicolus*	Mazeppa Bay	26		MN250565	MN250650		
PEM R19439	WC-DNA-423	*Leptotyphlops sylvicolus*	Hluleka NR	27		MN250508	MN250592		
PEM R24455	TB-L005	*Leptotyphlops sylvicolus*	Hluleka NR	28		MN250526	MN250610	MN250682	MN250705
PEM R24489	TB-L039	*Leptotyphlops sylvicolus*	Ntsikeni NR	29		MN250573	MN250659	MN250695	MN250719
PEM R24490	TB-L040	*Leptotyphlops sylvicolus*	Ntsikeni NR	29		MN250574	MN250660		
PEM R24480	TB-L030	*Leptotyphlops sylvicolus*	Nkandla Grassland	30		MN250551	MN250635		
PEM R24479	TB-L031	*Leptotyphlops sylvicolus*	Nkandla Grassland	30		MN250550	MN250634	MN250687	MN250710
PEM R25203	TB-L058	*Leptotyphlops sylvicolus*	Ashburton				MN250678		MN250723
PEM R24501	TB-L051	*Leptotyphlops sylvicolus*	Ncwadi	31		MN250584	MN250671	MN250697	
PEM R24491	TB-L041	*Leptotyphlops sylvicolus*	Elandskuil	32		MN250575	MN250661	MN250696	MN250720
PEM R24492	TB-L042	*Leptotyphlops sylvicolus*	Elandskuil	32		MN250576	MN250662		
PEM R24493	TB-L043	*Leptotyphlops sylvicolus*	Elandskuil	32		MN250577	MN250663		
PEM R24494	TB-L044	*Leptotyphlops sylvicolus*	Elandskuil	32		MN250578	MN250664		
PEM R24495	TB-L045	*Leptotyphlops sylvicolus*	Elandskuil				MN250665		
PEM R24488	TB-L038	*Leptotyphlops sylvicolus*	Matatiele	33		MN250557	MN250642	MN250692	MN250715
PEM R24496	TB-L046	*Leptotyphlops sylvicolus*	Matatiele	33		MN250579	MN250666		
PEM R24497	TB-L047	*Leptotyphlops sylvicolus*	Matatiele	34		MN250580	MN250667		
PEM R24498	TB-L048	*Leptotyphlops sylvicolus*	Matatiele	34		MN250581	MN250668		
PEM R24499	TB-L049	*Leptotyphlops sylvicolus*	Matatiele	34		MN250582	MN250669		
PEM R24500	TB-L050	*Leptotyphlops sylvicolus*	Matatiele	34		MN250583	MN250670		
PEM R18156	MBUR00439	*Leptotyphlops sylvicolus*	Fever Village	35		**GQ469168**			
PEM R18155	SBH268074; MBUR00438	*Leptotyphlops sylvicolus*	Fever Village	36		**GQ469147**			
PEMR18154	SBH268073; MBUR00435	*Leptotyphlops sylvicolus*	Fever Village	37		**GQ469146**			
PEM R22656	WC-5064	*Leptotyphlops sylvicolus*	Ntywenka	38		MN250585	MN250672		
PEM R24837	WC-6647	*Leptotyphlops sylvicolus*	Ongeluksnek NR				MN250674		
PEM R24827	WC-6667	*Leptotyphlops sylvicolus*	Ongeluksnek NR	39		MN250588	MN250676	MN250699	MN250722
PEM R24838	WC-6666	*Leptotyphlops sylvicolus*	Ongeluksnek NR	40		MN250589	MN250677		

80

PEM R24485	TB-L035	*Leptotyphlops sylvicolus*	Upper Tsitsana	41		MN250554	MN250639	MN250691	MN250714
PEM R24487	TB-L037	*Leptotyphlops sylvicolus*	Upper Tsitsana	41		MN250556	MN250641		
PEM R24486	TB-L036	*Leptotyphlops sylvicolus*	Upper Tsitsana	42		MN250555	MN250640		
PEM R24637	LJK-0018	*Leptotyphlops sylvicolus*	Morgan's Bay	43		MN250587	MN250675	MN250698	MN250721
	Lepto 1	*Leptotyphlops conjunctus*	Ladysmith KZN			MN250455			
PEM R18149	MBUR01235	*Leptotyphlops conjunctus*	Manyiseni region KZN			**GQ469167**			
PEM R 5913	SBH267160	*Leptotyphlops conjunctus*	Lebombo KZN			**GQ469103**			
PEM R17531	SBH268062	*Leptotyphlops conjunctus*	Phinda PGR KZN			**GQ469136**			
MBUR 00107	SBH268070	*Leptotyphlops conjunctus*	40 km S Lydenburg			**GQ469143**			
PEM R18153	SBH268071	*Leptotyphlops conjunctus*	40km W Nelspruit MP			**GQ469144**			
PEM R18152	SBH268072	*Leptotyphlops conjunctus*	40km W Nelspruit MP			**GQ469145**			
PEM R18157	SBH268077	*Leptotyphlops conjunctus*	Manyiseni region KZN			**GQ469149**			
PEM R17410	SBH268183	*Leptotyphlops conjunctus*	Mkhuze Game Reserve KZN			**GQ469159**			
PEM R17418	SBH268191	*Leptotyphlops conjunctus*	Mkhuze Game Reserve KZN			**GQ469160**			
PEM R17420	SBH268193	*Leptotyphlops conjunctus*	Mkhuze Game Reserve KZN			**GQ469161**			
PEM R24452	TB-L001	*Leptotyphlops conjunctus*	Harold Johnson NR			MN250456	MN250471	MN250487	MN250495
PEM R24453	TB-L002	*Leptotyphlops conjunctus*	Harold Johnson NR			MN250457	MN250472		
PEM R24454	TB-L003	*Leptotyphlops conjunctus*	Harold Johnson NR			MN250458	MN250473		
	TB-L004	*Leptotyphlops conjunctus*	Harold Johnson NR			MN250459	MN250474		
PEM R25205	TB-L052	*Leptotyphlops conjunctus*	Tugela Mouth			MN250468	MN250484	MN250494	MN250504
PEM R25207	TB-L055	*Leptotyphlops conjunctus*	Barberton			MN250469	MN250485		MN250505
PEM R25209	TB-L0565	*Leptotyphlops conjunctus*	Ndomu			MN250470	MN250486		MN250506
PEM R19175	WC 10-066	*Leptotyphlops conjunctus*	Rockridge			MN250460	MN250475	MN250488	MN250496
PEM R21093	WC-2666	*Leptotyphlops conjunctus*	Littleandbigthomas			MN250463	MN250478	MN250491	MN250499
PEM R21272	WC-2744	*Leptotyphlops conjunctus*	Fort Fordyce			MN250464	MN250479	MN250492	MN250500
PEM R21274	WC-2770	*Leptotyphlops conjunctus*	Fort Fordyce			MN250465	MN250480		MN250501
PEM R21851	WC-3615	*Leptotyphlops conjunctus*	Penhoekpass			MN250466	MN250481	MN250493	MN250502
PEM R22202	WC-3804	*Leptotyphlops conjunctus*	Fort Fordyce			MN250467	MN250482		
PEM R22562	WC-5034	*Leptotyphlops conjunctus*	MpofuNR				MN250483		MN250503
PEM R19003	WC-DNA-0037	*Leptotyphlops conjunctus*	Cathcart			MN250461	MN250476	MN250489	MN250497
PEM R20667	WC-DNA-1216	*Leptotyphlops conjunctus*	Wakkerstroom			MN250462	MN250477	MN250490	MN250498
PEM R18150	SBH268204	*Leptotyphlops distanti*	Phalaborwa			**GQ469162**			
	SBH268226	*leptotyphlops merkeri*	Kenya			**GQ469164**			

81

PEM R17392	SBH267159	*Leptotyphlops nigricans*	Port Elizabeth EC			**GQ469102**		
PEM R 12556	SBH268047	*Leptotyphlops nigricans*	Caledon WC			**GQ469128**		
CAS 207002	SBH268048	*Leptotyphlops nigricans*	Caledon WC			**GQ469129**		
MCZF 38479	SBH268049	*Leptotyphlops nigricans*	Grahamstown commonage EC			**GQ469130**		
CAS 207001	SBH268053	*Leptotyphlops nigricans*	Caledon WC			**GQ469134**		
PEM R23615	WC-6168	*Leptotyphlops nigricans*	Finella Falls			MN250725	MN250726	MN250727	MN250728
	SBH268067	*Leptotyphlops nigroterminus*	Tanzania			**GQ469142**		
	SBH268223	*Leptotyphlops pitmani*	Rwanda			**GQ469163**		
MB 20939	MB20939	*Leptotyphlops scutifrons*	Groblershoop NC			**GQ469169**		
MCZ R184522	SBH268043	*Leptotyphlops scutifrons*	Tshukudu Lodge L			**GQ469125**		
CAS 234220	SBH268044	*Leptotyphlops scutifrons*	Farm Fancy L			**GQ469126**		
MCZ R184538	SBH268045	*Leptotyphlops scutifrons*	33.1 km S Kgama L			**GQ469127**		
PEM R17393	SBH268061	*Leptotyphlops scutifrons*	65k NE Kuruman NW			**GQ469135**		
MB 327	SBH268063	*Leptotyphlops scutifrons*	Blouberg L			**GQ469137**		
MB 393	SBH268064	*Leptotyphlops scutifrons*	Blouberg L			**GQ469138**		
PEM R181151	SBH268076	*Leptotyphlops scutifrons*	E of Tsipise L			**GQ469148**		
	TB-M018	*Macrelaps microlepidotus*	Eshowe	1		MN250449	MN250409	
DNSM 1751	DNSM 1751	*Macrelaps microlepidotus*	Westville	2		MN250426	MN250385	
	TB-M020	*Macrelaps microlepidotus*	Eshowe	2		MN250450	MN250410	
PEM R24503	TB-M002	*Macrelaps microlepidotus*	Kloof	3		MN250428	MN250387	
PEM R25141	Kloof1	*Macrelaps microlepidotus*	Kloof	3		MN250420	MN250379	
PEM R25142	Kloof2	*Macrelaps microlepidotus*	Kloof	3		MN250421	MN250380	
PEM R20944	B male	*Macrelaps microlepidotus*	Hillcrest	3		MN250416	MN250375	
PEM R20946	D female	*Macrelaps microlepidotus*	Hillcrest	3		MN250417	MN250376	
DNSM 1753	DNSM 1753	*Macrelaps microlepidotus*	Westville	3		MN250437	MN250397	
PEM R20945	E female	*Macrelaps microlepidotus*	Hillcrest	3		MN250418	MN250377	
PEM R24502	TB-M001	*Macrelaps microlepidotus*	Waterfall	3		MN250427	MN250386	
	TB-M004	*Macrelaps microlepidotus*	Assagay	3		MN250430	MN250389	
	TB-M006	*Macrelaps microlepidotus*	Westville	3		MN250431	MN250391	
	TB-M008	*Macrelaps microlepidotus*	Ixopo	4		MN250438	MN250398	
	TB-M005	*Macrelaps microlepidotus*	Shelley Beach	5			MN250390	
PEM R24504	TB-M003	*Macrelaps microlepidotus*	Southbroom	6		MN250429	MN250388	

82

PEM R25202	TB-M015	*Macrelaps microlepidotus*	Southbroom		7	MN250445	MN250405
	TB-M007	*Macrelaps microlepidotus*	Gomo Forest		8	MN250432	MN250392
PEM R22475	WC-4440	*Macrelaps microlepidotus*	Mbotyi		8	MN250419	MN250378
PEM R24313	WC-6579	*Macrelaps microlepidotus*	Gomo Forest		8	MN250448	MN250408
PEM R20295	WC-DNA-973	*Macrelaps microlepidotus*	Manubi Forest		8	MN250415	MN250374
PEM R22660	WC-5070	*Macrelaps microlepidotus*	Nqadu		9	MN250424	MN250383
PEM R22659	WC-4975	*Macrelaps microlepidotus*	Baziya		10	MN250422	MN250381
PEM R19786	WC-DNA-621	*Macrelaps microlepidotus*	Dwesa NR		11	MN250412	MN250371
PEM R19786	WC-DNA-511	*Macrelaps microlepidotus*	Dwesa NR		12	MN250413	MN250372
	TB-M009	*Macrelaps microlepidotus*	Sunrise on Sea		13	MN250439	MN250399
	TB-M013	*Macrelaps microlepidotus*	Thorn Park		13	MN250443	MN250403
PEM R22997	WC-5419	*Macrelaps microlepidotus*	Manubi Forest		13	MN250434	MN250394
PEM R22998	WC-5442	*Macrelaps microlepidotus*	Manubi Forest		13	MN250435	MN250395
PEM R20294	WC-DNA-922	*Macrelaps microlepidotus*	Manubi Forest		13	MN250414	MN250373
PEM R22996	WC-5414	*Macrelaps microlepidotus*	Manubi Forest		14	MN250433	MN250393
	TB-M010	*Macrelaps microlepidotus*	Sunrise on Sea		15	MN250440	MN250400
	East London 1	*Macrelaps microlepidotus*	East London		16	MN250447	MN250407
	TB-M011	*Macrelaps microlepidotus*	Dorchester Heights		16	MN250441	MN250401
	Pirie 1	*Macrelaps microlepidotus*	Pirie		17	MN250425	MN250384
	TB-M012	*Macrelaps microlepidotus*	Dorchester Heights		17	MN250442	MN250402
	TB-M014	*Macrelaps microlepidotus*	Thorn Park		18	MN250444	MN250404
PEM R22999	WC-5447	*Macrelaps microlepidotus*	Isedenge		19	MN250436	MN250396
PEM R20167	WC-DNA-928	*Macrelaps microlepidotus*	Hogsback		20	MN250411	MN250370
	SG 117	*Macrelaps microlepidotus*	Hogsback		21	MN250423	MN250382
	TB-M017	*Macrelaps microlepidotus*	Hogsback		22	MN250446	MN250406
PEM R17369	618	*Amblyodipsas concolor*	SA: KwaZulu-Natal			**MG746802**	**MG775917**
	634	*Amblyodipsas concolor*	SA: KwaZulu-Natal			**MG746801**	**MG775916**
NMB R11375	MBUR 01624	*Amblyodipsas concolor*	SA: Limpopo Province			**MG746804**	**MG775920**
NMB R11376	MBUR 01659	*Amblyodipsas concolor*	SA: Limpopo Province			**MG746803**	**MG775918**
NMB R11377	MBUR 01660	*Amblyodipsas concolor*	SA: Limpopo Province				**MG775919**
	TB-M016	*Amblyodipsas concolor*	SA: Mpumalanga, Nelspruit			MN250452	MN250454
PEM R19437	WC 373	*Amblyodipsas concolor*	SA: Eastern Cape Province, Hluleka			**MG746806**	**MG775922**

PEM R19795	WC 483	*Amblyodipsas concolor*	SA: Eastern Cape Province, Dwesa Point		**MG746807**	**MG775923**
PEM R20284	WC 975	*Amblyodipsas concolor*	SA: Eastern Cape Province, Mazeppa Bay		**MG746805**	**MG775921**
	TB-M019	*Amblyodipsas concolor*	SA: Mpumalanga, Lydenburg		MN250451	MN250453
	CMRK311	*Amblyodipsas dimidiata*	Tanzania		**DQ486346**	**DQ486322**
	SP3	*Amblyodipsas microphthalma*	SA: Limpopo Province, Soutpansberg		**MG746808**	**MG775927**
PEM R18986	632	*Amblyodipsas polylepis*	SA: Limpopo Province, Phalaborwa		**MG746811**	**MG775930**
	2209N	*Amblyodipsas unicolor*	Chad: Baibokoum		**MG746817**	**MG775925**
PEM R23320	WC 3920	*Amblyodipsas ventrimaculata*	Angola: Moxico Province, Cuito River		**MG746819**	
PEM R17438	647	*Xenocalamus bicolor*	SA: Northern Cape Province, Kimberly		**MG746786**	**MG775902**
UTEP 21620	ELI 355	*Xenocalamus michelli*	DRC: Katanga Province, Manono		**MG746799**	**MG775915**
PEM R12103		*Xenocalamus transvaalensis*	SA: KwaZulu-Natal, Maputaland		**AY612025**	**FJ404344**

Appendix 3.2. Substitution models used for each dataset in the various molecular analyses.

Dataset	Garli	MrBayes	BEAST	STACEY
Leptotyphlops				
mtDNA	*ND4* (TrN+I+G)	*ND4* (TrN+I+G)	*ND4* (TrN+I+G)	
Concatenated	*cyt b* (TIM2+I+G)	*cyt b* (TIM2+I+G)	*cyt b* (TIM2+I+G)	
Total-evidence	*ND4* (TIM2+I+G) *cyt b* (TIM2+I+G) *PRLR* (TPM1uf+G) *RAG1* (HKY+G)	*ND4* (TIM2+I+G) *cyt b* (TIM2+I+G) *PRLR* (TPM1uf+G) *RAG1* (HKY+G)		*ND4* (HKY+I+G) *cyt b* (HKY+I+G) *PRLR* (TPM1uf+G) *RAG1* (HKY+G)
Macrelaps microlepidotus				
mtDNA	*ND4* (TPM2uf+G)	*ND4* (TPM2uf+G)	*ND4* (TPM2uf+G)	
Concatenated	*cyt b* (TPM2uf+G)	cyt *b* (TPM2uf+G)	cyt *b* (TPM2uf+G)	

Appendix 3.3. Morphological variables measured for voucher specimens of *Leptotyphlops sylvicolus*.

Morphological variables	Definition
Meristic characters	
Midbody scales (MBS)	Number of midbody scale rows counted around body at half the body length
Midtail scales (MTS)	Number of midtail scale rows counted around the tail at half its length
Middorsal scales (MDS)	Number of middorsal scale rows between the rostral scale and terminal spine
Sucaudal scales (SCS)	Number of subcaudal scales counted from the cloaca to the terminal spine
Supralabial scales (SLS)	Number of supralabial scales
Body measurements	
Total length (ToL)	Measured from the tip of the snout to the terminal spine
Tail length (TaL)	Measured from the cloaca to the terminal spine
Snout to vent Length (SVL)	Measured from the tip of the snout to the posterior edge of the cloacal shield
Head width (HW)	Measured across the eyes
Body width at cloaca (BWCI)	Body width measured at cloaca level
Scale measurements	
PF-RO	Prefrontal (PF) rostral (RO) suture length
PF-SO	Prefrontal (PF) supraocular (SO) suture length
SO-RO	Supraocular (SO) rostral (RO) suture length
OC-SO	Ocular (OC) supraocular (SO) suture length
SO-PN	Supraocular (SO) postnasal (PN) suture length
SO L	Supraocular (SO) length (L)
RW	Rostral width at PN/SO/R
PF+FR+IP L	Length of first 3 middorsals - prefrontal (PF) + frontal (FR) + interparietal (IP)
MDS L	Middorsal scale length measured 15 scales from the rostral
OC L	Occular length
OC-PN	Ocular (OC) postnasal (PN) suture length
UL-OC	Upperlabial (UL) ocular (OC) suture
EL	Eye to lip
PA L	Parietal (PA) length (L)
OCC L	Occipital (OCC) length (L)
PA W	Parietal width
OCC W	Occipital width
PA-OCC	Parietal occipital suture length
CI W	Cloaca shield width
CI L	Cloaca shield length
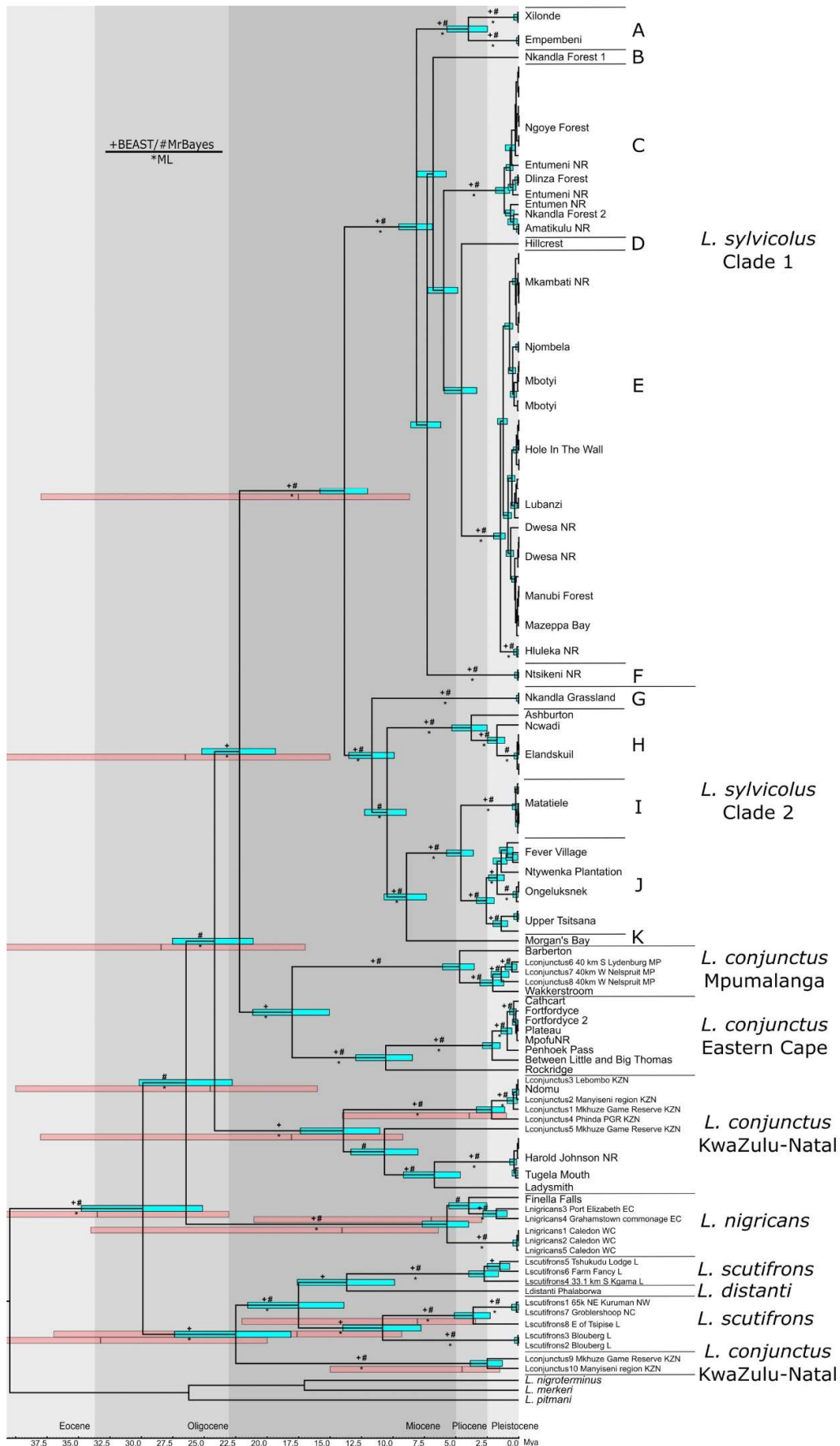
Appendix 3.4. *(see caption on the next page)*

Appendix 3.4. *(previous page)* Bayesian phylogeny derived from the two mtDNA loci, *cyt b + ND4* for all available *Leptotyphlops* sequences. Symbols represent support for maximum likelihood bootstrap >75% (*) and posterior probabilities >0.95 from the BEAST (+) and MrBayes (#) analyses. Blue node bars show 95% highest posterior distributions for each estimated divergence date in the present study. Red node bars show 95% highest posterior distributions and mean for each estimated divergence date from Adalsteinsson et al. (2009). Letters (A – K) denote the candidate lineages identified by the ABGD analysis within *L. sylvicolus*.

Appendix 3.5A

Pairwise F_{ST} values between *Leptotyphlops sylvicolus* sample localities for the *cyt b* locus. Bold values are statistically significant ($p < 0.05$).

Borders in the matrix outline pairwise F_{ST} values within lineages.

L		Locality	1	2	3	4	5	6	7	8	9	10	11	12	13	14
A	1	Xilonde	0.00000													
	2	Empembeni	1.00000	0.00000												
B	3	Nkandla Forest 1	1.00000	1.00000	0.00000											
C	4	Ngoye NR	**0.98934**	**0.98662**	0.98842	0.00000										
	5	Dlinza Forest	1.00000	1.00000	1.00000	**0.87589**	0.00000									
	6	Entumeni NR	0.96296	0.95652	0.92405	0.78469	0.40000	0.00000								
	7	Amatikulu NR	1.00000	1.00000	1.00000	**0.92199**	1.00000	0.66667	0.00000							
D	8	Hillcrest	1.00000	1.00000	1.00000	0.98639	1.00000	0.91045	1.00000	0.00000						
E	9	Mkambati NR	**0.99062**	0.99142	0.99079	**0.98789**	**0.98992**	**0.97959**	**0.99047**	0.98694	0.00000					
	10	Njabela	1.00000	1.00000	1.00000	**0.98846**	1.00000	0.95652	1.00000	1.00000	**0.89491**	0.00000				
	11	Mbotyi	**0.96542**	**0.96791**	0.96066	**0.97613**	**0.96250**	**0.94707**	**0.96450**	0.94894	**0.82139**	0.29412	0.00000			
	12	Hole-in-the-Wall	**0.98779**	0.98872	0.98710	**0.98584**	**0.98670**	0.97152	**0.98745**	0.98182	**0.93537**	0.88119	**0.80000**	0.00000		
	13	Lubanzi	**0.97457**	0.97644	0.97044	**0.98066**	**0.97237**	**0.95502**	0.97387	0.96026	**0.89579**	0.71292	**0.70865**	**0.53268**	0.00000	
	14	Dwesa NR	0.92718	0.92919	0.92581	**0.96127**	**0.92786**	**0.91395**	0.92853	0.90108	**0.88170**	**0.72888**	**0.75000**	**0.75455**	**0.66457**	0.00000
	15	Manubi Forest	1.00000	1.00000	1.00000	**0.98921**	1.00000	0.97087	1.00000	1.00000	**0.96977**	1.00000	**0.88000**	**0.94850**	0.88072	**0.34906**
	16	Mazzepa Bay	0.96308	0.96407	0.95122	**0.97930**	**0.96203**	0.93417	0.96203	0.93407	**0.93497**	0.86813	**0.83333**	**0.88327**	**0.80519**	**0.33077**
	17	Hluleka NR	0.98701	0.98795	0.97403	**0.98656**	0.98667	0.94737	0.98734	0.97015	**0.96645**	0.95238	**0.84348**	**0.94325**	0.88542	**0.80255**
F	18	Ntsikeni NR	1.00000	1.00000	1.00000	**0.98813**	1.00000	0.95652	1.00000	1.00000	**0.99047**	1.00000	0.96450	0.98812	0.97387	**0.92853**
G	19	Nkandla Grassland	1.00000	1.00000	1.00000	**0.99095**	1.00000	0.96774	1.00000	1.00000	**0.99351**	1.00000	0.97556	0.99118	**0.98130**	0.94965
H	21	Ncwadi	1.00000	1.00000	1.00000	0.99141	1.00000	0.94595	1.00000	1.00000	0.99210	1.00000	0.96943	0.98940	0.97581	0.93566
	22	Elandskuil	1.00000	1.00000	1.00000	**0.99332**	1.00000	0.98591	**1.00000**	1.00000	**0.99426**	1.00000	**0.98018**	**0.99311**	**0.98561**	**0.95971**
I	23	Matatiele	**0.99188**	**0.99256**	0.99059	**0.99154**	**0.99217**	0.98338	0.99217	0.99053	**0.99226**	**0.99243**	**0.98192**	**0.99030**	**0.98520**	**0.96824**
J	24	Fever Village	0.93287	0.93609	0.91579	**0.97736**	0.94231	0.92648	0.94231	0.91011	**0.97607**	0.94070	**0.95522**	**0.96564**	0.95454	**0.93414**
	25	Ntywenka	1.00000	1.00000	1.00000	0.99239	1.00000	0.95200	1.00000	1.00000	0.99349	1.00000	0.97391	0.99070	0.97931	0.94713
	26	Ongeluksnek NR	0.99083	0.99083	0.98400	**0.99129**	0.99174	0.96721	0.99174	0.98291	**0.99215**	0.99160	0.97497	0.98904	0.97962	**0.95206**
	27	Upper Tsitsana	**0.99188**	0.99188	0.98969	**0.99101**	0.99216	0.97468	0.99216	0.98864	**0.99183**	0.99202	**0.97624**	**0.98901**	**0.98075**	**0.95504**
K	28	Morgan's Bay	1.00000	1.00000	1.00000	0.99239	1.00000	0.95161	1.00000	1.00000	0.99349	1.00000	0.97303	0.99070	0.97945	0.94758

Appendix 3.5A continued.

| L		Locality	15	16	17	18	19	21	22	23	24	25	26	27	28
E	15	Manubi Forest	0.00000												
	16	Mazzepa Bay	0.00000	0.00000											
	17	Hluleka NR	0.97521	0.88550	0.00000										
F	18	Ntsikeni NR	1.00000	0.96203	0.98734	0.00000									
G	19	Nkandla Grassland	1.00000	0.97441	0.99065	1.00000	0.00000								
H	21	Ncwadi	1.00000	0.95775	0.98020	1.00000	1.00000	0.00000							
	22	Elandskuil	**1.00000**	0.98306	0.99484	1.00000	1.00000	1.00000	0.00000						
I	23	Matatiele	**0.99316**	**0.98314**	**0.98966**	**0.99268**	**0.99106**	0.98857	**0.99271**	0.00000					
J	24	Fever Village	0.95294	0.93642	0.93226	0.93970	0.92150	0.89041	**0.95592**	**0.94186**	0.00000				
	25	Ntywenka	1.00000	0.96610	0.98291	1.00000	1.00000	1.00000	1.00000	0.98261	0.38462	0.00000			
	26	Ongeluksnek NR	0.99409	**0.97104**	0.98246	0.99145	0.98851	0.97849	0.99461	**0.98035**	**0.28082**	0.84615	0.00000		
	27	Upper Tsitsana	0.99367	0.97516	0.98615	0.99216	0.98951	0.98701	**0.99480**	**0.98412**	0.78226	0.95652	0.93417	0.00000	
K	28	Morgan's Bay	1.00000	0.96591	0.98291	1.00000	1.00000	1.00000	1.00000	0.99059	0.90123	1.00000	0.98095	0.98750	0.00000

Appendix 3.5B

Pairwise F_{ST} values between *Macrelaps microlepidotus* sample localities for the concatenated *cyt b* and *ND4* loci. Bold values are statistically significant ($p < 0.05$). Borders in the matrix outline pairwise F_{ST} values within lineages.

L		Locality	29	30	31	32	33	34	35	36	37	38	39	40	42
A	29	Eshowe	0.00000												
	30	Kloof	0.25000	0.00000											
	31	Waterfall	0.00000	0.00000	0.00000										
	32	Assagay	0.00000	0.00000	0.00000	0.00000									
	33	Hillcrest	0.25000	0.00000	0.00000	0.00000	0.00000								
	34	Westville	0.20000	0.00000	0.00000	0.00000	0.00000	0.00000							
	35	Ixopo	0.33333	1.00000	1.00000	1.00000	1.00000	0.71429	0.00000						
	36	Shelley Beach	0.00000	1.00000	1.00000	1.00000	1.00000	0.50000	1.00000	0.00000					
	37	Southbroom	0.25000	0.25000	0.00000	0.00000	0.25000	0.15217	0.14286	0.00000	0.00000				
B	38	Gomo Forest	0.92308	1.00000	1.00000	1.00000	1.00000	**0.96407**	1.00000	1.00000	0.88000	0.00000			
	39	Mbotyi	0.84615	1.00000	1.00000	1.00000	1.00000	0.94595	1.00000	1.00000	0.76000	0.00000	0.00000		
	40	Nqadu	0.85714	1.00000	1.00000	1.00000	1.00000	0.95000	1.00000	1.00000	0.77778	1.00000	1.00000	0.00000	
	42	Dwesa NR	0.78571	**0.89565**	0.69231	0.69231	0.89565	0.86479	0.73333	0.66667	0.74074	0.00000	0.00000	0.33333	0.00000
	43	Manubi Forest	**0.88243**	**0.92302**	0.88333	0.88333	**0.92302**	**0.90680**	0.90000	0.87273	**0.86025**	0.36652	0.12500	0.46154	**0.41606**
	44	Sunrise on Sea	0.88889	0.97321	0.92000	0.92000	0.97321	0.93931	0.93103	0.91304	0.84615	0.80000	0.60000	0.71429	0.44444
	45	Dorchester Heights	0.88000	**0.97087**	0.91304	0.91304	0.97087	0.93417	0.92593	0.90476	0.83333	0.66667	0.33333	0.60000	0.28571
	46	Thorn Park	0.68750	0.81679	0.46667	0.46667	0.81679	0.79156	0.52941	0.42857	0.64516	0.20000	0.60000	0.33333	0.14286
	47	East London	0.84615	1.00000	1.00000	1.00000	1.00000	0.94595	1.00000	1.00000	0.76000	1.00000	1.00000	1.00000	0.00000
	48	Isedenge	0.85714	1.00000	1.00000	1.00000	1.00000	0.95000	1.00000	1.00000	0.77778	1.00000	1.00000	1.00000	0.20000
	49	Pirie	0.83333	1.00000	1.00000	1.00000	1.00000	0.94118	1.00000	1.00000	0.73913	1.00000	1.00000	1.00000	0.33333
	50	Hogsback	0.88587	0.94737	0.89474	0.89474	0.94737	**0.92308**	0.90909	0.88571	0.85552	0.67568	0.50000	0.63636	**0.50820**
C	41	Baziya	0.93939	1.00000	1.00000	1.00000	1.00000	0.97938	1.00000	1.00000	0.90769	1.00000	1.00000	1.00000	**0.87500**

Appendix 3.5B continued.

L		Locality	43	44	45	46	47	48	49	50	41
B	43	Manubi Forest	0.00000								
	44	Sunrise on Sea	0.02077	0.00000							
	45	Dorchester Heights	0.14729	0.50000	0.00000						
	46	Thorn Park	0.24612	0.00000	0.00000	0.00000					
	47	East London	0.30000	0.60000	0.00000	0.60000	0.00000				
	48	Isedenge	0.53333	0.71429	0.60000	0.00000	1.00000	0.00000			
	49	Pirie	0.40000	0.33333	0.00000	0.00000	1.00000	1.00000	0.00000		
	50	Hogsback	**0.48448**	0.61628	0.44068	0.32867	0.50000	0.63636	0.20000	0.00000	
C	41	Baziya	**0.95625**	0.96923	0.96825	0.76471	1.00000	1.00000	1.00000	0.95833	0.00000
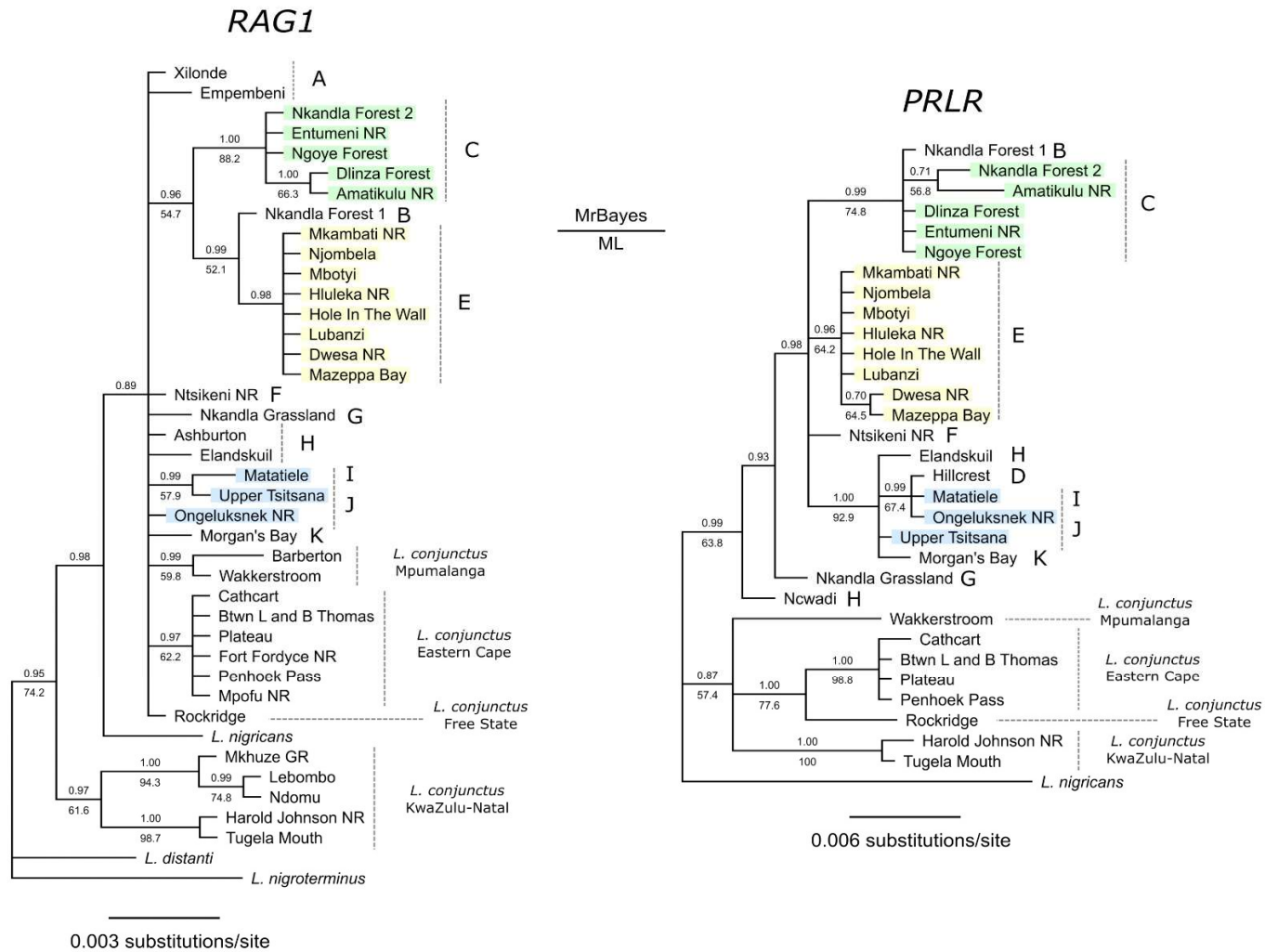
Appendix 3.6. Bayesian topologies derived from the individual nuDNA loci, *RAG1* and *PRLR*, with posterior probabilities from the MrBayes analysis above branches and maximum likelihood bootstrap values below branches. Letters denote *Leptotyphlops sylvicolus* lineages identified on the mtDNA phylogeny. Locality colors correspond to the three candidate species in the morphometric analyses.

Chapter 4
General conclusions

From the present study it is evident that diversification in the study taxa can be linked with paleoclimatic events since the late Miocene to the Pleistocene that would have been casual to the fragmentation of forest habitat. Population level divergence was evident in the larger and presumably more vagile Natal black snake, *Macrelaps microlepidotus,* where shallow Pleistocene differences were observed. By contrast, in both the forest thread snake, *Leptotyphlops sylvicolus,* and the Pondo flat gecko, *Afroedura pondolia*, deep divergence dated back to the late Miocene and both taxa represent species complexes. Despite different evolutionary histories, the taxa in the present study exhibited broadly congruent biogeographic breaks in the north eastern region of the Eastern Cape Province as well as a congruent break exhibited by *L. sylvicolus* and *A. pondolia* in the region of Durban in the KwaZulu-Natal Province.

Although the molecular data was sufficient to detect cryptic diversity and phylogeographic patterns among the three study taxa, the low sample sizes for certain localities revealed notable caveats, limiting the inferences made from the available molecular data. In the population genetic analyses low sample sizes resulted in most of the pairwise F_{ST} values between localities not being statistically significant. Furthermore, low sample sizes per locality also reduce the probability of detecting shared haplotypes, therefore limiting the inferences made regarding the gene flow among localities. Future studies would benefit from larger sample sizes and may provide more insight to the degree of interconnectivity and possible gene flow among isolated forest localities, which may be important for determining localities to be included in protected area networks in order to maintain gene flow among fragmented forest habitats. In addition, more sensitive markers such as microsatellite or next generation sequencing could complement our understanding of evolutionary process that sculpted the population genetic structure of these species.

The inferred breaks as well as the distributions of cryptic species in the present study are based on the current extent of sampling. Fine scale sampling, in the breaks between current sampling localities would be necessary to determine the total distribution of the cryptic species as well as the extent of the inferred biogeographic breaks. Sampling within the inferred breaks would reveal whether the breaks represent true biogeographic breaks and barriers to gene flow or simply reflect sampling gaps. These observations may warrant the inclusion additional forest-living taxa to test the inferred biogeographic breaks across a larger group of species. Including additional taxa would also allow for more robust statistical analyses in a comparative phylogeographic assessment of the inferred biogeographic breaks. Fine-scale sampling

would also be beneficial to quantify the total diversity among fragmented forest habitats, particularly within dispersal limited taxa such as *L. sylvicolus* where multiple cryptic lineages may be near sympatric and appear to be highly localized.

Low sample sizes per locality presented further limitations in the morphological analyses, since we used the genetic template to underpin the morphological groups. Due to permit constraints in KwaZulu-Natal, we were only permitted to sample two *A. pondolia* specimens per locality and the elusiveness of *L. sylvicolus* in some areas yielded few samples. Therefore, although the molecular analyses retrieved several lines of evidence to support the presence of several novel species within these taxa, the low sample sizes reduced the statistical power of the morphological analyses. One way to circumvent the problem of low sample sizes in morphological analyses is to make use of existing voucher specimens that were collected from the same localities, however, this approach brings in an element of uncertainty. Voucher specimens are predominantly preserved in formalin, which degrades genetic material, rendering these specimens useless for molecular analyses. Since the taxa under study exhibit cryptic diversity in geographically proximate localities, it would be imperative to know the phylogenetic position of the specimens examined in the morphological analyses to assign specimens to the correct genetic groups. Larger sample sizes in future studies would allow for additional morphological analyses such as cluster analyses, where the morphological data can be utilized independently of the molecular data to identify morphologically similar groups. With low sample sizes, these kinds of statistical analyses may yield spurious results mostly attributed to the overlap in inter- and intraspecific variation as well as human error while taking the morphometric measurements. Additionally, the lack of taxonomically informative characters among the study taxa warrants the investigation of novel approaches to phenotypically differentiate species. Future studies should investigate the usefulness of modern CT Scans and X-rays to investigating cranial and vertebral morphology which has been used to delineate cryptic species in other reptile groups.

Although both the molecular and morphological analyses were sufficient in identifying unknown diversity among the study taxa, phylogenetic relationships among the novel lineages remain dubious. This can be attributed to low sample sizes as well as the number and choice of loci used in the present study. The mitochondrial loci retrieved high divergence among lineages, comparable to other snake and gecko groups, however, the deeper nodes on the topologies were mostly poorly supported. The nuclear loci on the other hand exhibited low variation with generally poorly supported clades. Including additional loci, such as fast evolving nuclear loci or whole genome sequences, may resolve the taxonomic relationships among these novel lineages and by doing so provide a better understanding of the evolutionary history of these taxa. Additionally, incorporating niche modeling in future studies may reveal the drivers behind the inferred biogeographic breaks. We speculate that ancient climatic shifts

initiated cladogenesis, but contemporary climatic gradients may be maintaining lineage isolation. However, other than climatic gradients, physical barriers such as the deep gorges, large rivers or corridors of unfavorable habitat may be the main drivers of cladogenesis in some but not all taxa.

Revealing cryptic species among the study taxa have implications for the conservation status of the respective taxa as well as the management of forest habitat where these species occur. The cryptic species identified in *L. sylvicolus* and *A. pondolia* exhibit much narrower distributions than the nominal species they are currently classified under and in some lineages these distributions are highly localized, making them of high conservation concern as they could be more prone to extinction. For these geographically restricted species habitat loss and transformation would be among the greatest threats, emphasizing the importance of habitat conservation. Broadly congruent phylogeographic patterns among the study taxa as well as other forest-living reptiles could suggest that co-distributed forest-living species groups yet to be studied may reflect similar patterns. This would indicate that the forest biome along the east coast of South Africa most likely harbor significantly higher levels of diversity than currently recognized, further emphasizing the importance of identifying priority regions in need of conservation. Incorporating molecular diversity alongside species diversity in future forest conservation planning would be imperative to uncovering yet unknown priority regions with high endemism and diversity.

References

Adalsteinsson, S. A., Branch, W.R., Trape, S., Vitt, L.J., Hedges, S.B., 2009. Molecular phylogeny, classification, and biogeography of snakes of the family Leptotyphlopidae (Reptilia, Squamata). Zootaxa 50, 1–50.

Ahrens, D., Fujisawa, T., Krammer, H.J., Eberle, J., Fabrizi, S., Vogler, A.P., 2016. Rarity and incomplete sampling in DNA-based species delimitation. Syst. Biol. 65, 478–494.

Albert, E.M., Zardoya, R., García-París, M., 2007. Phylogeographical and speciation patterns in subterranean worm lizards of the genus *Blanus* (Amphisbaenia: Blanidae). Mol. Ecol. 16, 1519–1531.

Aragón, P., Lobo, J.M., Olalla-Tárraga, M.Á., Rodríguez, M.Á., 2010. The contribution of contemporary climate to ectothermic and endothermic vertebrate distributions in a glacial refuge. Glob. Ecol. Biogeogr. 19, 40–49.

Araújo, M.B., Nogués-Bravo, D., Diniz-Filho, J.A.F., Haywood, A.M., Valdes, P.J., Rahbek, C., 2008. Quaternary climate changes explain diversity among reptiles and amphibians. Ecography 31, 8–15.

Araújo, M.B., Thuiller, W., Pearson, R.G., 2006. Climate warming and the decline of amphibians and reptiles in Europe. J. Biogeogr. 33, 1712–1728.

Arévalo, E., Davis, S.K., Sites, J.W., 1994. Mitochondrial DNA sequence divergence and phylogenetic relationships among eight chromosome races of the *Sceloporus grammicus* complex (Phrynosomatidae) in central Mexico. Syst. Biol. 43, 387–418.

Balmford, A., 1996. Extinction filters and current resilience: the significance of past selection pressures for conservation biology. Trends Ecol. Evol. 11, 193–196.

Barlow, A., Baker, K., Hendry, C.R., Peppin, L., Phelps, T., Tolley, K.A., Wüster, C.E., Wüster, W., 2013. Phylogeography of the widespread African puff adder (*Bitis arietans*) reveals multiple Pleistocene refugia in southern Africa. Mol. Ecol. 22, 1134–1157.

Barnes, A., Daniels, S.R., 2019. On the importance of fine-scale sampling in detecting alpha taxonomic diversity among saproxylic invertebrates: a velvet worm (Onychophora: *Opisthopatus amaxhosa*) template. Zool. Scr. 48, 243–262.

Bates, M.F., Branch, W.R., Bauer, A.M., Burger, M., Marais, J., Alexander, G.J., De Villiers, M.S. (Eds.), 2014. Atlas and Red List of the Reptiles of South Africa, Lesotho and Swaziland. Suricata 1. South African National Biodiversity Institute, Pretoria.

Bauer, A.M., Lamb, T., 2002. Phylogenetic relationships among members of the *Pachydactylus capensis* group of southern African geckos. Afr. Zool. 37, 209–220.

Bauer, A.M., Lamb, T., Branch, W.R., 2006. A revision of the *Pachydactylus serval* and *P. weberi* groups (Reptilia: Gekkota: Gekkonidae) of Southern Africa, with the description of eight new species. Proc. Cal. Acad. Sci. 57, 595–709.

Blair, C., Bryson, R.W., 2017. Cryptic diversity and discordance in single-locus species delimitation methods within horned lizards (Phrynosomatidae: *Phrynosoma*). Mol. Ecol. Res. 17, 1168–1182.

Bonnet, X., Naulleau, G., Shine, R., 1999. The dangers of leaving home: dispersal and mortality in snakes. Biol. Conserv. 89, 39–50.

Bouckaert, R.R., Heled, J., Kühnert, D., Vaughan, T.J., Wu, C., Xie, D., Suchard, M.A., Rambaut, A., Drummond, A.J., 2014. BEAST 2: A Software platform for Bayesian evolutionary analysis. PLoS Comp. Biol. 10, e1003537.

Branch, W.R., 1998. Field guide to the snakes and other reptiles of southern Africa. Revised edition. Struik Publishers, Cape Town, South Africa.

Branch, W.R., Guyton, J.A., Schmitz, A., Barej, M.F., Naskrecki, P., Farooq, H., Verburgt, L., Rödel, M.O., 2017. Description of a new flat gecko (Squamata: Gekkonidae: *Afroedura*) from Mount Gorongosa, Mozambique. Zootaxa 4324, 142-160.

Branch, W.R., Tolley, K.A., Cunningham, M., Bauer, A.M., Alexander, G., Harrison, J.A., Turner, A.A., Bates, M.F. (Eds.), 2006. A Plan for Phylogenetic Studies of Southern African Reptiles: Proceedings of a Workshop Held at Kirstenbosch, February 2006. Biodiversity Series 5. South African National Biodiversity Institute, Pretoria.

Bredenkamp, G.J., Spada, F., Kazmierczak, E., 2002. On the origin of Northern and Southern Hemisphere grasslands. Plant Ecol. 163, 209–229.

Broadley, D.G., Broadley, S., 1999. A review of the African wormsnakes from south of latitude 12°S (Serpentes: Leptotyphlopidae). Syntarsus 5, 1–36.

Broadley, D.G., Wallach, V., 1997. A review of the genus *Leptotyphlops* (Serpentes: Leptotyphlopidae) in KwaZulu-Natal, South Africa, with the description of a new forest-dwelling species. Durban Mus. Novit. 22, 37–42.

Brown, W.L., Wilson, E.O., 1956. Character displacement. Syst. Zool. 5, 49–64.

Busschau, T., Conradie, W., Daniels, S.R., 2019. Evidence for cryptic diversification in a rupicolous forest-dwelling gecko (Gekkonidae: *Afroedura pondolia*) from a biodiversity

hotspot. Mol. Phylogenet. Evol. 139, 106549.

Busschau, T., Conradie, W., Jordaan, A., Daniels, S.R., 2017. Unmasking evolutionary diversity among two closely related South African legless skink species (Acontinae: *Acontias*) using molecular data. Zoology 121, 72–82.

Carranza, S., Arnold, E.N., 2012. A review of the geckos of the genus *Hemidactylus* (Squamata: Gekkonidae) from Oman based on morphology, mitochondrial and nuclear data, with descriptions of eight new species. Zootaxa 95, 1–95.

Clark, V.R., Barker, N.P., Mucina, L., 2011. The Great Escarpment of southern Africa: a new frontier for biodiversity exploration. Biodiv. Conser. 20, 2543–2561.

Clement, M., Posada, D., Crandall, K., 2000. TCS: a computer program to estimate gene genealogies. Mol. Ecol. 9, 1657–1660.

Coetzee, J.A., 1986. Microfloral elements in the Neogene of the southwestern Cape Province and their phytogeographic significance. Palaeoecol. Afr. 17, 21–30.

Coetzee, J.A., 1993. African flora since the Terminal Jurassic. In: Goldblatt, P. (Ed.), Biological Relationships between Africa and South America. Yale University Press, New Haven, Connecticut, pp. 37–61.

Conroy, C.J., Papenfuss, T., Parker, J., Hahn, N.E., 2009. Use of tricaine methanesulfonate (MS222) for euthanasia of reptiles. J. Am. Ass. Lab. Anim. Sci. 48, 28–32.

da Silva, J.M., Tolley, K.A., 2017. Diversification through ecological opportunity in dwarf chameleons. J. Biogeogr. 44, 834–847.

Daniels, S.R., 2017. Sympatric color morphs or distinct taxa? Examining species boundaries among two South African freshwater crabs (Decapoda: Potamonautidae: *Potamonautes* MacLeay, 1838), with the description of a new species. J. Crust. Biol. 37, 723–731.

Daniels, S.R., Dambire, C., Klaus, S., Sharma, P.P., 2016. Unmasking alpha diversity, cladogenesis and biogeographical patterning in an ancient panarthropod lineage (Onychophora: Peripatopsidae: *Opisthopatus cinctipes*) with the description of five novel species. Cladistics 32, 506–537.

Daniels, S.R., Dreyer, M., Sharma, P.P., 2017. Contrasting the population genetic structure of two velvet worm taxa (Onychophora: Peripatopsidae: *Peripatopsis*) in forest fragments along the south-eastern Cape, South Africa. Invert. Syst. 31, 781–796.

Daniels, S.R., Heideman, N.J.L., Hendricks, M.G.J., 2009. Examination of evolutionary relationships in the Cape fossorial skink species complex (Acontinae: *Acontias meleagris*

meleagris) reveals the presence of five cryptic lineages. Zool. Scr. 38, 449–463.

Daniels, S.R., Heideman, N.J.L., Hendricks, M.G.J., Crandall, K.A., 2006. Taxonomic subdivisions within the fossorial skink subfamily Acontinae (Squamata: Scincidae) reconsidered: a multilocus perspective. Zool. Scr. 35, 353–362.

Daniels, S.R., Heideman, N.J.L., Hendricks, M.G.J., Wilson, B A., 2002. A molecular phylogeny for the South African limbless lizard taxa of the subfamily Acontinae (Sauria: Scincidae) with special emphasis on relationships within *Acontias*. Mol. Phylogenet. Evol. 24, 315–323.

Daza, J.M., Smith, E.N., Páez, V.P., Parkinson, C.L., 2009. Complex evolution in the Neotropics: The origin and diversification of the widespread genus *Leptodeira* (Serpentes: Colubridae). Mol. Phylogenet. Evol. 53, 653–667.

de Queiroz, K., 1998. The general lineage concept of species, species criteria, and the process of speciation: a conceptual unification and terminological recommendations. In: Howard, D.J., Berlocher, S.H. (Eds.), Endless Forms: Species and Speciation. Oxford University Press, New York, pp. 57–75.

Deacon, H.J., 1983. Another look at the Pleistocene climates of South Africa. S. Afr. J. Sci. 79, 325–328.

Deacon, H.J., Jury, M.R., Ellis, F., 1992. Selective regime and time. In Cowling, R.M. (Ed.), The Ecology of Fynbos: Nutrients, Fire and Diversity. Cape Town, Oxford University Press. pp. 6–22.

Dellicour S., Flot J., 2015. Delimiting species-poor data sets using single molecular markers: a study of Barcode Gaps, Haplowebs and GMYC. Syst. Biol. 64, 900–908.

Díaz, J.A., Verdú-Ricoy, J., Iraeta, P., Llanos-Garrido, A., Pérez-Rodríguez, A., Salvador, A., 2017. There is more to the picture than meets the eye: adaptation for crypsis blurs phylogeographical structure in a lizard. J. Biogeogr. 44, 397–408.

Diedericks, G., Daniels, S.R., 2013. Ain't no mountain high enough, ain't no valley low enough? Phylogeography of the rupicolous Cape girdled lizard (*Cordylus cordylus*) reveals a generalist pattern. Mol. Phylogenet. Evol. 71, 234–248.

Edwards, S., Tolley, K.A., Vanhooydonck, B., Measey, G.J., Herrel, A., 2013. Is dietary niche breadth is linked to morphology and performance in Sandveld lizards *Nucras* (Sauria: Lacertidae)? Biol. J. Linn. Soc. 110, 674–688.

Edwards, S., Vanhooydonck, B., Herrel, A., Measey, G.J., Tolley, K.A., 2012. Convergent evolution associated with habitat decouples phenotype from phylogeny in a clade of lizards. PLoS ONE 7, e51636.

Eeley, H.A.C., Lawes, M.J., Piper, S.E., 1999. The influence of climate change on the distribution of indigenous forest in KwaZulu-Natal, South Africa. J. Biogeogr. 26, 595–617.

Engelbrecht, H.M., van Niekerk, A., Heideman, N.J.L., Daniels, S.R., 2013. Tracking the impact of Pliocene/ Pleistocene sea level and climatic oscillations on the cladogenesis of the Cape legless skink, *Acontias meleagris* species complex, in South Africa. J. Biogeogr. 40, 492–506.

Esselstyn, J.A., Evans, B.J., Sedlock, J.L., Anwarali Khan, F.A., Heaney, L.R., 2012. Single-locus species delimitation: a test of the mixed Yule-coalescent model, with an empirical application to Philippine round-leaf bats. Proc. R. Soc. Lond., B, Biol. Sci. 279, 3678– 3686.

Excoffier, L., Laval, G., Schneider, S., 2005. Arlequin ver. 3.0: an integrated software package for population genetics data analysis. Evol. Bioinform. Online, 1, 47–50.

Feakins, S.J., Demenocal, P.B., 2010. Global and African regional climate during the Cenozoic. In: Werdelin, L., Sanders, W.J. (Eds.), Cenozoic Mammals of Africa. University of California Press, CA, USA, pp. 45–56.

Ferguson, J.W.H., 2002. On the use of genetic divergence for identifying species. Biol. J. Linn. Soc. 75, 509–516.

Fujisawa, T., Barraclough, T.G., 2013. Delimiting species using single-locus data and the Generalized Mixed Yule Coalescent approach: a revised method and evaluation on simulated data sets. Syst. Biol. 62, 707–724.

Gaston, K.J., Blackburn, T.M., 2006. Range Size-Body Size Relationships: Evidence of Scale Dependence. Oikos 75, 479.

Geldenhuys, C.J., 1992. Richness, composition and relationships of the floras of selected forests in southern Africa. Bothalia 22, 205–233.

Geldenhuys, C.J., MacDevette, D.R., 1989. Conservation status of coastal and montane evergreen forest. In: Huntley, B.J. (Ed.), Biotic diversity in southern Africa: concepts and conservation. Oxford University Press, Cape Town, pp. 224–238.

Guo, P., Liu, Q., Zhu, F., Murphy, R.W., Zhong, G.H., Che, J., Wang, P., Xie, Y.L., Malhotra, A., 2019. Multilocus phylogeography of the brown-spotted pitviper *Protobothrops mucrosquamatus* (Reptilia: Serpentes: Viperidae) sheds a new light on the diversification

pattern in Asia. Mol. Phylogenet. Evol. 133, 82–91.

Hawlitschek, O., Toussaint, E.F.A., Gehring, P.S., Ratsoavina, F.M., Cole, N., Crottini, A., Nopper, J., Lam, A.W., Vences, M., Glaw, F., 2017. Gecko phylogeography in the Western Indian Ocean region: the oldest clade of *Ebenavia inunguis* lives on the youngest island. J. Biogeogr. 44, 409–420.

Hedges, S.B., 2008. At the lower size limit in snakes: two new species of threadsnakes (Squamata: Leptotyphlopidae: *Leptotyphlops*) from the Lesser Antilles. Zootaxa 1841, 1–30.

Heideman, N.J.L., Mulcahy, D.G., Sites, Jr., J.W., Hendricks, M.G.J., Daniels, S. R., 2011. Cryptic diversity and morphological convergence in threatened species of fossorial skinks in the genus *Scelotes* (Squamata: Scincidae) from the Western Cape coast of South Africa: implications for species boundaries, digit reduction and conservation. Mol. Phylogenet. Evol. 61, 823–833.

Heinicke, M.P., Adderly, L.M., Bauer, A.M., Jackman, T.R., 2011. A long-known new species of gecko allied to *Pachydactylus bicolor* (Squamata: Gekkonidae) from the central Namibian coast. Afr. J. Herp. 60, 113–129.

Heinicke, M.P., Daza, J.D., Bauer, A.M., Jackman, T.R., Greenbaum, E., 2014. Phylogeny, taxonomy and biogeography of a circum-Indian Ocean clade of leaf-toed geckos (Reptilia: Gekkota), with a description of two new genera. Syst. Biodivers. 12, 23–42.

Heinicke, M.P., Jackman, T.R., Bauer, A.M., 2017a. The measure of success: geographic isolation promotes diversification in *Pachydactylus* geckos. BMC Evol. Biol. 17, 1–17.

Heinicke, M.P., Turk, D., Bauer, A.M., 2017b. Molecular phylogeny reveals strong biogeographic signal and two new species in a Cape Biodiversity Hotspot endemic mini-radiation, the pygmy geckos (Gekkonidae: *Goggia*). Zootaxa 4312, 449–470.

Hewitt, B.J., 1925. On some new species of reptiles and amphibians from South Africa. Rec. Albany Mus. 3, 457.

Hewitt, G.M., 2000. The genetic legacy of the Quaternary ice ages. Nature, 405, 907–913.

Hewitt, G.M., 2003. Ice ages: their impact on species distributions and evolution. In Rothschild, L.J., Lister, A.M. (Eds.), Evolution on planet Earth. Academic Press, New York, pp. 339–361.

Hewitt, G.M., 2004. Genetic consequences of climatic oscillations in the Quaternary. Proc. R. Soc. Lond. [Biol] 359, 183–195.

Hosseinzadeh, M.S., Aliabadian, M., Rastegar-Pouyani, E., Rastegar-Pouyani, N., 2015. Morphometric study of *Hemidactylus* geckos (Squamata: Gekkonidae) in Iran. Iran. J. Anim. Biosyst. 10, 175–184.

Jacobs, S.J., Kristofferson, C., Uribe-Convers, S., Latvis, M., Tank, D.C., 2018. Incongruence in molecular species delimitation schemes: what to do when adding more data is difficult. Mol. Ecol. 27, 2397–2413.

Jacobsen, N.H.G., 1992. Flat geckos (genus *Afroedura*) in the Transvaal. Afr. J. Herpetol, 40, 22–25.

Jacobsen, N.H.G., 1994. The *Platysaurus intermedius* complex (Sauria: Cordylidae) in the Transvaal, South Africa, with descriptions of three new taxa. S. Afr. J. Zool. 29, 132–143.

Jacobsen, N.H.G., Kuhn, A.L., Jackman, T.R., Bauer, A.M., 2014. A phylogenetic analysis of the southern African gecko genus *Afroedura* Loveridge (Squamata: Gekkonidae), with the description of nine new species from Limpopo and Mpumalanga provinces of South Africa. Zootaxa 3846, 451–501.

Johnson, M.K., Russell, A.P., Bauer, A.M., 2005. Locomotor morphometry of the *Pachydactylus* radiation of lizards (Gekkota: Gekkonidae): a phylogenetically and ecologically informed analysis. Can. J. Zool. 83, 1511–1524.

Jones, G., 2017. Algorithmic improvements to species delimitation and phylogeny estimation under the multispecies coalescent. J. Math. Biol. 74, 447–467.

Jones, G., Aydin, Z., Oxelman, B., 2015. DISSECT: An assignment-free Bayesian discovery method for species delimitation under the multispecies coalescent. Bioinformatics 31, 991–998.

Jukes, T.H., Cantor, C.R., 1969. Evolution of protein molecules. In: Munro, H.N. (Ed.), Mammalian protein metabolism III. Academic Press Elsevier, New York, pp. 21–132.

Kimura M., 1980. A simple model for estimating evolutionary rates of base substitutions between homologous nucleotide sequences. J. Mol. Evol. 16, 111–120.

Kornilios, P., 2017. Polytomies, signal and noise: revisiting the mitochondrial phylogeny and phylogeography of the Eurasian blindsnake species complex (Typhlopidae, Squamata). Zool. Scr. 46, 665–674.

Kornilios, P., Kumlutaş, Y., Lymberakis, P., Ilgaz, Ç., 2018. Cryptic diversity and molecular systematics of the Aegean *Ophiomorus* skinks (Reptilia: Squamata), with the description of a new species. J. Zool. Syst. Evol. Res. 56, 364–381.

Kotsakiozi, P., Jablonski, D., Ilgaz, Ç., Kumlutaş, Y., Avcı, A., Meiri, S., Itescu, Y., Kukushkin, O., Gvoždík, V., Scillitani, G., Roussos, S.A., Jandzik, D., Kasapidis, P., Lymberakis, P., Poulakakis, N., 2018. Multilocus phylogeny and coalescent species delimitation in Kotschy's gecko, *Mediodactylus kotschyi*: hidden diversity and cryptic species. Mol. Phylogenet. Evol. 125, 177–187.

Kullenkampff, K., Van Zyl, F., Klaus, S., Daniels, S.R., 2019. Molecular evidence for cryptic species in the common slug eating snake *Duberria lutrix lutrix* (Squamata, Lamprophiidae) from South Africa. Zookeys 838, 133–154.

Kumar, S., Stecher, G., Li, M., Knyaz, C., Tamura, K., 2018. MEGA X: molecular evolutionary genetics analysis across computing platforms. Mol. Biol. Evol. 35, 1547–1549.

Kushata, J.N.T., 2018. Comparative phylogeography of three anuran species in the Eastern Cape Province forests. Unpublished M.Sc Thesis. Stellenbosch University, 103 pp.

Lajmi, A., Giri, V.B., Karanth, K.P., 2016. Molecular data in conjunction with morphology help resolve the *Hemidactylus brookii* complex (Squamata: Gekkonidae). Org. Divers. Evol. 16, 659–677.

Lamb, T., Biswas, S., Bauer, A.M., 2010. A phylogenetic reassessment of African fossorial skinks in the subfamily Acontinae (Squamata: Scincidae): Evidence for parallelism and polyphyly. Zootaxa 46, 33–46.

Laver, R.J., Doughty, P., Oliver, P.M., 2018. Origins and patterns of endemic diversity in two specialized lizard lineages from the Australian Monsoonal Tropics (*Oedura* spp.). J. Biogeogr. 45, 142–153.

Lavin, B.R., Wogan, G.O.U., McGuire, J.A., Feldman, C.R., 2018. Phylogeography of the Northern Alligator Lizard (Squamata, Anguidae): Hidden diversity in a western endemic. Zool. Scr. 47, 462–476.

Lawes, M.J., 1990. The distribution of the samango monkey (*Cercopithecus mitis erythrarchus* Peters, 1852 and *Cercopithecus mitis labiatus* I. Geoffroy, 1843) and forest history in southern Africa. J. Biogeogr. 17, 669–680.

Lawes, M.J., Eeley, H.A.C., Findlay, N.J., Forbes, D., 2007. Resilient forest faunal communities in South Africa: a legacy of palaeoclimatic change and extinction filtering? J. Biogeogr. 34, 1246–1264.

Lawes, M.J., Eeley, H.A.C., Piper, S.E., 2000a. The relationship between local and regional diversity of indigenous forest fauna in KwaZulu-Natal Province, South Africa. Biodivers. Conserv. 9, 683–705.

Lawes, M.J., Mealin, P.E., Piper, S.E., 2000b. Patch Occupancy and Potential Metapopulation Dynamics of Three Forest Mammals in Fragmented Afromontane Forest in South Africa. Conserv. Biol. 14, 1088–1098.

Lawson, L.P., 2010. The discordance of diversification: Evolution in the tropical-montane frogs of the Eastern Arc Mountains of Tanzania. Mol. Ecol. 19, 4046–4060.

Lee-Thorp, J.A., Sponheimer, M., Luyt, J., 2007. Tracking changing environments using stable carbon isotopes in fossil tooth enamel: an example from the South African hominid sites. J. Hum. Evol. 53, 595– 601.

Linder, H.P., 2003. The radiation of the Cape Flora. Biol. Rev. 78, 597–638.

Low, A.B., Rebelo, A.G., 1996. Vegetation of South Africa, Lesotho and Swaziland. Department of Environmental Affairs and Tourism, Pretoria, South Africa.

Luo, A., Ling, C., Ho, S.Y.W., Zhu, C.D., 2018. Comparison of methods for molecular species delimitation across a range of speciation scenarios. Syst. Biol. 67, 830–846.

MacDevette, D.R., MacDevette, K., Gordon, I.G., Bartholomew, R., 1989. The floristics of the Natal indigenous forests. In: Gordon, I.G. (Ed.), Natal indigenous forest: a preliminary collection of reports on indigenous forests. Natal Parks Board, Pietermaritzburg, pp. 1-20.

Macey, J. R., J. A. Schulte II, N. B. Ananjeva, A. Larson, N. Rastegar-Pouyani, S. M. Shammakov, and T. J. Papenfuss. 1998. Phylogenetic relationships among agamid lizards of the *Laudakia caucasia* species group: testing hypotheses of biogeographic fragmentation and an area cladogram for the Iranian Plateau. Mol. Phylogenet. Evol. 10:118–131.

Makhubo, B.G., Tolley, K.A., Bates, M.F., 2015. Molecular phylogeny of the *Afroedura nivaria* (Reptilia: Gekkonidae) species complex in South Africa provides insight on cryptic speciation. Mol. Phylogenet. Evol. 82, 31–42.

Martín, J., López, P., García, L. V, 2013. Soil characteristics determine microhabitat selection of the fossorial amphisbaenian Trogonophis wiegmanni. J. Zool. 290, 265–272.

Massot, M., Clobert, J., Ferriere, R., 2008. Climate warming, dispersal inhibition and extinction risk. Glob. Change Biol. 14, 461–469.

Matthee, C.A., Flemming, A.F., 2002. Population fragmentation in the southern rock agama, *Agama atra*: more evidence for vicariance in southern Africa. Mol. Ecol. 11, 65–71.

Mazus, H., 2000. Clues on the history of *Podocarpus* forest in Maputaland, South Africa, during the Quaternary, based on pollen analysis. AGR 7, 75– 82.

McKelvy, A.D., Burbrink, F.T., 2017. Ecological divergence in the yellow-bellied kingsnake (*Lampropeltis calligaster*) at two North American biodiversity hotspots. Mol. Phylogenet. Evol. 106, 61–72.

Medina, M.F., Bauer, A.M., Branch, W.R., Schmitz, A., Conradie, W., Nagy, Z.T., Hibbitts, T.J., Ernst, R., Portik, D.M., Nielsen, S. V, Colston, T.J., Kusamba, C., Behangana, M., Rödel, M.-O., Greenbaum, E., 2016. Molecular phylogeny of *Panaspis* and *Afroablepharus* skinks (Squamata: Scincidae) in the savannas of sub-Saharan Africa. Mol. Phylogenet. Evol. 100, 409–423.

Midgley, J.J., Cowling, R.M., Seydack, A.H.W. van Wyk, G.F., 1997. Forest. In: Cowling, R.M., Richardson, D.M., Pierce, S.M. (Eds.), Vegetation of Southern Africa. Cambridge University Press, Cambridge, pp. 278–299.

Morando, M., Avila, L.J., Sites Jr., J.W., 2003. Sampling strategies for delimiting species: genes, individuals, and populations in the *Liolaemus elongatuskriegi* complex (Squamata: Liolaemidae) in Andean–Patagonian South America. Syst. Biol. 52, 159–185.

Moura, M.R., Argôlo, A.J., Costa, H.C., 2016. Historical and contemporary correlates of snake biogeographical subregions in the Atlantic Forest hotspot. J. Biogeogr. 44, 640–650.

Mouton, P.LeF.N., van Wyk, J.H., 1994. Taxonomic status of geographical isolates in the *Cordylus minor* complex (Reptilia: Cordylidae): a description of three new species. J. Herpetol. Assoc. Afr. 43, 6–18.

Mucina, L. M. C., Rutherford, R., 2006. The Vegetation of South Africa, Lesotho and Swaziland. Strelitzia vol. 19. South African National Biodiversity Institute, Pretoria.

Mucina, L., Geldenhuys, C.J., 2006. Afrotemperate, subtropical and azonal forests. In: Mucina, L., Rutherford, M.C. (Eds.), The Vegetation of South Africa, Lesotho and Swaziland. Strelitzia, vol. 19. South African National Biodiversity Institute, Pretoria, pp. 585–614.

Mucina, L., Scott-Shaw, C.R., Rutherford, M.C., Camp, K.G.T., Matthews, W., Powrie, L., Hoare, D.B., 2006. Indian Ocean Coastal Belt. In: Mucina, L., Rutherford, M.C. (Eds.), The

Vegetation of South Africa, Lesotho and Swaziland. Strelitzia, vol. 19. South African National Biodiversity Institute, Pretoria, pp. 568–583.

Myers, E.A., Hickerson, M.J., Burbrink, F.T., 2017. Asynchronous diversification of snakes in the North American warm deserts. J. Biogeogr. 44, 461–474.

Neumann, F.H., Bamford, M.K., 2015. Shaping of modern southern African biomes: Neogene vegetation and climate changes. Trans. R. Soc. S. Afr. 70, 195–212.

Onderstall, D., 1984. Descriptions of two new subspecies of *Afroedura pondolia* (Hewitt) and a discussion of species groups within the genus (Reptilia: Gekkonidae). Ann. Trans. Mus. 33, 497–509.

Ornelas, J.F., Sosa, V., Soltis, D.E., Daza, J.M., González, C., Soltis, P.S., Gutiérrez-Rodríguez, C., de los Monteros, A.E., Castoe, T.A., Bell, C., Ruiz-Sanchez, E., 2013. Comparative Phylogeographic Analyses Illustrate the Complex Evolutionary History of Threatened Cloud Forests of Northern Mesoamerica. PLoS One 8, e56283.

Parham, J.F., Papenfuss, T.J., 2009. High genetic diversity among fossorial lizard populations (*Anniella pulchra*) in a rapidly developing landscape (Central California). Conserv. Genet. 10, 169–176.

Partridge, T.C., Maud, R.R., 2000. Macro-scale geomorphic evolution of southern Africa. In: Partridge, T.C., Maud, R.R. (Eds.), The Cenozoic of Southern Africa. Oxford University Press, Oxford, pp. 3–18.

Paz, A., Crawford, A.J., 2012. Molecular-based rapid inventories of sympatric diversity: a comparison of DNA barcode clustering methods applied to geography-based vs clade-based sampling of amphibians. J. Biosci. 37, 887–896.

Pentinsaari, M., Vos, R., Mutanen, M., 2017. Algorithmic single-locus species delimitation: effects of sampling effort, variation and non-monophyly in four methods and 1870 species of beetles. Mol. Ecol. Res. 17, 393–404.

Perera, S.J., Ratnayake-Perera, D., Procheş, Ş., 2011. Vertebrate distributions indicate a greater Maputoland-Pondoland-Albany region of endemism. S. Afr. J. Sci. 107, 49-63.

Perissinotto, R., Stretch, D.D., Taylor, R.H. (Eds.), 2013. Ecology and conservation of estuarine ecosystems: Lake St. Lucia as a global model. Cambridge University Press. Cambridge.

Pinto, B.J., Colli, G.R., Higham, T.E., Russell, A.P., Scantlebury, D.P., Vitt, L.J., Gamble, T., 2019. Population genetic structure and species delimitation of a widespread, Neotropical

dwarf gecko. Mol. Phylogenet. Evol. 133, 54–66.

Portillo, F., Branch, W.R., Conradie, W., Rödel, M.-O., Penner, J., Barej, M.F., Kusamba, C., Muninga, W.M., Aristote, M.M., Bauer, A.M., Trape, J.-F., Nagy, Z.T., Carlino, P., Pauwels, O.S.G., Menegon, M., Burger, M., Mazuch, T., Jackson, K., Hughes, D.F., Behangana, M., Zassi-Boulou, A.-G., Greenbaum, E., 2018. Phylogeny and biogeography of the African burrowing snake subfamily Aparallactinae (Squamata: Lamprophiidae). Mol. Phylogenet. Evol. 127, 288–303.

Portillo, F., Stanley, E.L., Branch, W.R., Conradie, W., Rödel, M.-O., Penner, J., Barej, M.F., Kusamba, C., Muninga, W.M., Aristote, M.M., Bauer, A.M., Trape, J.-F., Nagy, Z.T., Carlino, P., Pauwels, O.S.G., Menegon, M., Ineich, I., Burger, M., Zassi-Boulou, A.-G., Mazuch, T., Jackson, K., Hughes, D.F., Behangana, M., Greenbaum, E., 2019. Evolutionary history of burrowing asps (Lamprophiidae: Atractaspidinae) with emphasis on fang evolution and prey selection. PLoS One 14, e0214889.

Posada, D., 2008. jModelTest: phylogenetic model averaging. Mol. Biol. Evol., 25, 1253–1256.

Prell, W.L., Hutson, W.H., Williams, D.F., Be´, A.W.H., Geitzenauer, K., Molfino, B., 1980. Surface circulation of the Indian Ocean during the last glacial maximum, approximately 18,000 yr. B.P. Quat. Res. 14, 309–336.

R Core Team, 2014. R: A Language and Environment for Statistical Computing. R Foundation for Statistical Computing, Vienna, Austria. Available at: http://www.R-project.org/

Rambaut, A., 2016. Figtree v1.4.3. Available online: http://tree.Bio.Ed.Ac.Uk/software/figtree

Rambaut, A., Suchard, M.A., Xie, D., Drummond, A.J., 2014. Tracer v1.6. Available online: http://beast.bio.ed.ac.uk/Tracer

Reid, N.M., Carstens, B.C., 2012. Phylogenetic estimation error can decrease the accuracy of species delimitation: a Bayesian implementation of the general mixed Yule-coalescent model. BMC Evol. Biol. 12, 196.

Renner, M.A., Heslewood, M.M., Patzak, S.D., Schäfer-Verwimp, A., Heinrichs, J. 2017. By how much do we underestimate species diversity of liverworts using morphological evidence? An example from Australasian Plagiochila (Plagiochilaceae: *Jungermanniopsida*). Mol. Phylogenet. Evol. 107, 576–593.

Rice, W.R., 1989. Analyzing tables of statistical tests. Evolution 43, 223–225.

Roberts, D.L., Sciscio, L., Herries, A.I.R., Scott, L., Bamford, M.K., Musekiwa, C., Tsikos, H., 2013. Miocene fluvial systems and palynofloras at the southwestern tip of Africa:

Implications for regional and global fluctuations in climate and ecosystems. Earth Sci. 124, 184–201.

Röll, B., Pröhl, H., Hoffmann, K.P., 2010. Multigene phylogenetic analysis of *Lygodactylus* dwarf geckos (Squamata: Gekkonidae). Mol. Phylogenet. Evol. 56, 327–335.

Ronquist, F., Teslenko, M., van der Mark, P., Ayres, D.L., Darling, A., Höhna, S., Larget, B., Liu, L., Suchard, M.A., Huelsenbeck, J.P., 2012. MrBayes 3.2: efficient Bayesian phylogenetic inference and model choice across a large model space. Syst. Biol. 61, 539–542.

Russell, A.P., Bauer, A.M., 1989. The morphology of the digits of the golden gecko, *Calodactylodes aureus* (Reptilia: Gekkonidae) and its implications for the occupation of rupicolous habitats. Amph. Rep. 10, 125–140.

Rutherford, M.C., Westfall, R.H., 1994. Biomes of Southern Africa: an objective categorization. Mem. Bot. Surv. S. Afr. 63, 1–94.

Scott, L., Anderson, H.M., Anderson, J.M., 1997. Vegetation history. In: Cowling, R.M., Richardson, D.M., Pierce, S.M. (Eds.), Vegetation history of Southern Africa. Cambridge University Press, Cambridge, pp. 62–90.

Scott, L., Cadman, A., McMillan, I., 2006. Early history of Cainozoic Asteraceae along the southern African west coast. Rev. Palaeobot. Palynol. 142, 47–-52.

Sepulchre, P., Ramstein, G., Fluteau, F., Schuster, M., Tiercelin, J.J., Brunet, M., 2006. Tectonic uplift and eastern Africa aridification. Science 313, 1419–1423.

Shimodaira, H., 2002. An approximately unbiased test of phylogenetic tree selection. Syst. Biol. 51, 492–508.

Shimodaira, H., Hasegawa, M., 1999. Multiple comparisons of log-likelihoods with applications to phylogenetic inference. Mol. Biol. Evol. 16, 1114–1116.

Siesser, W.G., 1980. Late Miocene origin of the Benguela upwelling system off northern Namibia. Science 208, 283–285.

Siler, C.D., Diesmos, A.C., Alcala, A.C., Brown, R.M., 2011. Phylogeny of Philippine slender skinks (Scincidae: *Brachymeles*) reveals underestimated species diversity, complex biogeographical relationships, and cryptic patterns of lineage diversification. Mol. Phylogenet. Evol. 59, 53–65.

Šmíd, J., Shobrak, M., Wilms, T., Joger, U., Carranza, S., 2017. Endemic diversification in the mountains: genetic, morphological, and geographical differentiation of the *Hemidactylus* geckos in southwestern Arabia. Org. Divers. Evol. 17, 267–285.

Stanley, E.L., Bates, M.F., 2014. Here be dragons: a phylogenetic and biogeographical study of the *Smaug warreni* species complex (Squamata: Cordylidae) in southern Africa. Zool. J. Linn. Soc. 172, 892–909.

Stöver, B.C., Müller, K.F., 2010. TreeGraph 2: combining and visualizing evidence from different phylogenetic analyses. BMC Bioinformatics 11, 7.

Sukumaran, J., Knowles, L.L., 2017. Multispecies coalescent delimits structure, not species. Proc. Natl. Acad. Sci. 114, 1607–1612.

Swofford, D.L., 2002. PAUP*. Phylogenetic analysis using parsimony (*and other methods), version 4.0 b10. Sunderland, MA: Sinauer Associates.

Thomas, D.S.G., Shaw, P.A., 1993. The evolution and characteristics of the Kalahari, southern Africa. J. Arid Environ. 25, 97–108.

Thomas, R., Hedges, & S.B., 2007. Eleven new species of snakes of the genus *Typhlops* (Serpentes: Typhlopidae) from Hispaniola and Cuba. Zootaxa 1400, 1–26.

Tolley, K.A., Chase, B.M., Forest, F., 2008. Speciation and radiations track climate transitions since the Miocene Climatic Optimum: a case study of southern African chameleons. J. Biogeogr. 35, 1402–1414.

Tolley, K.A., Conradie, W., Harvey, J., Measey, J., Blackburn, D.C., 2018. Molecular phylogenetics reveals a complex history underlying cryptic diversity in the bush squeaker frog (*Arthroleptis wahlbergii*) in Southern Africa. Afr. Zool. 53, 83–97.

Tolley, K.A., Weeber, J., Maritz, B., Verburgt, L., Bates, M.F., Conradie, W., Hofmeyr, M.D., Turner, A.A., da Silva, J.M., Alexander, G.J., 2019. No safe haven: protection levels show imperiled South African reptiles not sufficiently safe-guarded despite low average extinction risk. Biol. Conserv. 233, 61–72.

Tomasello, S., 2018. How many names for a beloved genus? – Coalescent-based species delimitation in Xanthium L. (Ambrosiinae, Asteraceae). Mol. Phylogenet. Evol. 127, 135–145.

Townsend, T.M., Alegre, R.E., Kelley, S.T., Wiens, J.J., Reeder, T.W., 2008. Rapid development of multiple nuclear loci for phylogenetic analysis using genomic resources: an example from squamate reptiles. Mol. Phylogenet. Evol. 47,129–142.

Travers, S.L., Jackman, T.R., Bauer, A.M., 2014. A molecular phylogeny of Afromontane dwarf geckos (*Lygodactylus*) reveals a single radiation and increased species diversity in a South African montane center of endemism. Mol. Phylogenet. Evol. 80, 31–42.

Trifinopoulos, J., Nguyen, L.T., von Haeseler, A., Minh, B.Q., 2016. W-IQ-TREE: a fast online phylogenetic tool for maximum likelihood analysis. Nucleic Acids Res. 44, W232–W235. Available online: http://iqtree.cibiv.univie.ac.at

Turner, F.B., Jennrich, R.I., Weintraub, J.D., 1969. Home Ranges and Body Size of Lizards. Ecology 50, 1076–1081.

Tyson, P.D., 1986. Climatic change and variability in southern Africa. Oxford University Press, Cape Town.

Tyson, P.D., Partridge, T.C., 2000. Evolution of Cenozoic climate. In: Partridge, T.C., Maud, R.R. (Eds.), The Cenozoic of Southern Africa. Oxford University Press, Oxford, pp. 371–387.

Valente, J., Rocha, S., Harris, D.J., 2014. Differentiation within the endemic burrowing skink *Pamelaescincus gardineri*, across the Seychelles islands, assessed by mitochondrial and nuclear markers. Afr. J. Herpetol. 63, 25–33.

Van Wyk, A.E., 1990. The sandstone regions of Natal and Pondoland: Remarkable centers of endemism. In: Heine, K., Balkema, A.A. (Eds.), Palaeoecology of Africa, Rotterdam, pp. 243–257.

Van Wyk, A.E., Smith, G.F., 2001. Regions of floristic endemism in Southern Africa: a review with emphasis on succulents. Umdaus Press, Hatfield.

Van Zinderen Bakker, E.M. 1982. African palaeoenvironments 18000 years B.P. Palaeoecol. Afr. 15, 77-99.

Van Zinderen Bakker, E.M., Mercer, J.H., 1986. Major late Cainozoic climatic events and palaeoenvironmental changes in Africa viewed in a worldwide context. Palaeogeogr. Palaeoclimatol. Palaeoecol. 56, 217–235.

Vidal, N., Branch, W.R., Pauwels, O.S.G., Hedges, S.B., Broadley, D.G., Wink, M., Cruaud, C., Joger, U., Nagy, Z.T., 2008. Dissecting the major African snake radiation: a molecular phylogeny of the Lamprophiidae Fitzinger (Serpentes, Caenophidia). Zootaxa 1945, 51–66.

Vidal, N., Hedges, S.B., 2004. Molecular evidence for a terrestrial origin of snakes. Proc. R. Soc. Lond. B 271 (Suppl.), 226–229.

Vitecek, S., Kučinić, M., Previšić, A., Živić, I., Stojanović, K., Keresztes, L., Bálint, M., Hoppeler, F., Waringer, J., Graf, W., Pauls, S.U., 2017. Integrative taxonomy by molecular species delimitation: multi-locus data corroborate a new species of Balkan Drusinae micro-endemics. BMC Evol. Biol. 17, 129.

Von Maltitz, G., Mucina, L., Geldenhuys, C.J., Lawes, M., Eeley, H., Adie, H., Vink, D., Fleming, G., Bailey, C., 2003. Classification system for South African indigenous forests: An objective classification for the Department of Water Affairs and Forestry. Report ENV-P-C 2003-017, Environmentek, CSIR, Pretoria.

Weinell, J.L., Bauer, A.M., 2018. Systematics and phylogeography of the widely distributed African skink *Trachylepis varia* species complex. Mol. Phylogenet. Evol. 120, 103–117.

White, F., 1978. The Afromontane Region: in Biogeography and Ecology of southern Africa Monographiae Biologicae 31. In: Werger, M.J.A. (Ed.), Biogeography and Ecology of Southern Africa. Springer Netherlands, The Hague, Netherlands, pp. 463– 560.

White, F., 1983. The vegetation of Africa. UNESCO. Paris.

Whiting, A.S., Bauer, A.M., Sites, J.W., 2003. Phylogenetic relationships and limb loss in sub-Saharan African scincine lizards (Squamata: Scincidae). Mol. Phylogenet. Evol. 29, 582–598.

Wollenberg, K.C., Vieites, D.R., Glaw, F., Vences, M., 2011. Speciation in little: The role of range and body size in the diversification of Malagasy mantellid frogs. BMC Evol. Biol. 11.

Xia, X., 2013. DAMBE5: a comprehensive software package for data analysis in molecular biology and evolution. Mol. Biol. Evol. 30, 1720–1728.

Zhang, J., Kapli, P., Pavlidis, P., Stamatakis, A., 2013. A general species delimitation method with applications to phylogenetic placements. Bioinformatics 29, 2869–2876.

Zwickl, D.J., 2006. Genetic Algorithm Approaches for the Phylogenetic Analysis of Large Biological Sequence Datasets Under the Maximum Likelihood Criterion. Ph.D. dissertation, The University of Texas, Austin, 115 pp.